ADVERTIMENT. La consulta d'aquesta tesi queda condicionada a l'acceptació de les següents condicions d'ús: La difusió d'aquesta tesi per mitjà del servei TDX (www.tesisenxarxa.net) ha estat autoritzada pels titulars dels drets de propietat intel·lectual únicament per a usos privats emmarcats en activitats d'investigació i docència. No s'autoritza la seva reproducció amb finalitats de lucre ni la seva difusió i posada a disposició des d'un lloc aliè al servei TDX. No s'autoritza la presentació del seu contingut en una finestra o marc aliè a TDX (framing). Aquesta reserva de drets afecta tant al resum de presentació de la tesi com als seus continguts. En la utilització o cita de parts de la tesi és obligat indicar el nom de la persona autora.

ADVERTENCIA. La consulta de esta tesis queda condicionada a la aceptación de las siguientes condiciones de uso: La difusión de esta tesis por medio del servicio TDR (www.tesisenred.net) ha sido autorizada por los titulares de los derechos de propiedad intelectual únicamente para usos privados enmarcados en actividades de investigación y docencia. No se autoriza su reproducción con finalidades de lucro ni su difusión y puesta a disposición desde un sitio ajeno al servicio TDR. No se autoriza la presentación de su contenido en una ventana o marco ajeno a TDR (framing). Esta reserva de derechos afecta tanto al resumen de presentación de la tesis como a sus contenidos. En la utilización o cita de partes de la tesis es obligado indicar el nombre de la persona autora.

WARNING. On having consulted this thesis you're accepting the following use conditions: Spreading this thesis by the TDX (www.tesisenxarxa.net) service has been authorized by the titular of the intellectual property rights only for private uses placed in investigation and teaching activities. Reproduction with lucrative aims is not authorized neither its spreading and availability from a site foreign to the TDX service. Introducing its content in a window or frame foreign to the TDX service is not authorized (framing). This rights affect to the presentation summary of the thesis as well as to its contents. In the using or citation of parts of the thesis it's obliged to indicate the name of the author

Scaling of Subsurface Processes in Heterogeneous Aquifers: From Hydraulic Testing to the Use of Memory Functions

PhD Thesis

Department of Geotechnical Engineering and Geosciences (ETCG)
Technical University of Catalonia, UPC

Matthias Willmann

October, 2008

UPC
HYDROGEOLOGY GROUP
TECHNICAL UNIVERSITY OF CATALONIA

This thesis was funded by AGAUR (Agència de Gestió d'Ajuts Universitaris i de Recerca) of the Catalan Regional Government with a FI doctoral grant and was developed in the framework of the European project, *FUNMIG*.

Für meine Eltern

Abstract

Heterogeneity of hydraulic conductivity is known to vary orders of magnitudes within small distances. This affects our observations of natural processes. To explain reality we usually rely on simplified models. But to apply them properly information of aquifer properties has to be transferred from local scale where the process can be described directly to the support scale of the measurement and to the grid scale of a numerical model. This procedure is termed upscaling and might involve changing the parameters of the known local scale equation or derivation of a new upscaled equation. Upscaling depends strongly on the complexity of the process under consideration. The objective of this thesis is to investigate these changes of scales for different subsurface processes with increasing complexity: radial flow, conservative transport and reactive transport.

First, flow upscaling is investigated for the example of the interpretation of a hydraulic test in a heterogeneous aquifer. Recovery tests are based on estimating transmissivity, T, from the heads that rebound after pumping has stopped. Recovery tests can be performed in wells where conventional constant-rate pumping tests would not be possible. Test interpretation is based on the simple Jacob's method, related to late time drawdown in an infinite homogeneous aquifer. Yet, field data often cannot be explained by the homogeneous theory. Numerical simulations are performed to show that heterogeneity in T can explain these field observations. It is also shown that the local T value around the well can be inferred from early time recovery data, assuming ideal conditions, whereas late time data yield a large scale (regional) representative value. Even when recovery is observed for a short time, indirect information about the regional value can also be obtained.

Second, conservative transport upscaling is considered by interpreting the tailing of breakthrough curves of tracer tests. Tailing is attributed to heterogeneity of aquifer properties and cannot be properly modelled by means of the homogeneous advection-dispersion equation (ADE). Mass-transfer models (e.g., CTRW, MRMT or fADE) using memory have been widely applied for reproducing observed tails. The relationship between memory parameters obtained from BTC fitting and the parameters characterizing the heterogeneity of hydraulic properties is still unclear. Here, the conditions are investigated under which heterogeneity produces the type of tailing observed in the field and how memory functions are influenced by measurable heterogeneity parameters (e.g., variance of the underlying transmissivity field). The slope of a BTC in a log-log plot is found to be mainly influenced by the connectivity of the underlying permeability field, but insensitive to its variance. The slope BTC reaches asymptotically 2 as connectivity increases.

And finally, the above model is extended to mixing controlled multi-component reactive transport. At the field scale, reactive transport equations based on the ADE are known to overestimate reactions. The objective is to test whether a model based on effective dynamics, such as e.g. the Multi-Rate Mass Transfer Method (MRMT), derived from conservative transport observations, can be used to describe effective reactive transport in heterogeneous media. The numerical solution of conservative transport MRMT is extended to the reactive case. The reaction rates are then compared for a binary system computed with the heterogeneous transport model to those corresponding to the reactive MRMT. An excellent agreement is found between the two models in terms of cumulative precipitated mass, and depending on the local heterogeneous structure the match is also very good regarding the spatial distribution of precipitated mineral. These results indicate that mass transfer models are an excellent tool for upscaling of mixing controlled reactive transport.

Resum

L'heterogeneïtat de la conductivitat hidràulica és ben coneguda, podent canviar varis ordres de magnitud en poca distància. Això afecta les nostres observacions dels processos naturals. Per explicar la realitat normalment ens basem en models simplificats. Però per incorporar correctament en ells les propietats dels aqüífers, s'ha de passar de l'escala local a l'escala de suport i a l'escala de la malla del model numèric. Aquest procés s'anomena Upscaling i pot comportar canviar els paràmetres de l'equació coneguda a escala local, o bé la derivació d'una nova equació d'Upscaling. L'Upscaling depèn fortament de la complexitat dels processos que es consideren. L'objectiu d'aquesta tesis és investigar aquests canvis d'escala a partir de diferents processos subterranis, incrementant la complexitat: flux radial, transport conservatiu i transport reactiu.

En primer lloc s'investiga el Upscaling de flux per medi de la interpretació d'un assaig hidràulic en un medi heterogeni. Els assajos de recuperació es basen en l'estimació de la transmissivitat, T, a partir de la recuperació dels nivells un cop s'ha parat el bombeig. Aquests tipus d'assaig es pot realitzar en pous on no és possible dur a terme un assaig convencionals a cabal constant. La interpretació de l'assaig de recuperació es basa en el mètode simplificat de Jacob, tenint en compte els últims temps de la recuperació, en un aqüífer infinit homogeni. Però, sovint les dades de camp no es poden interpretar amb la teoria basada en l'homogeneïtat. S'han realitzat simulacions per demostrar que l'heterogeneïtat de T pot explicar aquestes observacions de camp. També es mostra que el valor local de T al voltant del pou pot ser deduït dels primers temps de la recuperació del bombeig, assumint condicions ideals, mentre que les dades del últims temps de la recuperació corresponen a valors representatius a escala regional. A més a més, els primers temps de la recuperació també contenen informació indirecta del valor regional de T.

En segon lloc, es considera l'Upscaling en transport conservatiu a partir de la interpretació de les cues de les corbes d'arribada (BTC) d'un assaig de traçadors. La cua s'atribueix a l'heterogeneïtat de l'aqüífer, i no pot ser modelada per medi de l'equació d'advecció-dispersió (ADE) en medi homogeni. Per tal de reproduir les cues observades s'han aplicat àmpliament models de transferència de massa utilitzant memòria (e.g, CTRW, MRMT o fADE). La relació entre els paràmetres de memòria obtinguts de l'ajust de les BTC i els paràmetres que caracteritzen l'heterogeneïtat de les propietats hidràuliques enara està per aclarir. En aquesta tesis s'investiga sota quines condicions l'heterogeneïtat produeix el tipus de cues observades al camp, i com les funcions de memòria estan influenciades per paràmetres de l'heterogeneïtat que es poden mesurar (e.g, variança dels camps de transmissivitat). S'ha observat que el pendent d'una BTC en un log-log plot està majoritàriament influenciat per la connectivitat del camp de permeabilitats, però és insensible a la seva variança. El pendent del BTC arriba assimpdòticament a un valor de 2 quan s'augmenta la connectivitat.

I finalment, el model exposat anteriorment s'extén al transport reactiu multi-component controlat per la barreja. És ben conegut que a l'escala de camp, les equacions de transport reactiu basades en la ADE sobreestimen les reaccions. L'objectiu és assajar si un model basat en la dinàmica efectiva, tal com per exemple MRMT derivat de les observacions de transport reactiu, pot ser utilitzat per descriure el transport reactiu efectiu en medi heterogeni. La solució numèrica del MRMT de transport conservatiu s'extén al cas reactiu. Les taxes de reacció es comparen per un sistema binari, entre un model heterogeni i el seu corresponent model MRMT. S'ha trobat un excel.lent acord entre els dos models en termes de massa precipitada acumulada i, depenent de l'estructura heterogènia local, l'ajust és també molt bò pel que respecta a la distribució espacial del mineral precipitat. Aquests resultats indiquen que els models de transferència de massa són una eina excel.lent per l'Upscaling del transport reactiu controlat per la barreja.

Resumen

La heterogeneidad de la conductividad hidráulica es bien conocida, pudiendo cambiar varios órdenes de magnitud en poca distancia. Esto afecta nuestras observaciones de los procesos naturales. Para poder explicar la realidad normalmente nos basamos en modelos simplificados. Pero para incorporar correctamente en ellos las propiedades de los acuíferos, se debe pasar de escala local a escala de soporte y a escala de la malla del modelo numérico. Este proceso se llama Upscaling y puede comportar cambiar los parámetros de la ecuación conocida a escala local, o bien la derivación de una nueva ecuación de Upscaling. El Upscaling depende fuertemente de la complejidad de los procesos que se consideran. El objetivo de esta tesis es investigar estos cambios de escala a partir de diferentes procesos subterráneos, incrementando la complejidad: flujo radial, transporte conservativo y transporte reactivo.

En primer lugar se investiga el Upscaling de flujo por medio de la interpretación de un ensayo hidráulico en un medio heterogéneo. Los ensayos de recuperación se basan en la estimación de la transmisividad, T, a partir de la recuperación de los niveles una vez parado el bombeo. Este tipo de ensayo se puede realizar en pozos donde no es posible llevar a cabo un ensayo convencional a caudal constante. La interpretación del ensayo de recuperación se basa en el modelo simplificado de Jacob, teniendo en cuenta los últimos tiempos de la recuperación, en un acuífero infinito homogéneo. Pero, a menudo los datos de campo no se pueden interpretar usando la teoría basada en la homogeneidad. Se han realizado simulaciones para demostrar que la heterogeneidad de T puede explicar estas observaciones de campo. También se muestra que el valor local de T alrededor del pozo puede ser deducido de los primeros tiempos de la recuperación del bombeo, asumiendo condiciones ideales, mientras que los datos de los últimos tiempos de la recuperación corresponden a valores representativos a escala regional. Además, los primeros tiempos de la recuperación también contienen información indirecta del valor regional de T.

En segundo lugar, se considera el Upscaling en transporte conservativo a partir de la interpretación de las colas de curvas de llegada (BTC) de un ensayo de trazadores. La cola se atribuye a la heterogeneidad del acuífero, y no puede ser modelada por medio de la ecuación de advección-dispersión (ADE) en medio homogéneo. Para reproducir las colas observadas se han aplicado ampliamente los modelos de transferencia de masa utilizando memoria (e.g, CTRW, MRMT o fADE). La relación entre los parámetros de memoria obtenidos del ajuste de las BTC y los parámetros que caracterizan la heterogeneidad de las propiedades hidráulicas aun esta por aclarar. En esta tesis se investiga bajo qué condiciones la heterogeneidad produce el tipo de colas observadas en campo, y como las funciones de memoria están influenciadas por parámetros de la heterogeneidad que se pueden medir (e.g, varianza de los campos de transmisividad). Se ha observado que la pendiente de una BTC en un log-log plot está mayoritariamente influenciada por la conectividad del campo de permeabilidades, pero es insensible a su varianza. La pendiente del BTC llega asindóticamente a un valor de 2 cuando aumenta la conectividad.

Y finalmente, el modelo expuesto anteriormente se extiende al transporte reactivo multicomponente controlado por la mezcla. Es bien conocido que a escala de campo, las ecuaciones de transporte reactivo basadas en la ADE sobrestiman las reacciones. El objetivo es ensayar si un modelo basado en la dinámica efectiva, tal como por ejemplo MRMT derivado de las observaciones de transporte reactivo, puede ser utilizado para describir el transporte reactivo en medio heterogéneo. La solución numérica del MRMT de transporte conservativo se extiende al caso reactivo. Las tasas de reacción se comparan para un sistema binario, entre un modelo heterogéneo y su correspondiente modelo MRMT. Se ha encontrado un excelente acuerdo entre los dos modelos en términos de masa precipitada acumulada y, dependiendo de la estructura heterogénea local, el ajuste es también muy bueno en relación a la distribución espacial del mineral precipitado. Estos resultados indican que los modelos de transferencia de masa son una herramienta excelente para el Upscaling del transporte reactivo controlado por la mezcla.

Acknowledgements

First of all, I want to thank my advisers, Jesús Carrera y Xavier Sánchez-Vila for the continuous support throuout my thesis. I always found your doors open. And I learned a lot from you, also scientifically. Also, I want to thank Alberto Guadagnini, Michela de Simoni and Monica Riva for your hospitality during my time in Milan.

Thanks also to my colleagues from the Hydrology Group at the Department of Geotechnical Engineering and Geosciences at the UPC. It's a great working environment and I am glad to say that I found some very good friends there. Marco, I miss already our discussions in the Cinemateca. I also want to thank Agustin Medina, who was always helpful with my needs for TRANSIN.

Thanks to all my friends, particularly to those in Barcelona and those from my other life in the Baix Penedes. And Roser, many thanks for your support all this time, particularly the last months were not easy for you. I promise from now on we will go to the mountains more often.

Und schlieslich möchte ich meiner Familie danken, meinem Bruder Christian und vor allem meinen Eltern. Ihr habt immer an mich geglaubt, oft mehr als ich, und ohne Euch hätte ich diese Arbeit nicht einmal angefangen.

Table of Contents

1 Introduction 1

1.1 Objectives 3

1.2 Thesis outline 4

2 Flow: Interpretation of Recovery Tests 5

2.1 Introduction 5

2.2 Methodology for the numerical simulations 11

2.2.1 Transmissivity fields 11

2.2.2 Simulation of recovery tests 12

2.2.3 Analysis of the simulated tests 14

2.3 Discussion of results 15

2.4 A reinterpretation of the field tests 20

2.4.1 Tests at Park Escorxador 21

2.4.2 Test at Villalba Street 21

2.4.3 Test at Mallorca Street 21

2.5 Conclusions and recommendations 22

3 Conservative Transport: Memory parameters 25

3.1 Introduction 25

3.2 Background 30

3.3 Methodology 32

3.3.1 Generation of transmissivity fields 33

3.3.2 Fine-scale transport simulations within the heterogeneous fields 36

3.3.3 Obtaining memory functions from breakthrough curves 38

3.3.4 Modeling of BTCs using the memory term 40
3.4 Results 41
3.4.1 Effects of mass input and detection mode; scaling 41
3.4.2 Effects of different heterogeneous fields 43
3.4.3 Effects of the local-scale equation 47
3.4.4 Comparison with BTCs using mass transfer 49
3.5 Discussion and Conclusions 49

4 Reactive Transport: MRMR-R **53**

4.1 Introduction 53
4.2 The Multi-Rate Mass Transfer Reactive (MRMT-R) Model 56
4.2.1 Conservative transport model based on Multi-Rate Mass Transfer 57
4.2.2 Reactive transport in a single porosity model 59
4.2.3 Multi-Rate Mass Transfer Reactive (MRMT-R) model 61
4.3 The MRMT-R Model: Sensitivity Analysis 63
4.3.1 Reaction Rate Spatial Distributions in the Mobile and Immobile Zones . 64
4.3.2 Sensitivity to the equilibrium constant 66
4.3.3 Variation of Parameters that Alter the Shape of the Conservative BTC . . 66
4.3.4 Variation of parameters conserving the shape of the BTC 69
4.4 MRMT-R upscaling methodology 70
4.4.1 Creation of heterogeneous transmissivity fields 70
4.4.2 Reactive transport simulations 71
4.4.3 Derivation of memory function for conservative transport 72
4.5 Reproducing the observations in the heterogeneous media by means of an effective model 74
4.5.1 Reproducing anomalous transport behavior 74
4.5.2 Reproducing Quasi-ergodic transport 76
4.6 Sensitivity to boundary condition and transverse dispersivity 77
4.6.1 Boundary conditions 77
4.6.2 Transverse dispersion 80
4.7 Conclusions 80

5 General conclusions 83

A Apendix A: Numerical implementation 89

A.1 Implementation of a discrete mass-transfer scheme 89

A.2 Implementation of the discrete MRMT-R 91

Bibliography 92

List of Figures

2.1 ”Ideal” Theis recovery plot (also called Horner plot), displaying residual drawdown versus equivalent time, defined as t* = (t + tP)/t. Transmissivity can be calculated from the slope m through equation 2. The validity limit of the Theis recovery method u is r2S/4Tt. 8

2.2 Examples of field recovery tests performed within the city of Barcelona, Spain. The Theis recovery plots are plotted as residual drawdown versus dimensionless equivalent time. Escorxador 1 and 2 are tests performed at Park Escorxador, Villalba is a test at Villalba Street and Mallorca is a test at Mallorca Street? Only Fig 2a (Escorxador 1) displays a shape similar to that in a homogeneous aquifer. Notice that even in this test, early time data ($t* > 100$) departs from the ideal condition, reflecting well effects, such as skin, wellbore storage, etc. (negative skin in this case). 10

2.3 a) Transmissivity fields F1 through F4. F1 and F2 show a disc around the well with T one order of magnitude lower (F1) or higher (F2) than the regional value. F3 and F4 are simulated heterogeneous T fields conditioned at the well location to a value one order of magnitude higher (F3) or lower (F4) with respect to the geometric mean of the T point values. b) Set-up of the numerical simulations. The fields in a) correspond to the zone of interest. In the outer domain, the grid becomes increasingly coarse towards the boundary, whereas it is refined at the well. Plot b) is not to scale. The characteristic length, Lc, is 20, equal to the radius of the inner disc in fields F1 and F2 and equal to the correlation length in fields F3 and F4. All numbers are unit length. 12

2.4 Two different calculations of slope m in a heterogeneous aquifer at the example test site Villalba. At any point P, the slope can be calculated as that of the tangent (m1) or as that of the secant, the line between the origin and P (m2). Note that m1 and m2 should be identical for late time data in an ideal homogeneous aquifer. . . 15

2.5 Numerical results for fields F1 and F2. (a) Dimensionless drawdown for 3 different pumping durations for F1, and (b) corresponding estimated transmissivities (T* = T/Tloc) derived from either (4) or (5). (c) Dimensionless drawdown for three different pumping durations for F2, and (d) corresponding estimated transmissivities. Shown are only the portions of the curves meeting the condition of validity of the Theis recovery method (u ¡ 0.01). 16

2.6 Numerical results for fields F3 and F4. (a) Dimensionless drawdown for 3 different pumping durations for F3, and (b) corresponding estimated transmissivities. (c) Dimensionless drawdown for three different pumping durations for F4 with additional pumping time $t_P D = 100$, and (d) corresponding estimated transmissivities. Shown are only the portions of the curves meeting the condition of validity of the Theis recovery method ($u < 0.01$). 19

2.7 Reinterpretation of the field test data presented in Fig. 2.2. The tests results are plotted as transmissivities versus equivalent time. Tm1 and Tm2 are defined in equations 4 and 5 but not normalized by T_{loc} as it is not known. In Fig. 2.7 a T_{m1} and T_{m2} are basically the same but in Fig. 2.7b-d they differ particularly for early times. 20

3.1 Breakthrough curve of iodine measured at the EL Cabril site (UPC, 1990). A power-law tail is observed with a slope of 2.0 (indicated as a grey line). The power-law behavior spans over 1.5 orders of magnitude until the background concentration was reached. This curve cannot be reproduced by using a homogeneous ADE. Mass transfer models using a memory function can reproduce this behavior. But the causes of the tailing need to be properly understood in order to use such memory function for predictions under different flow conditions or transport distances. 26

3.2 Representation of a memory function (black). It can be viewed as the superposition of 10 individual memory functions each corresponding to an immobile zone (grey) (Eq. 3). The memory function exhibits three independent variables: characteristic time t_1 when power-law decay starts, characteristic time t_2 when power-law behavior ends; and the power-law slope, m_g. 32

3.3 Five types of transmissivity fields used in this work. They show different ranges of scales and different degrees of connectivity: (a) multi-gaussian field with a single exponential variogram and a small correlation length; (b) field comprising of two nested variograms with different correlation lengths; (c) power variograms representing a continuous distribution of heterogeneity scales; (d) similar to type 3 but conditioned to leave a preferential flow path (white and black crosses indicate conditioning point with low and high T values respectively; and (e) highly connected fields. 34

3.4 Derivation of the memory function of a breakthrough curves taken in a heterogeneous aquifer BTC_{het}. Early time data is fitted against the corresponding BTC derived by means of the ADE (BTC_{ADE}). t_1 is read directly from the point where the two curves deviate. Starting from t_1 a straight line is fitted to the tail to get m_{BTC}. Finally, the cut-off, t_2 is taken as the point where the BTC starts to decrease exponentially. 39

3.5 Snapshots of concentrations for a type 3 field at three different time steps. The shape of the plume clearly indicates non-Fickian behavior (marked asymmetry) that cannot be described by an ADE-like equation with upscaled parameters, whether constant or time dependent. Actually, two different preferential flow paths can be observed where the upper is more conductive than the lower one. 42

3.6 Comparison of breakthrough curves for two different initial conditions (uniform initial concentration or flux averaged mass inflow) and two detection modes (resident or flux averaged concentration). All 8 tests are performed in the type 3 field example of Figs. 3 and 5, where the left boundary is highly heterogeneous and the right boundary is relatively homogeneous. In four tests, the solute moves from left to right and in the remaining four from right to left with all the possible combinations of detection mode (flux or resident concentration) and initial conditions (uniform or flux averaged). Test results do not depend on the condition applied at the homogeneous boundary, which consistently display a slope around 2.2. The slope decreases by about 0.9 for the four cases where either resident concentrations are measured or fixed concentrations are applied at the heterogeneous boundary. Notice that the effect of the two preferential flow paths of Fig. 5 is reflected as two, more or less smoothed, humps in the BTC. 44

3.7 Breakthrough curves for different types of heterogeneity: a) the multi-gaussian fields (type 1). The curves do not show power-law tail and the curves can be reproduced using an ADE with upscaled parameters. b) A type 3 field with varying variance. When variance is decreased, we observe no change of slope, m_{BTC}, but a significant delay in first arrival and reduction of late time cutoff, t_2. c) A type 3 field with different values for the Hurst coefficients. It indicates that small scale heterogeneity has little effect on any of the parameters of g and d) type 3 field with BTC measured at uniformly increasing distances between 100 and 1000. No change in m_{BTC} is observed with increasing sampling volume. 45

3.8 Slopes for different types of transmissivity fields versus: a) the correlation lengths of the underlying multi-gaussian field in Type 5 fields(recall that increasing this correlation length results in broader, better connected channels); b) flow connectivity index; and c) transport connectivity index. They all show that the slope m_{BTC} decreases (i.e., tailing becomes increasingly marked) as connectivity increases. The slope appears to tend $m_{BTC} = 2$, but does not decrease further. 47

3.9 BTCs investigating the local scale equation: a) Subgrid heterogeneity is modeled using dispersivity (ADE). When the local transverse dispersivity is varied, the effect on the resulting BTCs is minor. The longitudinal dispersivity was kept constant. b) A non-local small-scale equations is used: a mass transfer term is added with varying memory functions, which causes m_{BTC} to decreases when a large final cutoff time is used. 48

3.10 Fitted breakthrough curve using the memory function derived from the heterogeneous small scale simulations. The only fitting parameters are dispersivity and mobile porosity. As part of the heterogeneity can be modeled either with the mobile zone dispersion or with the memory function, more than one set of parameters fit the original BTC. When t_1 is chosen small, the mobile zone dispersivity is equal to the local dispersivity of the original heterogeneous field simulation. 50

4.1 Evaluation of the spatial distribution of mineral precipitation: a) total precipitated mass for three different times (1000, 11000, 51000); b) spatial distribution of reaction rate for an early time step (t t1); reaction rate in the mobile zones shows some ADE like behavior with the characteristic double peak and is much stronger than reaction rate in the immobile zone; c) the same plot for a later time step, where no double peaks are displayed anymore (the modeling domain was enlarged here); d) distribution of selected single immobile zones for the same time as c); the total number of immobile zones is 20. 65

4.2 a) Speciation factor as a function of concentration for different pK values (notice, that the speciation factor increases with pK for low values of$u$, but decreases for high values); b) spatial distribution of the reaction rate as a function of K. The reaction rates are non-monotonic with K. 67

4.3 Sensitivity of the spatial distribution of total reaction rates (recall Fig.4.1) and total precipitated mass to: a,b) longitudinal dispersivity, c,d) t2, and e,f) slope of the memory function, mg. The curves in a, c and e correspond to a fixed time t=51000 68

4.4 Spatial distributions of reaction rate for three combinations of ratios of mobile and immobile porosity, t_1 and dispersivity, that lead to virtually identical conservative tracer BTCs. Notice that the total reaction rate is not affected dramatically though the separation between mobile and immobile precipitation is. 69

4.5 Transmissivity fields and corresponding breakthrough curves (BTCs) obtained from conservative transport simulations. BTC's are the cumulated mass collected at the domain's right boundary. The three fields correspond respectively to single realizations of: A) a Multi-Gaussian field with short correlation length, B) a non-stationary field based on a power variogram, and C) a field where connectivity between the high transmissive pixels have been enhanced with respect to those of low conductivity. 73

4.6 Model results for field type C (connected field). a-c) Comparison between the spatial distribution of the vertically averaged precipitated mass in the heterogeneous media with those derived from the effective MRMT-R model for three different time steps (1000, 11000, 51000) and for (a) pK = 2, (b) pK = 4 ,and (c) pK = 6. d) The instantaneous reaction rate for both models at a given time step at pK = 2.. 75

4.7 Model results for field type B (non-stationary variogram). a-c) Comparison between the spatial distribution of the vertically averaged precipitated mass in the heterogeneous media with those derived from the effective MRMT-R model for three different time steps (1000, 11000, 51000) and for (a) pK = 2, (b) pK = 4 ,and (c) pK = 6. d) The instantaneous reaction rate for both models at a given time step at pK = 2. 76

4.8 Model results for field type A, the multi-Gaussian field. a) Comparison between the spatial distribution of the vertically averaged precipitated mass in the heterogeneous media with those derived from the effective MRMT-R model for three different time steps (1000, 11000, 51000) and for pK = 2. b) The instantaneous reaction rate for both models at a given time step. 78

4.9 Sensitivity analysis for: a) Boundary conditions, including an flux averaged input pulse and initial uniform concentration at the boundary nodes. After a distance of 200 the curves have the same shape but the precipitated mass when a pulse is considered is 5 times larger than for fixed initial concentration. The smoother cures are the effective MRMT-R models which both reproduce very well the heterogeneous solution. b) Transverse dispersivities (0.1, 1.0, 10.0) is varied. The curves look similar but smooth out with increasing dispersivity. The corresponding effective solution represents very well all the heterogeneous curves. 79

Chapter 1

Introduction

Heterogeneity remains a major difficulty in the interpretation of field observations. Hydraulic conductivity measured at some small representative scale is known to vary by orders of magnitude from one point to another, even in apparently homogeneous aquifers (e.g. *Gelhar*, 1993). This makes it important to know the scales involved: the scale where the local equation is valid, the support scale of the measurements, the scale of numerical resolution and the scale of the problem. The shift between these scales is called upscaling (or down-scaling). Their effects depends strongly depending on the complexity of the process under consideration. For flow problems only the total flux is important and neither travel time of water particles not their trajectory. For conservative transport also the travel time becomes important, but integrated values over the path way is sufficient. Considering reactive transport on the other side makes it important to consider as well the distributions along the pathways.

For flow this problem is generally well understood. Various methods are known to determine effective parameters (e.g. *Renard and de Marsily*, 1997; *Wen and Gómez-Hernández*, 1996; *Sánchez-Vila et al.*, 1995). Hydraulic tests performed under radial flow conditions are a common way to measure hydraulic conductivity. *Meier et al.* (1998) found for pumping tests that the late time behavior of heads, measured by the slope of drawdown versus log time was characterized by the effective transmissivity of the aquifer, thus, making Jacob's method also valid for heterogeneous media. *Meier et al.* (1999) showed that specific-capacity measurements depend strongly on the local transmissivity next to the well.

Conservative transport has been traditionally modeled using the advection dispersion equation (ADE). Yet, transport in natural aquifers usually displays anomalous (i.e., inconsistent with the ADE) behavior. Observed deviations are numerous (*Carrera*, 1993). They include scale dependence of dispersivity (e.g., *Lallemand-Barres and Peaudecerf*, 1978; *Neuman*, 1990), directional and time dependence of apparent porosity (*Sánchez-Vila and Carrera*, 1997; *Guimerà and Carrera*, 2000) and tailing of breakthrough curves (e.g., *Valocchi*, 1985; *Freyberg*, 1986; *Cortis and Berkowitz*, 2004). Stochastic hydrology has succeeded in qualitatively explaining these deviations and in quantifying the scale dependence of dispersivity, (e.g., *Dagan*, 1989; *Gelhar*, 1993). In the process, tools have been developed to predict the evolution of dispersivity with scale given a stochastic description of variability of hydraulic conductivity (*Kitanidis*, 1988; *Dentz et al.*, 2000). However, much less efforts have been devoted to understanding the causes of tailing (*Haggerty et al.*, 2000; *Shapiro*, 2001; *Cortis and Berkowitz*, 2004; *Dentz et al.*, 2004).

A number of non-local methods have been proposed to describe anomalous transport. Multi-Rate Mass Transfer (MRMT) (*Haggerty and Gorelick*, 1995; *Wang et al.*, 2005) and memory functions (*Carrera et al.*, 1998), which are equivalent (*Haggerty et al.*, 2000), can be viewed as dividing the medium into overlapping mobile and immobile continua (hence the generic term multicontinuum models). Each immobile zone exchanges solute mass with the mobile zone by linear mass transfer (i.e., mass exchange is proportional to concentration gradient). These models may be expressed as a function of only the mobile concentration by introducing a memory term into the ADE to account for mass transfer between mobile and immobile zones. The name ”memory” reflects the fact that this term represents the system memory (i.e., how current mobile concentrations are affected by past events). Multicontinuum models have been successfully applied to interpret anomalous transport (*McKenna et al.*, 2001; *Haggerty et al.*, 2004; *Zinn et al.*, 2004; *Carrera et al.*, 1998; *Sánchez-Vila and Carrera*, 2004; *Zhang et al.*, 2007). At present, memory functions are calibrated against tracer test data, without explicit reference to heterogeneity. This is unsatisfactory both from conceptual and practical viewpoints.

Reactive transport modeling at the field scale is more complex. *De Simoni et al.* (2005, 2007) showed that equilibrium reaction rates are controlled by mixing rates. The distinctive characteristic of the upscaled equations with respect to the ADE is how these equations can separate the concepts of spreading and mixing. Spreading, directly related to hydrodynamic dispersion, provides a measure of the area that could potentially be affected by a pollution problem, incorporating the uncertainty in the location of the center of gravity of the polluted area. Mixing, on the other side, indicates the extent of the polluted area, regardless of its location. The ADE equates the concepts of mixing and spreading.

The question is whether the success of non-local formulations for representing conservative transport can be extended to reactive transport.

1.1 Objectives

The objective of this thesis is to study the effects of upscaling for different subsurface processes in heterogeneous aquifers: particularly on flow, conservative and reactive transport. The specific objectives are:

For flow it is studied if the classical interpretation of recovery tests yields meaningful and useful hydraulic parameter values in heterogeneous aquifers. If yes, as conjectured by extrapolating the results of *Meier et al.* (1998), then the practical question would be how long to pump or to observe recovery in order to obtain meaningful results.

For conservative transport the objective is to investigate the physical meaning of mass transfer models used for upscaling. First, conditions are explored under which heterogeneity can explain the kind anomalous transport observed in tracer tests, namely power law decay in tailing. Second, the relationship between field properties describing heterogeneity and the parameters describing the memory function are investigated.

For reactive transport the goal is to show the applicability of mass transfer models for upscaling of multi-component reactive. For this purpose the model proposed above is revisited and extended for reactive transport. It is then investigated if the physically based upscaling of conservative transport is sufficient to upscale reactive transport.

1.2 Thesis outline

This thesis is presented in terms of journal publications, partly already published or still in the review process. This results in stand-alone chapters with own introduction, own methodology and conclusions. Unfortunately, this leads to some repetitions of concepts and methods for which I want to apologize. Still, reading this work one will realize that the same concepts are different for the different problems considered here. The general conclusion are then added as a final chapter.

Chapter 2

On the meaning of transmissivity values obtained from recovery tests*

2.1 Introduction

A large body of work in hydrogeology has been devoted to the design of hydraulic tests that can provide good estimates of aquifer parameters. Specifically, recovery tests are easy to perform and provide reliable estimates of transmissivity, T. Recovery tests consist of observing the build-up (or recovery) of hydraulic heads after pumping has stopped. If possible, measurements should continue until the head has recovered to its prior-to-pumping value.

The advantages of a recovery test stem from its simplicity: (1) a recovery test follows naturally from a pumping test, because it only requires the recording of heads after pumping has ceased; (2) it can be used even when pumping rates are difficult to control; (3) it is fairly inexpensive and no equipment or additional observation wells are required apart from a water level measuring device;

---

*This chapter is based in the article: Willmann, M., J. Carrera, X. Sánchez-Vila, and E. Vásquez, 2007, On the meaning of transmissivity values obtained from recovery tests, *Hydrogeol. J.*, Vol. 15, 833-842., doi10.1007/s10040-006-0147-8 and (4) results are usually not sensitive to well losses.

The analysis of a recovery test follows the Theis solution to pumping a fully penetrating well of zero radius in an infinite, homogeneous aquifer. The most common and easiest way to interpret a recovery test is to use the Theis recovery method (*Theis*, 1935), an approximation to late time data which leads to:

$$s = \frac{2.303Q}{4\pi T} \log(\frac{t + t_P}{t}) = 0.183\frac{Q}{T} \log(t*) \quad , \tag{2.1}$$

where s is the residual drawdown, Q (constant) is the pumping rate, T is the transmissivity,t_P is the pumping time, and t is the elapsed time since pumping stopped. The variable $t^* = (t + t_P)/t$ is termed equivalent time. In dimensionless form, Eq. (2.1) can be rewritten as:

$$s_D = \log(\frac{t_D + t_{PD}}{t_D}) = \log(t*) \tag{2.2}$$

where $s_D = 4\pi Ts/2.303Q$ and $t_D = Tt/SL^2$ with L_c some characteristic length of the problem and S storage coefficient. The variable t_{PD} corresponds to the dimensionless pumping duration. Equations (2.1) and (2.2) are valid for large times, meeting the condition $u = r^2S/4Tt < 0.01$ (e.g. *Freeze and Cherry*, 1979), where r is the distance between pumping and observation points. In terms of equivalent time, this condition is $t* < 1 + 0.04t_{PD}\frac{L_c^2}{r^2}$. In recovery tests, heads are usually observed at the pumping well, so that r is the well radius, which tends to be small, making this condition easy to meet. Q can be approximated as V_w/t_P, where V_w is the total volume of water pumped. This result is useful when Q is not constant even if this variability might affect early time recovery.

The interpretation of a recovery test is performed by plotting residual drawdown against equivalent time on a semi-logarithmic plot (Fig. 2.1). The use of equivalent time causes late time data to be displayed on the left side, corresponding to small residual drawdown. Equation (2.1) shows that late time data displays a straight line passing through the origin, provided that no residual drawdown remains when the aquifer reaches equilibrium. The slope, m, of this line is the coefficient in

Eq. (2.1). Knowing m allows estimating transmissivity as:

$$T = 0.183\frac{Q}{m} \tag{2.3}$$

In principle, the interpretation of one recovery test using a semi-log plot would not allow estimating S. Recent research on recovery tests has concentrated on overcoming this limitation (*Agarwal*, 1980; *Banton and Bangoy*, 1996; *Goode*, 1997; *Chenof*, 2002; *Zheng et al.*, 2005). They focus on finding an alternative interpretation to estimate the storage coefficient by using also heads at observation points different from the pumping well.

The Theis solution and, thus, the Theis recovery method are based on some assumptions that are not met in reality, but may affect test results: infinite aquifers, negligible well radius, perfectly confined aquifer, constant pumping rate, and homogeneous hydraulic parameters. Actually, aquifers in the field are bounded, wells do have a finite radius, flow to a pumping well may not be purely horizontal but have a vertical component, pumping rate may be kept constant with difficulty, and transmissivity and storativity are not homogeneous. Some of these departures from the ideal hydrologic conditions have been thoroughly studied for hydraulic tests and several methodologies to account for them are available in the literature (e.g. *Streltsova*, 1988; *Bourdet*, 2002). Heterogeneity remains a major difficulty in the interpretation of field hydraulic testing. Hydraulic conductivity measured at some small representative scale is known to vary by orders of magnitude from one point to another, even in apparently homogeneous aquifers (e.g. *Gelhar*, 1993). This result makes it important to know the individual support scale of the measurements. If the sampled volumes of an aquifer are too large, estimated parameters would be artificially homogenized. In large projects, it is not unusual to perform different types of tests involving several support scales in order to find the adequate input value for numerical models (*Shapiro and Hsieh*, 1998; *Martinez-Landa and Carrera*, 2005)

A few results are available for the response of heads to pumping in a heterogeneous aquifer. Analytical solutions are available for simplified heterogeneities like a disk of transmissivity T_1 em-

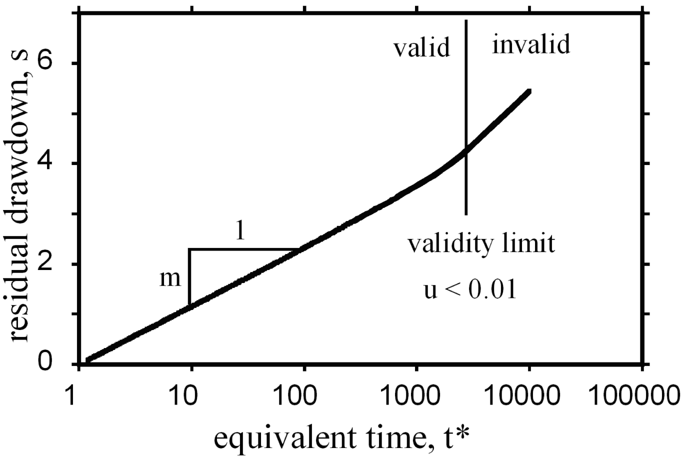

Figure 2.1: "Ideal" Theis recovery plot (also called Horner plot), displaying residual drawdown versus equivalent time, defined as t* = (t + tP)/t. Transmissivity can be calculated from the slope m through equation 2. The validity limit of the Theis recovery method u is r2S/4Tt.

bedded in a homogeneous matrix of transmissivity T_2 (*Moench and Hsieh*, 1985; *Butler*, 1990), geometries with three different zones, each one with a different T value shaping as disks (*Butler and Liu*, 1993), or with complicated, but, in any case, prefixed geometries (*Chu and Grader*, 1999). *Schad and Teutsch* (1994) analyzed the support scale of pumping tests by looking at an extensive set of field tests, and thus, being able to characterize an effective heterogeneity length scale. *Meier et al.* (1998) found that the late time behavior of heads, measured by the slope of drawdown versus log time was: (1) the same for all points independent of their relative location with respect to the well, and (2) characterized by the effective transmissivity of the aquifer, thus, making Jacob's method also valid for heterogeneous media. These findings were confirmed analytically by *Sánchez-Vila et al.* (1999) using a small perturbation approach. *Meier et al.* (1999) showed that specific-capacity measurements depend strongly on the local transmissivity next to the well. More recently, *Copty and Findikakis* (2004) and *Neuman et al.* (2004) have focused on the possibility of obtaining the integral scale and the variance of local log-conductivity from a small number of pumping tests in a given aquifer. None of the above results was derived for recovery tests but these results are directly applicable here.

Heterogeneity affects recovery data at all times. Heterogeneity also affects lateral boundaries that can be conceptualized as extreme cases of heterogeneity. There are, as well, certain effects that influence early time data. The most important effects considered here are vertical leakage, wellbore storage, and skin effect. In case of a large amount of available drawdown data, it is possible to analyze these effects in both pumping and recovery tests, and there is extensive literature on this subject (*Streltsova*, 1988; *Bourdet*, 2002). In any case, the point is that they are limited in time. Using the results of *Papadopulus and Cooper* (1967) and *Agarwal et al.* (1970), wellbore storage and skin effect can be ruled out if:

$$t > \frac{S r_s^2}{2.25T}. \tag{2.4}$$

$$t > 10\frac{S_W e^{2\sigma}}{T}. \tag{2.5}$$

where r_S is the radius of the region sampled by the test, S_W is the well storage (water surface area in open wells), and σ is the skin factor. Using rough estimates of S and T, pumping and recovery time can be defined so as to eliminate these perturbations from the ideal case. Oppositely, following Eq. 2.4 for interpreting a given test, the sampling radius, $r_S = 1.5\sqrt{Tt/S}$, can be solved. Depending on the scale of the sampling radius and additional data, the analyst of the pumping test has to judge whether all these early effects can be ruled out and, thus, the remaining data are governed by the underlying heterogeneous T field.

In order to grasp the behavior of recovery tests in aquifers in the field, four selected plots of recovery tests are shown in Fig. 2.2. It is clearly visible that, in most cases, the shapes of the curves are far from that of *Fig*. 1 (that is, far from ideal). First, drawing a single straight line is in most cases difficult. Second, the extrapolation of these straight lines rarely crosses the origin as predicted by the homogeneous theory. Local scale heterogeneity of transmissivity can explain these two effects (variable slope and extrapolation line not passing through the plot origin). Proper accounting for heterogeneity needs to be done in the context of geostatistical

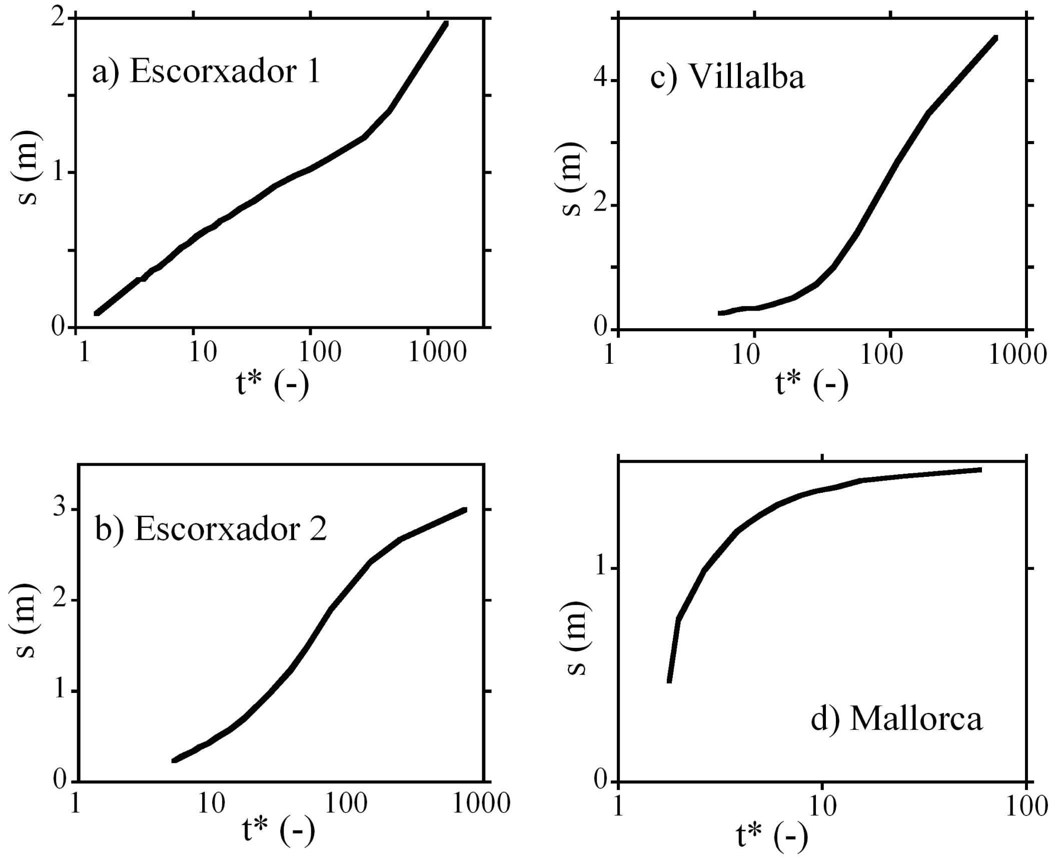

Figure 2.2: Examples of field recovery tests performed within the city of Barcelona, Spain. The Theis recovery plots are plotted as residual drawdown versus dimensionless equivalent time. Escorxador 1 and 2 are tests performed at Park Escorxador, Villalba is a test at Villalba Street and Mallorca is a test at Mallorca Street? Only Fig 2a (Escorxador 1) displays a shape similar to that in a homogeneous aquifer. Notice that even in this test, early time data ($t* > 100$) departs from the ideal condition, reflecting well effects, such as skin, wellbore storage, etc. (negative skin in this case).

inversion. In practice, however, this accounting is only done when several pumping tests and/or several observation wells are available (*Yeh and Liu*, 2000; *Meier et al.*, 2001; *Vesselinov et al.*, 2001). The scope of recovery tests is usually much more limited than when several pumping and observation wells are available. Interpretation of recovery tests is usually done by using the simple homogeneous model. The immediate question arising is what is the meaning of the value obtained using this simple interpretation?

The objective of the chapter described here is to answer the above question and specifically to study if the classical interpretation of recovery tests yields meaningful and useful hydraulic parameter values in heterogeneous aquifers. If yes, as conjectured by extrapolating the results of *Meier et al.* (1998), then the practical question would be how long to pump or to observe recovery in order to obtain meaningful results. To address these issues, numerical simulations are performed first and then the results to the tests of Fig. 2.2 are applied.

2.2 Methodology for the numerical simulations

The methodology is adapted from that of *Meier et al.* (1998). The methodology can be summarized into four basic steps: (1) generation of heterogeneous transmissivity fields; (2) numerical simulation of recovery tests within these fields; (3) interpretation and (4) comparison of interpretation results with hydraulic parameters representative of the original transmissivity field. These steps are discussed below.

2.2.1 Transmissivity fields

The problem domain is identical for all transmissivity fields. The domain consists of a 256 x 256 zone of interest. An inner disc of radius 20 around the pumping well is also defined to specify heterogeneity patterns. Four different heterogeneous transmissivity fields (F1 - F4) were generated (see Fig. 2.3a). F1 and F2 are deterministic with $T = T_{loc}$ for all elements located within the inner disc, and a different value, $T = T_{reg}$, outside of the disc. In field F1, T_{loc} is one order of magnitude lower than T_{reg}, whereas the opposite holds for F2. F3 and F4 are defined as individual realizations of a random stationary field with a spherical covariance function with a correlation length, λ, of 20 and a variance of 1 in terms of ln T. Both fields are conditional to the T value around the well, T_{loc}, which is one order of magnitude lower (F3) or larger (F4) than the effective large scale transmissivity, T_{reg}. The random ln T fields were generated using the Gaussian random simulator GCOSIM3D (*Gómez-Hernández and Journel*, 1993). The correlation length was chosen equal to the radius of the disc in F1 and F2 for later comparison. Notice that only two realizations are used. The underlying idea is not to follow a Monte Carlo procedure, but to generate individual realizations to see whether information could be obtained about recovery tests in a given aquifer.

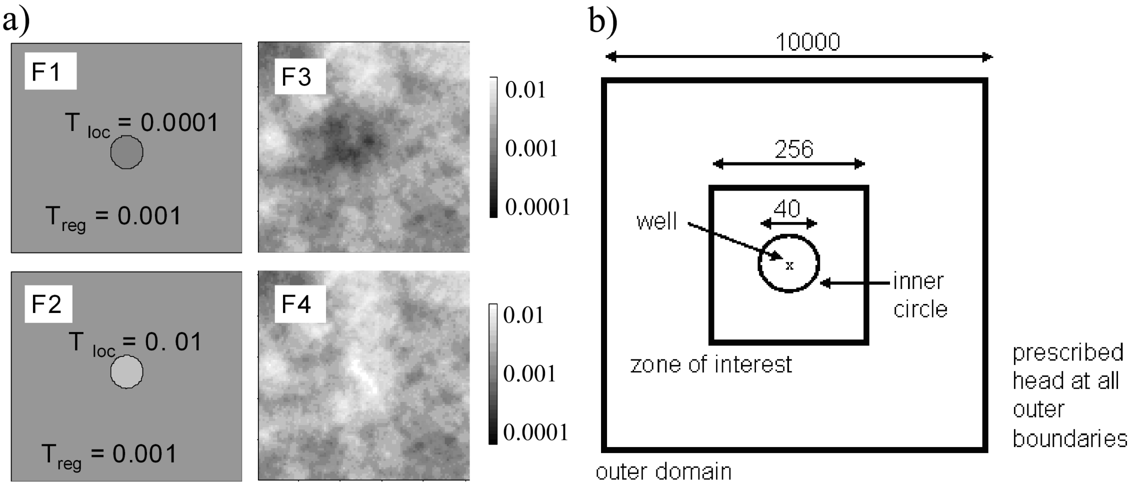

Figure 2.3: a) Transmissivity fields F1 through F4. F1 and F2 show a disc around the well with T one order of magnitude lower (F1) or higher (F2) than the regional value. F3 and F4 are simulated heterogeneous T fields conditioned at the well location to a value one order of magnitude higher (F3) or lower (F4) with respect to the geometric mean of the T point values. b) Set-up of the numerical simulations. The fields in a) correspond to the zone of interest. In the outer domain, the grid becomes increasingly coarse towards the boundary, whereas it is refined at the well. Plot b) is not to scale. The characteristic length, Lc, is 20, equal to the radius of the inner disc in fields F1 and F2 and equal to the correlation length in fields F3 and F4. All numbers are unit length.

2.2.2 Simulation of recovery tests

Pumping and recovery was simulated using the finite-element flow modeling code FAITH (*Sánchez-Vila et al.*, 1993). The zone of interest (Fig. 2.3b) consists of a grid containing 256 x 256 heterogeneous regular square cells. The boundary conditions applied to this ideal grid are, first, zero drawdown at the outer boundaries and, second, a constant pumping rate prescribed at the well (located in the center of the grid). The pumping rate is set to zero after pumping stops. These boundary conditions allow a total drawdown recovery for very large times.

The grid is modified in order to avoid boundary effects (Fig. 2.3b). First, the grid is enlarged outside zone of interest to ensure that the outer boundary is far enough and does not affect the results. In this outer domain, T is homogeneous and set to value outside the disc (T_{reg}) in the case of F1 and F2 and to the geometric mean (T_{reg}) in F3 and F4. Second, the grid was refined around the well to improve simulation accuracy. The level of refinement was verified by comparison with the analytical solution for a homogeneous medium (for $u < 0.01$). This refinement does not affect the regular shape of the transmissivity fields generated. The same approach was shown by (*Meier et al.*, 1998) to provide drawdown results that are not affected by boundary conditions.

One of the objectives is to obtain insight into the recommended pumping duration. Therefore, three tests durations were simulated for each field: A short- term test with a dimensionless pumping time t_{PD}= 0.1, an intermediate-term test with $t_{PD} = 1$, and a long-term test witht_{PD}= 10. Here, t$_{PD}$ is defined as in Eq. 1b, using the disc radius (F1 and F2) or the correlation length (F3 and F4) as characteristic length, L_c, and as the transmissivity value the (constant) T_{loc}. Because T_{loc} is either 10 T_{reg} (F1 and F3) or $0.1T_{reg}$ (F2 and F4), actual pumping is different for each field: (1) t_{PD}= 0.1 corresponding to a local (short) test with a very small radius of influence, so that the perturbation in terms of drawdown has barely reached the limit of the inner disc or the correlation length. Therefore, the support volume sampled by the test during pumping is a small area around the well; (2) $t_{PD} = 1$, an intermediate test where pumping lasts long enough to bring the drawdown signal to a distance comparable to the characteristic length, L_c; and (3) $t_{PD} = 10$, a very long test that samples areas well beyond the characteristic distance, thus, affecting the area corresponding to$T = T_{reg}$. In all cases, the recovery time was set to five times the pumping time. Notice that measurements in field tests are seldom performed after elapsed time of one to two times the pumping time. Usually, the recovery time is often shorter (a fraction of the pumping time).

2.2.3 Analysis of the simulated tests

A number of methods are available for interpretation of recovery tests. Possibly, diagnostic plots (displaying the derivative of residual drawdown with respect to log $t_{DP}/t*$) are the most informative method. A large body of literature is available in the oil industry, where recovery tests are termed "shut-in" tests, about ideal features that can be identified with diagnostic plots. Unfortunately, diagnostic plots require pumping rates to be well monitored. Moreover, existing tools are better suited for analyzing early time behavior. For the study of large scale effects, the variations of the Theis recovery method described below were applied.

The interpretation consists of three steps. First, dimensionless drawdown is plotted against the logarithm of the equivalent time ($t*$). Second, two different slopes are defined at any given time. Slope m_1, which is defined as the tangent of the residual drawdown data, that is its derivative with respect to $t* = (t + t_P)/t$ (Fig. 2.4) is considered here. This slope is computed by using moving windows in order to avoid numerical artifacts. A second slope, $m_{2,}$ is defined as that corresponding to the secant that joins any given point of the semi-log plot with the origin $(s = 0, t^* = 1)$. Third, slopes are converted into normalized estimates of transmissivities $T^* = T/T_{loc}$by means of

$$T^*_{m1} = 0.183\frac{Q}{T_{loc}m_1} \tag{2.6}$$

$$T^*_{m2} = 0.183\frac{Q}{T_{loc}m_2} \tag{2.7}$$

which are simple extensions of equation (2.3) but normalized by the well (local) T value. Note that in the case of a homogeneous medium (Fig. 2.1), $T^*_{m1} = T^*_{m2} = 1$ should be obtained in the range of validity of the method. Notice also that $T^*_{loc} = 1$ for all fields but $T^*_{reg} = 10$ in fields F1 and F3, whereas $T^*_{reg} = 0.1$in fields F2 and F4.

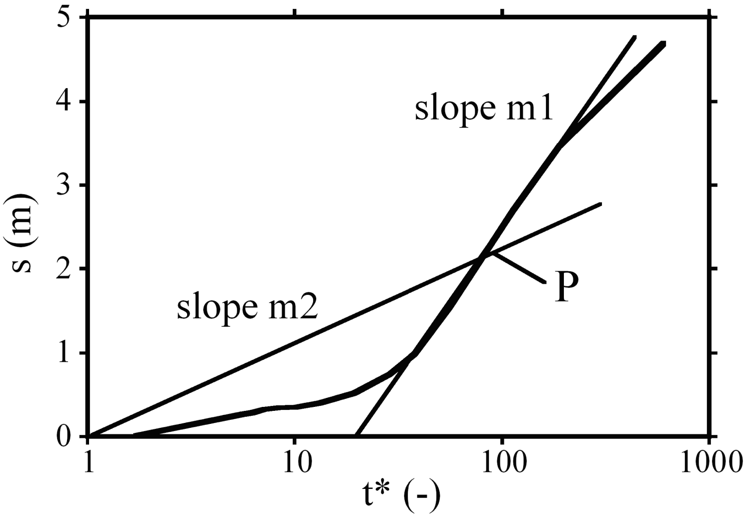

Figure 2.4: Two different calculations of slope m in a heterogeneous aquifer at the example test site Villalba. At any point P, the slope can be calculated as that of the tangent (m1) or as that of the secant, the line between the origin and P (m2). Note that m1 and m2 should be identical for late time data in an ideal homogeneous aquifer.

2.3 Discussion of results

Results are presented in terms of both residual dimensionless drawdown and equivalent transmissivities versus equivalent time for all fields and pumping durations.

The short-term test with t_{PD}= 0.1 in Field F1 (T^*_{reg}= T_{reg}/T_{loc} = 10) looks basically like the homogeneous case (Fig. 2.5a). The resulting late time straight line crosses the axes close to the origin of the semi-log plot, as would happen in a homogeneous field. Furthermore, the estimated transmissivity is very close to the local value. Only for very long times (several times the pumping period) would a deviation from this behavior be found. Therefore, the estimated transmissivity value would increase with recovery time. In short, it would not be possible to resolve (find) the regional value with such a short test. The reason is that in such a short pumping time the signal has barely gone beyond the inner circle and the test behaves mostly as if performed in a homogeneous medium.

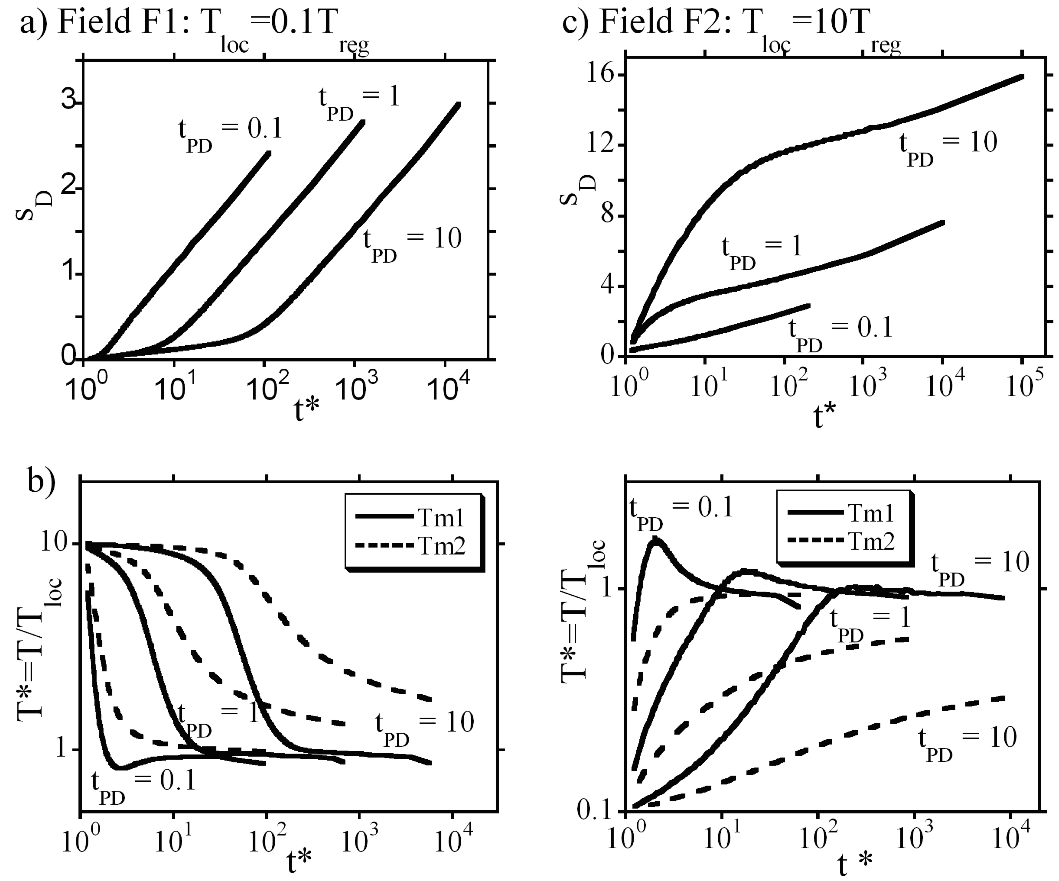

Figure 2.5: Numerical results for fields F1 and F2. (a) Dimensionless drawdown for 3 different pumping durations for F1, and (b) corresponding estimated transmissivities (T* = T/Tloc) derived from either (4) or (5). (c) Dimensionless drawdown for three different pumping durations for F2, and (d) corresponding estimated transmissivities. Shown are only the portions of the curves meeting the condition of validity of the Theis recovery method (u ¡ 0.01).

With a longer test, $t_{PD} = 1$, drawdown at the well is affected by the transmissivity beyond the inner circle. Estimated transmissivities obtained from T^*_{m1} at early times are close to $T*_{loc}$ (equal to 1). As time increases ($t*$ tends to 1), transmissivity tends to $T^*_{reg}.T^*_{m2}$; on the other hand, transmissivity always lies between T^*_{loc} and T^*_{reg}, converging to T^*_{reg} only for long recovery times. Extrapolating the early time data crosses the time axis at $t* > 1$. Similar results, but even more pronounced, can be seen for $t_{PD} = 10$ (Fig. 2.5a). The extrapolation of early time data crosses the equivalent time axis at an even higher value than for the case t_{PD}= 1 and the one for late time data crosses exactly $t* = 1$. For these latter two cases, $t_{PD} = 1$ and 10, a very short recovery test would lose all the relevant potential information regarding T_{reg}. Further, in both cases, $T^*_{m2}$is at all points between T^*_{loc} andT^*_{reg} and larger thanT^*_{m1}.

In field F2, T^*_{reg} is 0.1. The short-term test (t_{PD}= 0.1) is essentially identical to the corresponding test with T^*_{reg}= 10 (difference between Figs. 2.5a, c for $t_{PD} = 0.1$ are limited to changes in vertical scales, except for very late recovery, i.e. small t*). T_{loc} is well resolved and the extrapolation of the data passes through the origin (zero drawdown at infinite time). This test again behaves like a test performed in a homogeneous medium as the heads are insensitive to the T_{reg} value. The intermediate test, t_{PD}= 1 (see Fig. 2.5a, d), displays a behavior very different from the corresponding test in field F1. T_{loc} is well defined from the short-time data. However, T^*_{m1}tends to the regional value, but it does not stabilize as in the F1 case. This difference can be attributed to the fact that T_{reg} is now smaller than T_{loc}. As a result, drawdowns progress slowly beyond the inner circle. Therefore, only a relatively small area of T_{reg} is actually sampled. The extrapolation of the slope corresponding to early time data would cross the zero drawdown line at $t* < 1$. In the homogeneous interpretation of a field test, this extrapolation is usually interpreted as if the original water level were never to be recovered. If the recovery is observed for very long times, the line bends, and the slope of the late time data would really cross the y-axis at a value close to 1. This result is again a reason for extending the recovery time as much as possible. These effects are similar but more pronounced in the case of $t_{PD} = 10$ (Fig. 2.5) with both T^*_{loc} and T^*_{reg} resolved visibly by T^*_{m1}. Again, the extrapolation of the early time slope leads to a crossing point well beyond $t*$= 1. The late time slope crosses exactly through the origin. T^*_{m2}lies, in all the cases, between T^*_{loc} and T^*_{reg}, but converges to T^*_{reg} faster than T^*_{m1}. This implies that T^*_{m2}can be used as an estimate for the not resolved T^*_{reg} when recovery is short. When applying equation (2.4) to the turning points in the semi-log plots for fields F1 and F2, values of $r = 14$ and 25, respectively, are obtained. As the real distance is 20, this value shows that equation (2.4) does indeed lead to a rough estimate of heterogeneity scale.

Transition from T_{loc} to T_{reg} estimated from T_{m1} is preceded by a small trough when $T_{loc} < T_{reg}$ (Fig. 2.5b) and by a small peak when $T_{reg} > T_{loc}$ (Fig. 2.5d). These results are caused by the change in transmissivity (they occur for $t_{DP} \approx 0.1$, regardless of the pumping duration) that causes recovery initially to speed up (when $T_{reg} < T_{loc}$, Fig. 2.5d). The effect is similar to double porosity, linear flow, or boundary effects.

Fields F1 and F2 can be viewed as a simplistic representation of realistic heterogeneous media. Field sites will rarely display a single geometric feature separating local and regional T values. The spatial distribution of T values will not be radially symmetric. Recovery tests in fields F3 and F4 (Fig. 2.6) display some similarities to those in F1 and F2, but there are a number of distinct differences. For the shortest test ($t_{PD} = 0.1$), only the local value can be well resolved in both fields, even though T^*_{m2} is slightly bent towards the regional value (recall that now T_{reg} is the effective transmissivity, the geometric mean of point values). Notice that the local value corresponds here to the one used for conditioning the fields. Because the correlation length is large compared to the cell size, this local value would correspond also to some integrated value of the local T values around the well.

Results from the intermediate test ($t_{PD} = 1$) in fields F3 and F4 are similar to those of the short-term test, but late time data provide an improved estimation of the regional value with respect to the shortest test. However, the behavior of the two fields is qualitatively different in that both T^*_{m1} and T^*_{m2} identify regional transmissivity much better in field F4 (high T_{loc}, Fig. 2.6d) than in F3 (low T_{loc}, Fig. 2.6c). It is clear that the low T zone is "screening" the high T regional value in field F3. Contrarily, T_{reg} becomes well defined if the pumping duration is long enough (see *Fig6.* for $t_{PD} = 10$) when T_{loc} is small. In order to register a sharp definition of T_{reg} when it is smaller than T_{loc}, a larger t_{PD} value is required. The results corresponding to $t_{PD} = 100$, also shown in Fig. 2.6, also confirms this requirement.

In summary, T_{m1} provides good estimates of T_{loc} with early time data and eventually tends to T_{reg} if both pumping time and recovery durations are long enough.$T_{m2,}$ on the other hand, helps

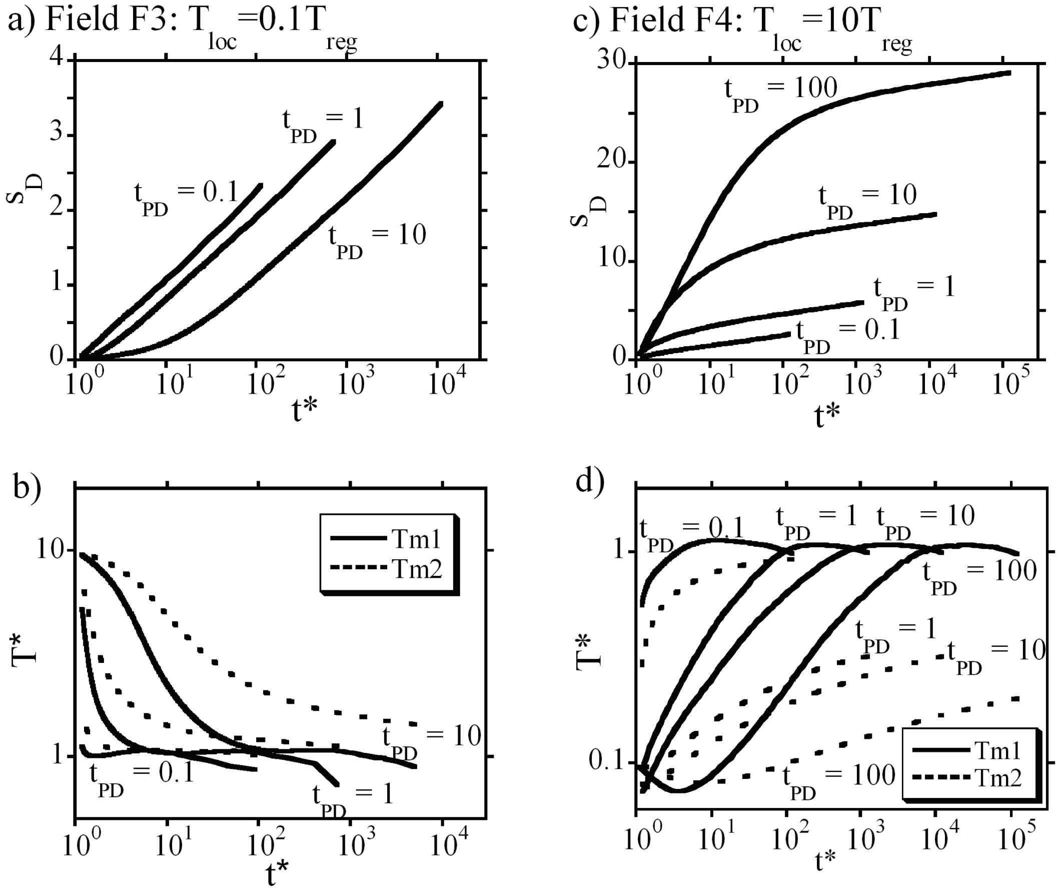

Figure 2.6: Numerical results for fields F3 and F4. (a) Dimensionless drawdown for 3 different pumping durations for F3, and (b) corresponding estimated transmissivities. (c) Dimensionless drawdown for three different pumping durations for F4 with additional pumping time $t_PD = 100$, and (d) corresponding estimated transmissivities. Shown are only the portions of the curves meeting the condition of validity of the Theis recovery method ($u < 0.01$).

identifying departure from ideality, as it consistently lies between T_{loc} and T_{reg}. At late times, both values converge for sufficiently long pumping and recovery times.

2.4 A reinterpretation of the field tests

In this section, the above results are used to discuss the interpretation of the field tests shown in Fig. 2.2. Curves of estimated transmissivity versus equivalent time resulting from equations (2.6) and (2.7) are shown in Fig. 2.7. The only difference with respect to the numerical simulations from synthetic fields presented in Fig. 2.5 and Fig. 2.6 is that now the values of T_{m1} and T_{m2} shown are dimensional, because the local value of T at the well is not known.

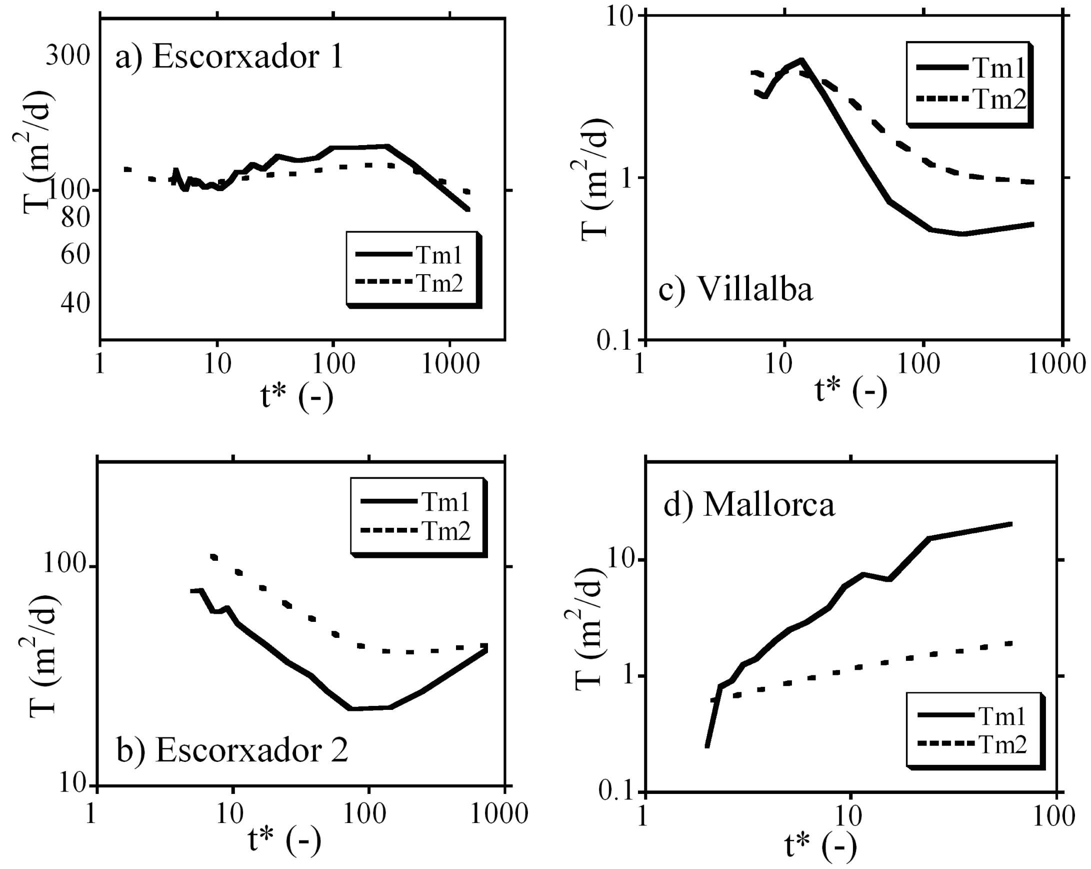

Figure 2.7: Reinterpretation of the field test data presented in Fig. 2.2. The tests results are plotted as transmissivities versus equivalent time. Tm1 and Tm2 are defined in equations 4 and 5 but not normalized by T_{loc} as it is not known. In Fig. 2.7 a T_{m1} and T_{m2} are basically the same but in Fig. 2.7b-d they differ particularly for early times.

2.4.1 Tests at Park Escorxador

Two long-term recovery tests ($t_p = 12h$, constant rate) were performed at different times at two wells located 74 m apart (Fig. 2.2 a, b). The shapes of the recovery curves are appreciably different. Whereas test 1 follows a straight line for $t* < 300$ and looks like the expected result for a homogeneous aquifer, the same is not true for test 2, where the slope increases with time (decreases with $t*$) without reaching a plateau. Despite these differences, very similar late time transmissivity estimates were determined from both tests. These estimates are consistent with$T$ values derived from long-term pumping tests (**?**). Early time data lead to a difference in estimated transmissivities, T_{loc}, of about one order of magnitude between the two tests. From the methodology already explained, skin effect and effect of wellbore storage can be out- ruled. This result would mean that well 2 is located in an area less conductive than well 1, which is consistent with the fact that observed drawdowns are larger in well 2.

2.4.2 Test at Villalba Street

Recovery data of test Villalba ($t_p = 9$ h, constant rate) are displayed in Fig. 2.2c. As for the Escorxador 2 test, the shape of the curve does not display a homogeneous behavior. Using equations (2.4) and (2.5), skin effect and wellbore storage can be neglected. The apparent transmissivity as a function of time is plotted in Fig. 2.7c. From the plot, it can be conclude that T_{reg} is larger than T_{loc}. In this test, an external confirmation of the estimation of T_{reg} is confirmed as it is very close to the value calibrated in a regional groundwater model of the area (**?**).

2.4.3 Test at Mallorca Street

The short recovery test ($t_p = 0.32$ h, constant rate) in Fig. 2.2d displays clearly two different slopes. The corresponding estimated transmissivities in Fig. 2.7d suggest an increase from T_{loc} to T_{reg} of almost two orders of magnitude. The check with equation (2.4) renders a sampling radius, r_s, of around 10 cm for the time where the change in slope takes place. This result clearly indicates that both the pumping and recovery times were too short. The different T_{loc} is most likely caused by skin effect or wellbore storage. This result was confirmed by interpreting the test using an automatic fitting tool (*Ondiviela et al.*, 2001) that provides about the same result for T as our estimated value T_{loc} and a very high skin factor.

2.5 Conclusions and recommendations

Interpretation of recovery tests using the simple Theis recovery method can provide valuable information about representative parameters in heterogeneous aquifers, even though the method was developed for homogeneous media. Actually, it may be possible to discriminate between at least two representative transmissivity values, corresponding to the local T values (T_{loc}) surrounding the well, and some regional representative value (T_{reg}). The analysis presented here implies that the rate of early time recovery is informative of T_{loc}, whereas that of late time data yields information about T_{reg}. This result is valid as long as early time effects can be filtered out. The latter was shown for pumping tests by Butler (1988) for a radially symmetric structure and then confirmed by (*Meier et al.*, 1998) for general heterogeneity. The results presented here have several practical implications about the design and interpretation.

Regarding test design the following recommendations are advisable:

1. Pumping duration. Pumping duration should be chosen depending on the scale, L_c, to be characterized. At the very least, t_p should equal SL_c^2/T, where S and T are local estimates of storativity and transmissivity, respectively. Preferably, pumping durations should be much longer, for example, 10 SL_c^2/T, especially if T_{reg} is expected to be smaller than T.

2. Recovery period. The design should allow for a long recovery period, not shorter than twice the pumping duration, and, if possible, much longer than twice the duration. Notice that this increase in time can be achieved at very low cost because time scale is logarithmic and only a few

measurements have to be added. Because drawdowns become small for late time recovery, the reliability of these drawdowns needs to be assessed by comparing them to measurement errors.

3. Pumping rate. Late time residual drawdown is sensitive to total volume of water pumped, V_W, as $s \sim V_W/4\pi T t$ (that is, it does not depend on the time evolution of pumping rate). Average pumping rate, V_W/t_P, should be designed for a sizable value of s. Recovery tests are not highly sensitive to high frequency changes in flow rate, but early time recovery is sensitive. Still, using V_W/t_P may become the only realistic option when pumping rate cannot be controlled.

4. Natural head trends. Heads should be monitored prior to the test so as to ensure either that they have stabilized prior to pumping or that a natural trend can be fitted. It should be noticed that much information is contained in late time residual drawdowns that are small. Residual drawdowns are equal to the difference between heads during recovery, which can be measured accurately, and natural heads. Efforts should be made to estimate the latter natural heads as accurately as possible. These efforts include not only prior stabilization, but also monitoring boreholes unaffected by the test. Mistaken natural head evolution would lead to wrong T_{reg} estimation.

Regarding the interpretation the following recommendations are advisable:

1. At any given time the head recovery plot can yield two slopes: m_1, tangent, and m_2, secant though the origin. Using them, T_{m1} and T_{m2} can be calculated.

2. When both pumping and recovery times are large it is possible to obtain good estimates of both T_{loc} and T_{reg}. Better estimations are obtained when the local value at the well is smaller than the regional T value, provided that sizable pumping rates can be sustained.

3. T_{loc} is better represented by T_{m1}. Early time effects (for example, skin effect) should be ruled out by calculating the corresponding sampling radius. A small radius indicates that these effects are still relevant and mask T_{loc} that cannot be estimated.

4. If pumping duration and recovery are long enough, late time T_{m1} and T_{m2} will tend to T_{reg}.

The advantage of using T_{m2} is that it converges to the large scale value much faster than T_{m1}. If recovery is too short to resolve T_{reg} ($T_{m1} \neq T_{m2}$), T_{m2} can be used to approximate T_{reg}. The resulting value should be suspected. T_{m2} lies between T_{loc} and T_{reg}. Therefore, T_{reg} will be larger than T_{m2} if T_{loc} is small, and vice versa.

These recommendations are valid for the interpretation of recovery in the pumping well. Recovery in observation wells renders usually only an intermediate value of transmissivity as early time responses are delayed and late time responses are usually not resolved as well. This lack of resolution results in that total drawdown is smaller at an observation well and measurement errors become more important.

Chapter 3

Relationship between aquifer parameters and parameters of memory functions controlling transport models*

3.1 Introduction

Contaminant transport has been traditionally modeled using the advection dispersion equation (ADE). Yet, transport in natural aquifers usually displays anomalous (i.e., inconsistent with the ADE) behavior. Observed deviations are numerous (*Carrera*, 1993). They include scale dependence of dispersivity (e.g., *Lallemand-Barres and Peaudecerf*, 1978; *Neuman*, 1990), directional and time dependence of apparent porosity (*Sánchez-Vila and Carrera*, 1997; *Guimerà and Carrera*, 2000) and tailing of breakthrough curves (e.g., *Valocchi*, 1985; *Freyberg*, 1986; *Cortis and Berkowitz*, 2004). Stochastic hydrology has succeeded in qualitatively explaining these deviations

---

*This chapter is based in the article: Willmann, M., J. Carrera, and X. Sánchez-Vila, 2008, Transport upscaling in heterogeneous aquifers: What physical parameters control memory functions?, *Water Resour. Res.*, doi:10.1029/2007WR006531, in press.

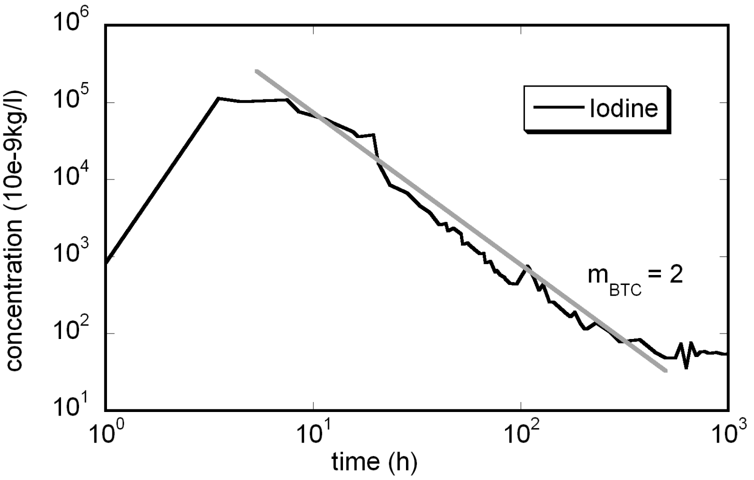

Figure 3.1: Breakthrough curve of iodine measured at the EL Cabril site (UPC, 1990). A power-law tail is observed with a slope of 2.0 (indicated as a grey line). The power-law behavior spans over 1.5 orders of magnitude until the background concentration was reached. This curve cannot be reproduced by using a homogeneous ADE. Mass transfer models using a memory function can reproduce this behavior. But the causes of the tailing need to be properly understood in order to use such memory function for predictions under different flow conditions or transport distances.

and in quantifying the scale dependence of dispersivity, (e.g., *Dagan*, 1989; *Gelhar*, 1993). In the process, tools have been developed to predict the evolution of dispersivity with scale given a stochastic description of variability of hydraulic conductivity (*Kitanidis*, 1988; *Dentz et al.*, 2000). However, much less efforts have been devoted to understanding the causes of tailing (*Haggerty et al.*, 2000; *Shapiro*, 2001; *Cortis and Berkowitz*, 2004; *Dentz et al.*, 2004).

Tailing is defined as the markedly asymmetric shape of breakthrough curves (BTCs), which cannot be reproduced by the homogeneous medium ADE. Field BTCs typically display a sharp rising limb for the early arrival but a slowly decaying limb at late time (Fig.3.1). More important, the decay limb often displays a power law behavior. That is, late-time concentrations decay as $t^{-m_{BTC}}$, so that they plot as a straight line on a log-log scale (*Farrell and Reinhard*, 1994; *Hadermann and Heer*, 1996; *Werth et al.*, 1997; *Becker and Shapiro*, 2000; *Shapiro*, 2001; *Meigs and Beauheim*, 2001).

A proper description of this ”late time” behavior is important not only for practical reasons (i.e., time for clean-up below a threshold or reactive transport modeling), but also because the apparent ubiquity of power-law decay suggests it must reflect something of a fundamental nature.

Different mechanisms are known to cause tailing. These include heterogeneity of permeability, diffusion or chemical heterogeneity. Tailing was initially attributed to matrix diffusion and/or sorption kinetics (*Neretnieks et al.*, 1982; *Neretnieks and Rasmuson*, 1984). In fact, the 1.5 slope usually observed in fractured media was soon attributed to diffusion into rock matrix (*Hadermann and Heer*, 1996). Actually, different slopes can be obtained by acknowledging that low permeability blocks exhibit a distribution of sizes and diffusion coefficients. As a result, the memory function of diffusion dominated mass transfer is predictable (*Rasmuson and Neretnieks*, 1986; *Zhang et al.*, 2007; *Gouze et al.*, 2008b). However, here we concentrate on the role of hydraulic heterogeneity. Heterogeneity of permeability leads to conductive paths that carry most of the water and arrive early (hence the sharp rising limb of BTCs) and less conductive paths that trail behind and cause tailing. This is referred to as ”slow advection”.

Becker and Shapiro (2000, 2003) performed field tracer tests such that they could neglect other causes for tailing. They found power-law slopes $m_{BTC} = 2$ caused by slow advection. *Di Donato et al.* (2003) modeled slow advection in a heterogeneous system using the streamline method. They found a slope for 2.2. *Zhang et al.* (2007) modeled a heterogeneous 3D sedimentary aquifers where the dominant process in the low conductive zones was diffusion. They found a power-law tail of about 2. Most interestingly, *Gouze et al.* (2008a) and *Shapiro et al.* (2008) found for field tracer tests slopes between 2 and 2.2 at intermediate times and 1.5 at very late time.

A number methods have been proposed to describe tailing. Multi-Rate Mass Transfer (MRMT) (*Haggerty and Gorelick*, 1995; *Wang et al.*, 2005) and memory functions (*Carrera et al.*, 1998), which are equivalent (*Haggerty et al.*, 2000), can be viewed as dividing the medium into overlapping mobile and immobile continua (hence the generic term multi-continuum models). Each immobile zone exchanges solute mass with the mobile zone by linear mass transfer (i.e., mass exchange is proportional to concentration gradient). These models may be expressed as a function of only the mobile concentration by introducing a memory term into the ADE to account for mass transfer between mobile and immobile zones. The name ”memory” reflects the fact that this term represents how current mobile concentrations are affected by past events. Multi-continuum models have been successfully applied to interpret anomalous transport (*McKenna et al.*, 2001; *Haggerty et al.*, 2004; *Zinn et al.*, 2004; *Medina and Carrera*, 1996; *Sánchez-Vila and Carrera*, 2004; *Zhang et al.*, 2007). While these models were originally developed to represent diffusion into immobile regions, they can also be used to reproduce the effect of slow advection.

The most widely used method for representing tailing is the Continuous Time Random Walk Method (CTRW) (*Berkowitz and Scher*, 1998; *Dentz et al.*, 2004). CTRW can be viewed as a generalization of Random Walk methods in that not only spatial displacements, but also time step lengths are random variables (*Berkowitz et al.*, 2006, Section 7.1). The effective transport equation results from ensemble averaging the transport of individual particles. As it turns out, CTRW is broader in scope than multi-continuum representations, which can be viewed as a particular case of CTRW (*Dentz and Berkowitz*, 2003). However, the most commonly adopted form of CTRW is equivalent to the memory function approach and the corresponding memory functions can be derived from each other. CTRW has been successful not only in reproducing field BTCs, but also in reproducing appropriate scaling behavior. That is, CTRW models calibrated against BTCs measured at one scale have been successful in predicting BTCs at different scales (*Berkowitz and Scher*, 1998; *Kosakowski et al.*, 2001; *Levy et al.*, 2003; *Cortis and Berkowitz*, 2004; *Le Borgne and Gouze*, 2008). CTRW models have also accurately reproduced the outcome of pore network models, reproducing the dependence of dispersion on molecular diffusion (*Bijeljic and Blunt*, 2006).

A further method to describe tailing are the fractional order advection-dispersion equations (fADE) (*Benson et al.*, 2000). As with CTRW, the model is rather general, but can also be characterized by a power law memory function when only the time derivative term in the ADE is fractional. *Berkowitz et al.* (2006) showed that, in such case, fADE can be considered as a limiting case of CTRW.

In summary, multi-continuum models, CTRW and fADE, all sharing a time non-locality, must be considered as excellent representations of transport in natural media. Moreover, they allow discriminating between mixing and spreading. Mixing controls many chemical reactions (e.g., *De Simoni et al.*, 2005, 2007; *Cirpka and Valocchi*, 2007). Therefore, a proper representation of mixing is a prerequisite for proper reactive transport modeling. Yet, the ADE (and all formulations that base dispersion solely on the spreading of plumes) equate dispersion and mixing (thus overestimating mixing and mixing-driven reactions). Non-local in time formulations separate these two processes. Therefore, they shed some hope on the possibility of predicting reactive transport accurately.

Despite the above nice properties, non local formulations have been subject to criticism (*Neuman and Tartakovsky*, 2008). All these formulations require specifying some (arbitrary) memory function. At present, memory functions are calibrated against tracer test data, without explicit reference to heterogeneity. This is unsatisfactory both from conceptual and practical viewpoints. Conceptually, it is generally agreed that tailing can be caused by heterogeneity. In fact, *Berkowitz and Scher* (1997, 1998); *Berkowitz et al.* (2008) suggest deriving the memory function from the velocity pdf. However, *Le Borgne et al.* (2008a,b) point out that velocity correlation along a stream tube (Lagrangian correlation) may be a key factor. Since there is no way to obtain the full statistical characterization of the velocity field, other than numerical simulation, it is clear that no explicit link is available between memory function parameters and measurable properties of the heterogeneity in hydraulic conductivity. This casts a shadow of doubt on the predictive capabilities of non-local formulations for scales dramatically different than those for which they were calibrated. There are also practical implications. Tracer tests cannot be performed on the long scales often needed for transport predictions. Certainly, using non-local formulations for reactive transport requires ascertaining the conditions under which they are valid. On the other hand, stochastic approaches offer no clear alternative. In fact they are criticized because, with rare exceptions (e.g., *Di Donato et al.*, 2003; *Alcolea et al.*, 2008; *Luo et al.*, 2008), they usually fail to reproduce the kind of tailing observed in the field.

Accepting that spatial variability of hydraulic conductivity is a frequent cause of tailing, the objective of this paper is twofold. First, we explore some conditions under which heterogeneity can explain the kind of tailing observed in tracer tests, namely power law decay. Second, we investigate the relationship between certain field properties describing heterogeneity and the parameters describing the memory function.

3.2 Background

We conceptualize solute transport by assuming a superposition of a (homogeneous) mobile zone and an infinite number of immobile zones. Mass is exchanged between the mobile and the immobile ones by diffusion-like processes. This results in the following transport equation:

$$\phi_m \frac{\partial c}{\partial t} = \nabla \cdot (\mathbf{D}\nabla c) - \mathbf{q} \cdot \nabla c - \Gamma \tag{3.1}$$

where c is solute concentration in the mobile zone, $\mathbf{D}$ is the dispersion tensor, ϕ_m is the mobile porosity and Γ is the source/sink term controlling the mass transfer between the mobile and a continuum of immobile zones. In the case of a discrete description with a finite number of immobile zones Γ can be expressed in terms of immobile concentrations resulting in a system of $n + 1$ equations for n immobile zones. *Carrera et al.* (1998) showed that Γ can be expressed in terms of mobile concentration by using a convolution product noted by (*) with a memory function g:

$$\Gamma = \phi_{im} g * \frac{\partial c}{\partial t} \tag{3.2}$$

$$g(t) = \sum_{n=1}^{N} \alpha_n b_n e^{-\alpha_n t} \tag{3.3}$$

$$\sum_{n=1}^{N} b_n = 1 \tag{3.4}$$

where N is the number of immobile zones, α_n are first order rate coefficients and b_n is the fraction of total immobile porosity characterized by α_n (inverse of the characteristic time of zone n). Note, that the memory function (Eq. 3) is slightly different to the one of previous authors. The constant characteristic diffusion of *Carrera et al.* (1998) is accounted for by α_n. *Haggerty et al.* (2000) define their memory function in terms of the full aquifer, while we prefer to define it in only in terms of immobile zone parameters. Thus our memory function does not depend on mobile porosity. By excluding the immobile porosity our memory function does not depend on the size of the immobile zone, but only on its geometry. In Appendix A we show how Eq. 1-4 can be easily implemented into a standard numerical code. Throughout this paper, we will only refer to conservative transport and 1D transport equation. This implies that we could solve the transport equation in Laplace space and then invert the solution. This would avoid discretization of the memory function. However, our ultimate goal is to apply these results on to reactive transport, which is simpler in the discrete version of g (Eq. 3).

A memory function can be of irregular shape. But as power-law behavior in BTCs is observed frequently, we use memory functions that display power-law behavior. *Haggerty et al.* (2000) related late time concentrations to the memory function and found that a power-law behavior in a BTC is caused by a power-law behavior of the memory function. Similar findings are reported by *Berkowitz and Scher* (1997, 1998) in the context of CTRW. Therefore, we choose α_n and b_n in Eq. 3 so as to ensure this power law behavior (Fig. 3). A truncated power-law (TPL) seems to represent best anomalous transport because it allows an evolution to Fickian transport (*Dentz et al.*, 2004; *Berkowitz and Scher*, 2008).

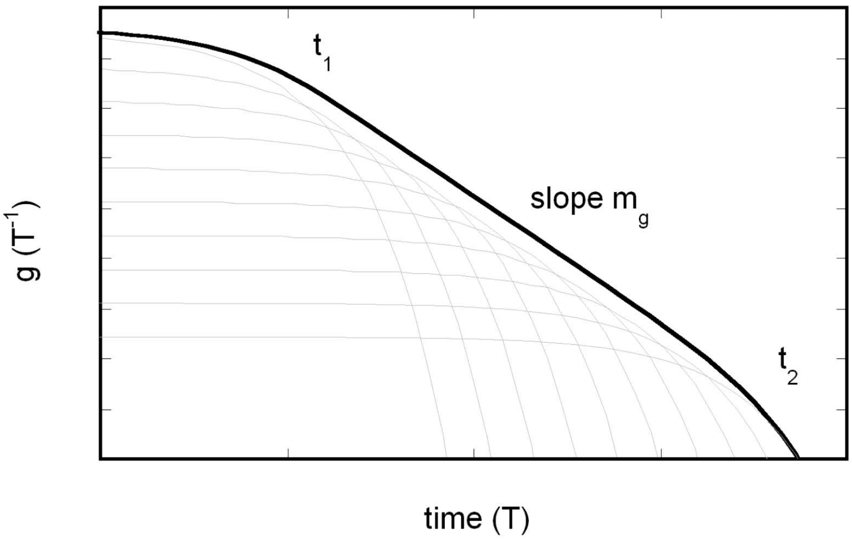

Figure 3.2: Representation of a memory function (black). It can be viewed as the superposition of 10 individual memory functions each corresponding to an immobile zone (grey) (Eq. 3). The memory function exhibits three independent variables: characteristic time t_1 when power-law decay starts, characteristic time t_2 when power-law behavior ends; and the power-law slope, m_g.

This reduces the number independent unknown parameters describing a memory function to three: two characteristic times, power-law behavior initial (t_1) and final (t_2) cut-off times and the power-law slope m_g (Fig. 3.2).

3.3 Methodology

We use a numerical approach based on synthetic aquifer analysis to study the heterogeneous features that control tailing. The methodology consists of 4 major steps: (1) Generation of heterogeneous transmissivity fields, (2) transport simulation on the heterogeneous fields using the ADE at the local scale, (3) analysis of vertically integrated BTCs at selected locations and derivation of a representative memory function, and (4) simulation of transport though a homogeneous medium with the above memory function. All simulations are performed within a domain of 1024 times

512 cells of unit size. Water flow is steady-state, prescribed by constant heads at the left and the right boundaries and no-flow conditions on top and bottom, resulting in mean uniform flow with a mean gradient of 0.0098.

3.3.1 Generation of transmissivity fields

We generate 2D transmissivity fields with different heterogeneity characteristics. First, we need varying heterogeneity scales, as we expect in nature, evolving over a range of scales (*Neuman*, 1990). We also need poorly connected and well connected fields, that is where high transmissivity, T zones extend over long distances. We analyze transport in individual realizations of heterogeneous aquifers, as opposed to a Monte Carlo approach, because we are interested in what happens in a given aquifer rather than in an ensemble. The realizations are generated with the Gaussian Sequential Simulation Method (*Gómez-Hernández and Journel*, 1993). The method uses a single or a combination of variograms, always exponential in this work, to generate simulations conditioned to field data. We used five types of heterogeneous lognormal transmissivity, lnT, fields (Fig. 3.3) with a default variance of 6.

Type 1 fields are unconditioned multi-gaussian fields generated with a correlation length of 20, which is small compared to the domain size (1024). The variance of the lnT fields was set to 2 and 6. The resulting fields display neither multiple scales nor preferential flow paths. Therefore, no anomalous transport behavior is expected for long travel distances, compared to the domain size.

Type 2 fields are obtained with a nested variogram consisting of two exponential variograms, one describing small scale heterogeneity with a correlation length between 8 and 128, and one with a large correlation length between 128 and 1024. The sill of the two different variograms are varied between between 1 and 5, but the total variance always adds up to 6. The resulting fields display two distinct scales of heterogeneity scales but no apparent preferential flow paths.

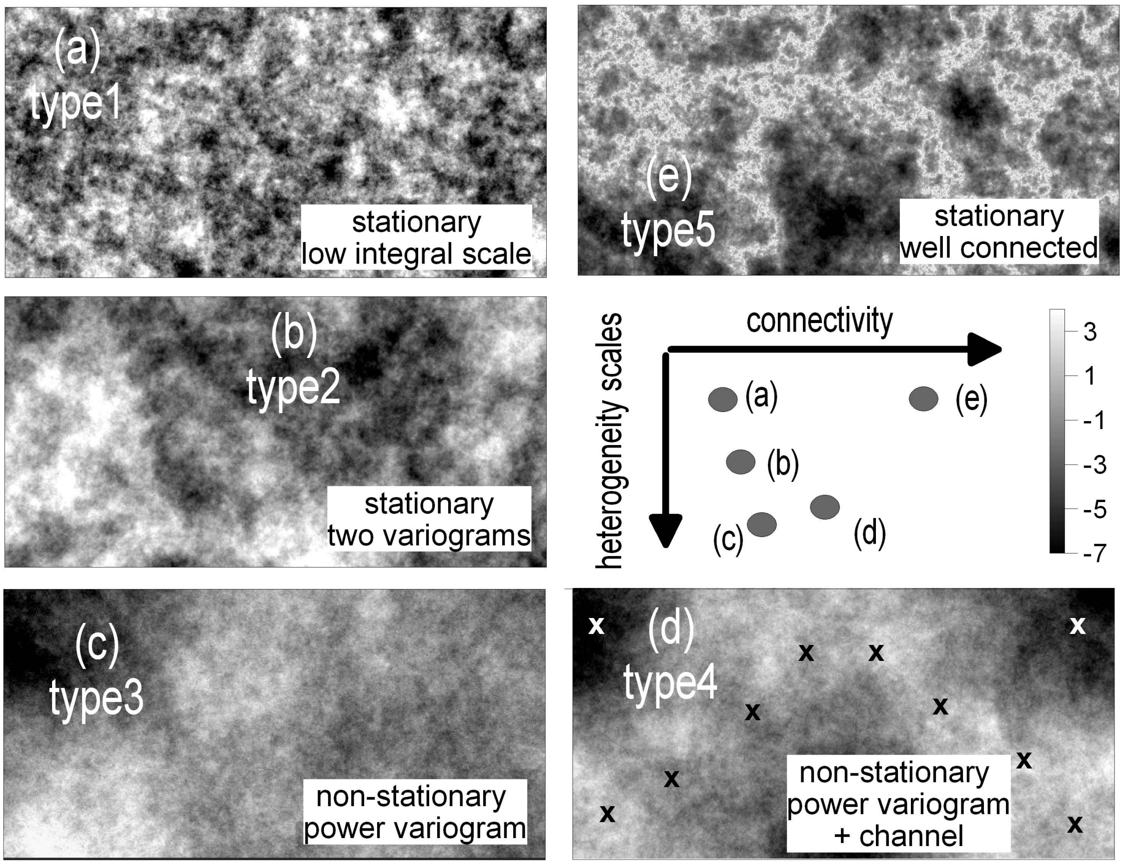
(a)
type1
stationary
low integral scale
(e)
type5
stationary
well connected
(b)
type2
stationary
two variograms
connectivity
heterogeneity scales
(a)
(e)
(b)
(c)
(d)
3
1
-1
-3
-5
-7
(c)
type3
non-stationary
power variogram
(d)
type4
x
non-stationary
power variogram
+ channel

Figure 3.3: Five types of transmissivity fields used in this work. They show different ranges of scales and different degrees of connectivity: (a) multi-gaussian field with a single exponential variogram and a small correlation length; (b) field comprising of two nested variograms with different correlation lengths; (c) power variograms representing a continuous distribution of heterogeneity scales; (d) similar to type 3 but conditioned to leave a preferential flow path (white and black crosses indicate conditioning point with low and high T values respectively; and (e) highly connected fields.

Type 3 heterogeneous fields show an evolving range of scales. We use a power law variogram:

$$\gamma(s) = C_0 s^{2H} \tag{3.5}$$

where s is distance, C_0 is a constant and H is the Hurst coefficient. The power law variogram can be seen as an infinite series of nested variograms (*Neuman and Di Federico*, 2003). We generated fields with H values of either 0.1, 0.25 or 0.4 and scale them for comparison with the other fields to a variance of 6. Such a variogram was postulated by *Neuman* (1990) to account for increasing variance and correlation length of aquifers as their size increases. Whether such a variogram would be still valid at very large scales can be neither profen nor discarded. The fields display a continuous range of heterogeneity scales but the existence of interconnected zones of high T depends on the individual realization.

Type 4 fields are a modification of type 3 fields, where the simulations are now conditioned to 14 points to ensure interconnected zones of high T (Fig. 3.3). These fields still display a continuous range of heterogeneity scales, but also a well defined preferential flow path. Still, the results may be affected by the conditioning process.

The type 5 fields are built with the methodology of *Zinn and Harvey* (2003) to ensure good connectivity. The original multi-gaussian fields display connectivity only for intermediate T values. These are transformed to high T values to enhance hydraulic connectivity. To ensure consistency we use here an exponential variogram with correlation lengths between 20 and 200.

We quantify here connectivity using the indexes of *Knudby and Carrera* (2005):

$$CF = \frac{T_{eq}}{T_G}. \tag{3.6}$$

where T_{eq} is the equivalent transmissivity (i.e., the transmissivity of a homogeneous medium allowing the same flux as the actual heterogeneous medium) and T_G is the geometric mean of point transmissivity values. CF is considered a measure of connectivity because it reflects the increase in flow caused by highly transmissive channels transversing the domain. The transport connectivity index is defined as

$$CT = \frac{t_{peak_{hom}}}{t_{peak_{het}}}. \tag{3.7}$$

where $t_{peak_{het}}$ is the peak arrival time for transport across the heterogeneous field and $t_{peak_{hom}}$ is the peak arrival time for the equivalent homogeneous field. CT is considered a connectivity measure because it reflects the early arrival caused by channels. *Cortis and Knudby* (2006) use a CTRW formulation for representing flow through heterogeneous media. We expect their memory function to contain information on connectivity, but it has not yet been quantified as an index.

Fig. 3.3 displays an schematic plot comparing the 5 types of lnT fields in terms of regional connectivity and scales of heterogeneity. This is a qualitative plot aimed at indicating the features that are explored in each of the realizations.

3.3.2 Fine-scale transport simulations within the heterogeneous fields

Fine scale conservative transport simulations are performed on the heterogeneous fields following the steady-state flow conditions described above. Transport is simulated at the local scale with the ADE using the finite element code FAITH (*Sánchez-Vila et al.*, 1993). Local dispersivities are assumed to be 10 units in longitudinal and 1 unit in transverse direction. To test the effect of local dispersivities, these values are varied for one specific set-up between 0.1 and 10. The porosity is set to 0.3 in all cases. The time step starts with 100, increases up to 5000, and then remains constant until the end of the simulation period. The simulation is stopped when only 10^{-4} % of the initial mass remains in the domain. Breakthrough curves are measured as integrated values at selected sections, perpendicular to the mean flow and at several distances from the source.

The above mentioned assumption (validity of the ADE at the local scale) has been questioned by some authors (e.g., *Berkowitz et al.*, 2006). To test this we add some additional runs with a local scale equation based on the mass transfer scheme presented in Appendix A. We used the same input value as before but add an additional porosity of 0.05 be accessible to mass transfer. To keep the analogy of intragranular diffusion we use $m_g = 0.5$, the value of matrix diffusion. We use different characteristic diffusion times (t_1/t_2) to define three local memory functions: 0.017/17, 0.017/1.7, and 0.17/17 for memory functions 1, 2 and 3 respectively.

Concentration is initially zero throughout the domain. Solute mass input into the system can be expressed either as resident or as flux averaged. Most of the runs were performed by imposing a flux dependent mass of 1 at the left boundary. That is, mass inflow at every node is proportional to the water inflow. The boundary condition was applied during an initial time interval of 1000 which is small compared to the characteristic transport times. After this time interval, the boundary condition is changed to let clean water enter the domain. To test the effect of using initial resident concentration, one test case was performed by evenly distributing the unit mass over the first column.

Integrated breakthrough curves are sampled along transects at several distances. To avoid boundary effects these measurements are taken always at least 24 cells away from the aquifer boundaries. The distinction between resident and flux concentrations (*Kreft and Zuber*, 1978; *Zhang et al.*, 2006) is relevant for our work. While resident concentrations represent the mass within a certain domain (e.g., numerical grid cell) at a certain time, flux concentrations provide the mass passing a cross section during a time interval. Resident concentrations are relevant for chemical reactions (i.e., reactive transport). Flux concentrations are the ones to be used when all mass flowing across a boundary has to be taken into account, which is the case in tracer tests. The relationship between both concentrations is based on the definition of flux concentration at control plains as the vertically averaged solute flux component along the mean flow direction normalized by the vertically averaged fluid flux in mean flow direction:

$$c_f = \frac{\int_0^{Ly} j_x dy}{\int_0^{Ly} q_x dy} \tag{3.8}$$

$$j_x = q_x c_r - D_{xx}\frac{\partial c_r}{\partial x} - D_{xy}\frac{\partial c_r}{\partial y} \tag{3.9}$$

where c_f is the flux concentration, c_r is the resident concentration, j_x is the mass flux in mean flow direction, q_x is the fluid flux in mean flow direction, D_{xx} and D_{xy} are the corresponding components of the dispersion tensor, and Ly is the length of the cross section.

3.3.3 Obtaining memory functions from breakthrough curves

Fig. 3.2 shows the memory function defined in Eq. 3 for 10 immobile zones ($N = 10$). *Haggerty et al.* (2000) related the late time slope of BTCs (m_{BTC}) with the slope of memory functions depending on the initial conditions, provided that the longest characteristic times of the memory function are much longer than the advection time. A BTC with initial concentration specified throughout the mobile and immobile zones is linear on the memory function, g. A BTC resulting from an initial mass pulse into the mobile zone is linear on the time derivative of the memory function, $\partial g/\partial t$. For a tracer test BTC with the initial pulse and detection mode c_f, the relation between the slopes m_g and m_{BTC} is $m_g = m_{BTC}$ -1. For example, m_{BTC} for a matrix diffusion tracer test is 1.5 and the slope of the corresponding memory function, m_g, is 0.5.

We take advantage of the above properties to identify the memory function from the BTC obtained from the heterogeneous fields simulations. It should be noticed that the objective here is just to fit the BTC, which could be done by any conventional fitting procedure. In fact, we use TRANSIN (*Medina and Carrera*, 1996), which is an inverse problem code, for fitting runs, which should facilitate estimation. However, direct inversion of the memory function shown in Eq. 3 is extremely ill-posed (a potentially large number of α_n and b_n coefficients just to fit the BTC tail). Therefore, g must be parameterized. As mentioned in Section 2, we have used a standard parametrization in terms of m_g, t_1 (time for which the slope m_g starts) and t_2 (time for which power law behavior ends), as shown in Fig. 3.4. Time t_2 represents the time for which the immobile zone equilibrates with the mobile zone and corresponds roughly with the time for which the BTC departs from power law behavior and drops to zero exponentially, hence the name cut-off time. Time t_1 is the characteristic time of the smallest heterogeneity scale encountered (*Bijeljic and Blunt*, 2006; *Berkowitz et al.*, 2008). For the case of slow advection, both characteristic times scale with flow rate (*Berkowitz et al.*, 2008) while the slope remains constant. Additionally, if t_1 is smaller than t_{peak}, t_1 can be chosen larger and the contribution of the missed part can be modeled using an upscaled dispersivity. TRANSIN does not handle this parametrization. Moreover, we

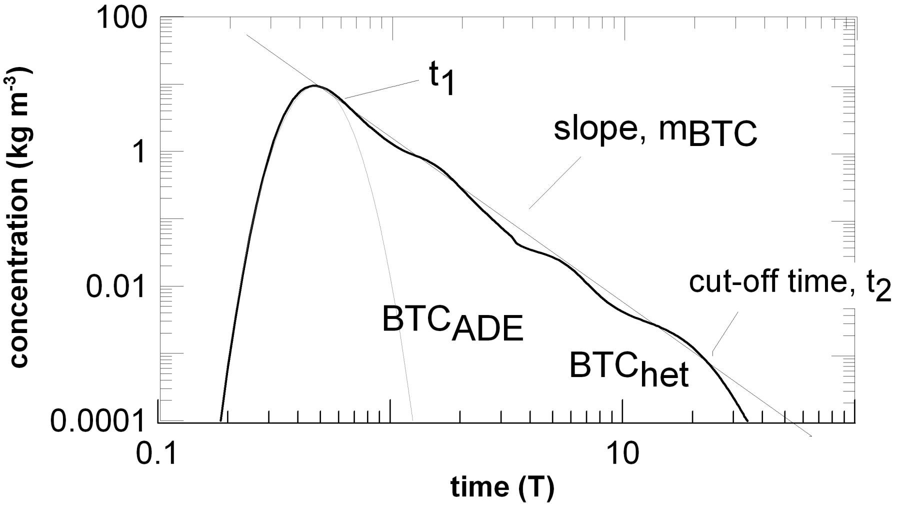

Figure 3.4: Derivation of the memory function of a breakthrough curves taken in a heterogeneous aquifer BTC_{het}. Early time data is fitted against the corresponding BTC derived by means of the ADE (BTC_{ADE}). t_1 is read directly from the point where the two curves deviate. Starting from t_1 a straight line is fitted to the tail to get m_{BTC}. Finally, the cut-off, t_2 is taken as the point where the BTC starts to decrease exponentially.

preferred a generic methodology which could be easily applied with any code. Therefore, we use the following steps: First, we fit an ADE to the first arrival and the peak of the BTC by applying the same boundary conditions and using the T_{eq} as upscaled T (T_{up}). The fitting parameters are initial mass, porosity and dispersivity. Second, overlaying the resulting BTC (BTC_{ADE}) with the measured one, we define t_1 as the time when the two curves start departing from each other (again, this is somewhat arbitrary, shorter times would work as well). Second, a straight line is fitted starting at the point where t_1 crosses the original BTC, which renders the slope m_{BTC}. And third, t_2 is read from the BTC. Sometimes, the BTC does not display a well defined cut-off time t_2. In such cases, t_2 is defined by extrapolating the power-law behavior until the full mass is recovered. Finally, the immobile porosity controls the size (height) of the tail. Therefore, some trial runs may be needed to obtain ϕ_{im} (this we did automatically with TRANSIN). Ideally, ϕ_{im} should be equal to the total minus the mobile porosity (*Sánchez-Vila and Carrera*, 2004). But t_2 may have to be adjusted for this condition to be met (increasing t_2 lowers the tail). Once t_1, t_2 and m_g are known, coefficients α_n and b_n are adjusted as explained below.

3.3.4 Modeling of BTCs using the memory term

As a last step we take the memory function derived above and implement it in a homogeneous 1D mass transfer model. Again, the finite element code TRANSIN (*Medina and Carrera*, 1996) was used for solving the ADE with general mass transfer (Appendix A). Dispersivity values and mobile porosity are estimated from early time data. When possible, dispersivity is set to its local value. The total porosity is kept at its true value of 0.3, except for the cases in which BTCs were obtained with a local mass transfer scheme, when total porosity is 0.35. The immobile porosity is calculated from the mobile one. N = 20 was found sufficient in most cases. The α_n values are bounded by (the inverse of) cut-off times, within which the power-law behavior takes place ($\alpha_1 = t_2^{-1}$ and $\alpha_N = t_1^{-1}$). If we chose the rate coefficients, α_n, evenly distributed on a logarithmic scale, the corresponding b_N can be easily calculated using the slope of the memory function and Eq. 1 together with:

$$b_n^* = \alpha_n^{m-1} \tag{3.10}$$

$$b_{tot}^* = \sum b_n^* \tag{3.11}$$

$$b_n = \frac{b_n^*}{b_{tot}^*} \tag{3.12}$$

b_n^* and b_{tot}^* are introduced to normalize b_n. Note, that $b_n \phi_{im} = \phi_{im_n}$ where ϕ_{im_n} is the corresponding immobile porosity fraction characterized by α_n.

3.4 Results

Plume snapshots (Fig. 3.5) show that transport is non-Fickian at this scale. Spatial distributions of solute mass are highly asymmetric, with peak values trailing behind early arrivals. It is clear that properly reproducing the geometry of these plumes would require a thorough knowledge of the medium, which is unrealistic. Instead, the main features of this and other simulations are captured with a homogeneous transport equation with mass-transfer term, which motivates the type of upscaling proposed here.

3.4.1 Effects of mass input and detection mode; scaling

Fig. 3.6 shows eight BTCs investigating solute mass input conditions and detection (sampling) mode. They are all obtained with the same heterogeneous field (type 3 field in Fig. 3.3). This particular field displays a relatively homogeneous right boundary, but a highly heterogeneous left one. The homogeneous boundary is characterized by an almost uniform distribution of velocities while the heterogeneous boundary displays a high velocity variance along the cross section (low values on top and high values on bottom). Four tests are performed with flow from left to right and four from right to left with all possible combinations of detection mode (flux or resident concentration) and input conditions (flux- averaged input pulse or fixed initial concentration). In our numerical set-up, the input conditions are affected by the upstream boundary, while the detection mode is influenced by the downstream boundary (where measurements are taken). BTCs separate all tests into two distinct groups. The individual behavior depends only on the condition applied at the heterogeneous boundary. When a heterogeneous boundary is used as inflow, the curves corresponding to constant initial concentration display a smaller slope than those of an input pulse proportional the local velocity at each point. When the heterogeneous boundary corresponds to the outflow, the same effect is displayed for resident concentrations detection mode with respect to flux concentration. The difference between the slopes in the log-log plots from the two groups

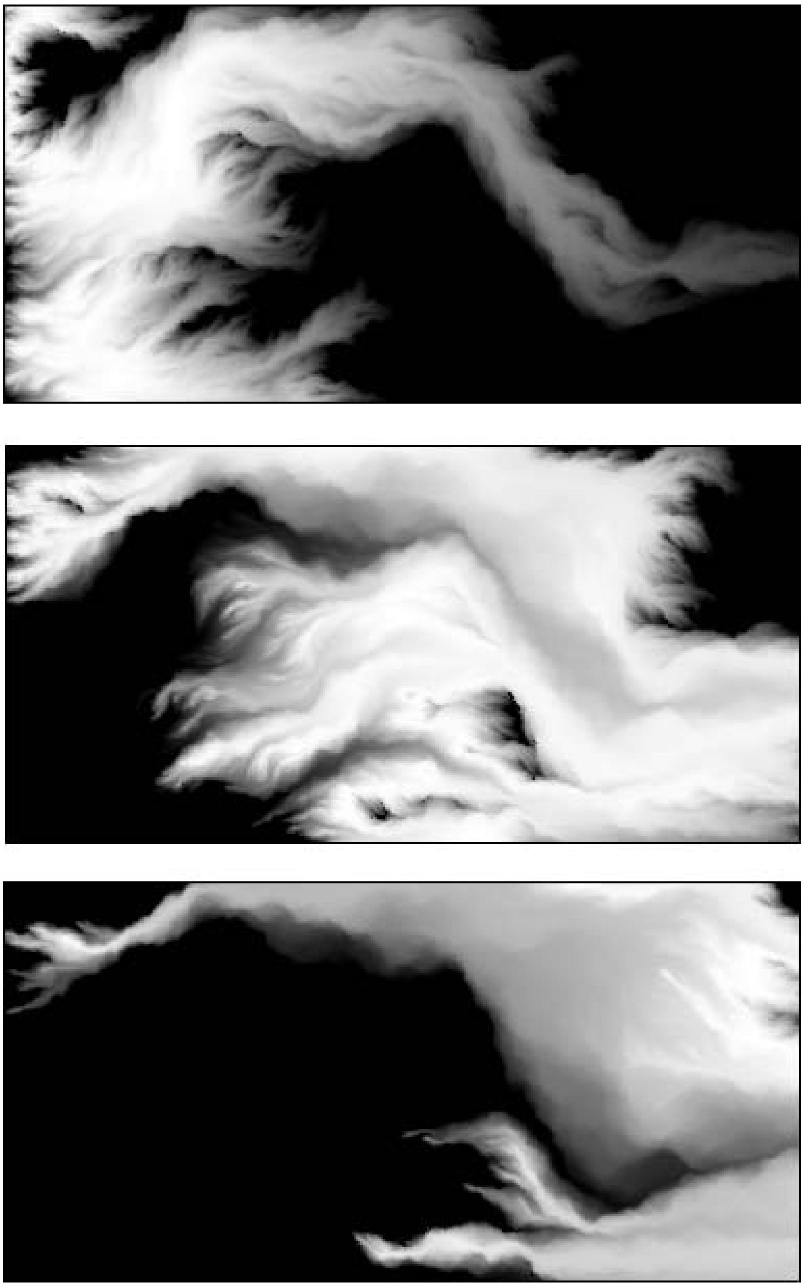

Figure 3.5: Snapshots of concentrations for a type 3 field at three different time steps. The shape of the plume clearly indicates non-Fickian behavior (marked asymmetry) that cannot be described by an ADE-like equation with upscaled parameters, whether constant or time dependent. Actually, two different preferential flow paths can be observed where the upper is more conductive than the lower one.

of curves is 0.9, which agrees quite well with a difference of 1.0 derived analytically by *Haggerty et al.* (2000) for different initial conditions. This result agrees also with *Di Donato et al.* (2003) where they found a difference of 0.83. It is also worth pointing out that the peak would have been poorly reproduced with a single ADE for the mobile zone. All BTCs display two, more or less explicit, humps (arguably corresponding to the two main flow paths that can be discerned in Fig. 3.5). Clearly, an accurate fit would require the superposition of at least two homogeneous solutions (*Luo et al.*, 2008). This implies that indeed, the BTC spread is reflecting the variability in travel times of different stream tubes (only to some extent, lateral mass transfer between adjacent stream tubes smooths out part of the spread). It also implies that, as opposed to memory functions representing actual diffusion into mobile zones, the portion of memory functions representing reversible slow advection (*Gouze et al.*, 2008a), must be scaled by advection.

3.4.2 Effects of different heterogeneous fields

We now compare BTCs corresponding to the simulations performed in the different field types. BTCs of type 1 fields (multi-gaussian) do not show anomalous features (Fig. 3.7a). Some tailing is observed, for a *lnT* variance of 6 there, but no power-law slope is developed. These curves could be well reproduced by the ADE with an upscaled dispersivity. As our BTC samples about 50 correlation lengths, we can consider transport here to be ergodic, so that macrodispersive behavior is observed.

The type 2 fields (nested variograms, BTCs not shown) allow us to investigate the influence of two clearly separate heterogeneity scales. The breakthrough curves display anomalous (i.e., non ADE-like) behavior, some with a clear tail. Still, the shape of the log-log scale tail is irregular. This might be due to the fact that heterogeneity only exists at two specific scales. In any case, no clear connected paths are observed in these fields (Fig. 3.3).

Transport in type 3 fields (power-law variogram) is always anomalous. Whether strong tailing

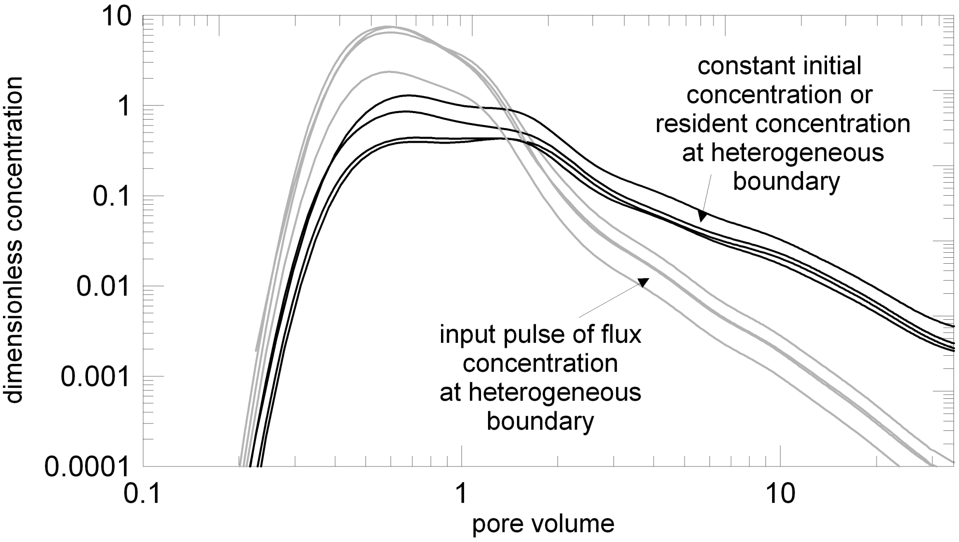

Figure 3.6: Comparison of breakthrough curves for two different initial conditions (uniform initial concentration or flux averaged mass inflow) and two detection modes (resident or flux averaged concentration). All 8 tests are performed in the type 3 field example of Figs. 3 and 5, where the left boundary is highly heterogeneous and the right boundary is relatively homogeneous. In four tests, the solute moves from left to right and in the remaining four from right to left with all the possible combinations of detection mode (flux or resident concentration) and initial conditions (uniform or flux averaged). Test results do not depend on the condition applied at the homogeneous boundary, which consistently display a slope around 2.2. The slope decreases by about 0.9 for the four cases where either resident concentrations are measured or fixed concentrations are applied at the heterogeneous boundary. Notice that the effect of the two preferential flow paths of Fig. 5 is reflected as two, more or less smoothed, humps in the BTC.

develops in a given realization depends on how high T values align to form a certain connected path, which in these realizations happens randomly. The slopes of BTCs are smoother than those obtained with type 2 fields and look similar to those often found in field tests, such as that presented in Fig 3.1. This supports the conjecture that aquifers are heterogeneous over a range of scales (*Neuman*, 1990) and that the power-law tails result from this range of scales (*Berkowitz and Scher*, 1997, 1998).

The influence of the overall variance of transmissivity can be seen in Fig. 3.7b. The slope is not sensitive to variance of lnT, but both early arrival and cut-off times change dramatically. As the variance decreases, early arrival is delayed and late time cut-off, t_2, is reduced. This is

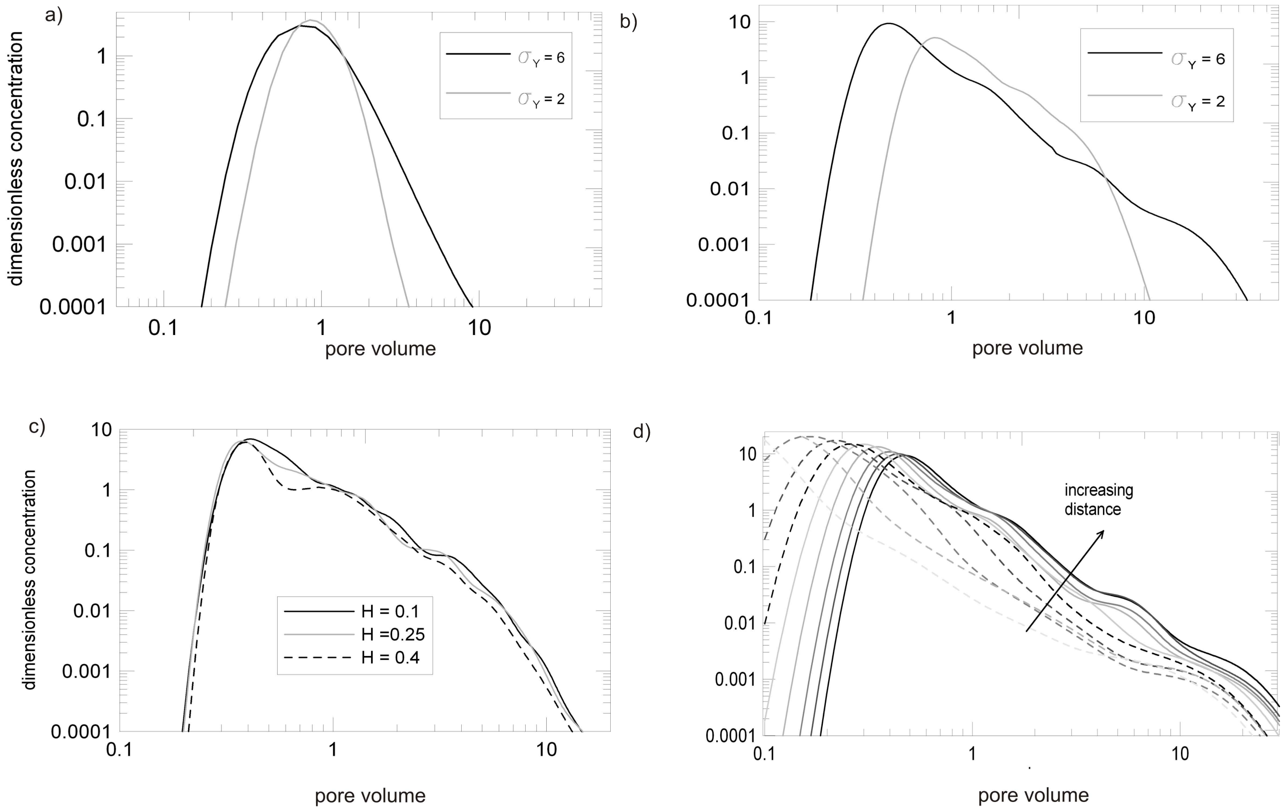

Figure 3.7: Breakthrough curves for different types of heterogeneity: a) the multi-gaussian fields (type 1). The curves do not show power-law tail and the curves can be reproduced using an ADE with upscaled parameters. b) A type 3 field with varying variance. When variance is decreased, we observe no change of slope, m_{BTC}, but a significant delay in first arrival and reduction of late time cutoff, t_2. c) A type 3 field with different values for the Hurst coefficients. It indicates that small scale heterogeneity has little effect on any of the parameters of g and d) type 3 field with BTC measured at uniformly increasing distances between 100 and 1000. No change in m_{BTC} is observed with increasing sampling volume.

consistent with the view of the memory function reflecting the spread of travel times. In fact, in the limiting case of zero variance (homogeneous medium), t_2 becomes so small that a memory term is not needed. These results suggest that t_2 scales up with σ_y^2. That is, increasing variance with a factor f implies increasing t_2 by the same factor while reducing immobile porosity.

To assess the effect of Hurst coefficient, independently of lnT variance, we changed H while total variance and geometrical patterns (i.e., location of high and low T regions) remained unchanged. This way, H reflects the relative importance of small scale variability. With increasing

Hurst coefficient (i.e., reduced small scale variability) we get a slightly delayed first arrival but also a slightly delayed cut-off (Fig. 3.7c). Again, the slope remains constant independently of H. This indicates that small scale structures do not affect the large scale slope, but only the characteristic times. In any case, the dependence is weak, which we find surprising.

Transport in type 4 fields is always anomalous. Due to the conditioning process, all fields exhibit a preferential flow path that leads to a well defined power-law tail in the BTC (not shown). Results are similar to those of type 3 curves. Fig. 3.7d displays a series of BTCs taken at varying distances from the source within the same field. Tail slopes do not change with distance (or time). However, the late time cut-off, t_2, increases more or less linearly with travel distance. This confirms the earlier assertion about the scaling of t_2 with advection.

Type 5 fields allow us to investigate the influence of connectivity. Recall that these fields are obtained by imposing connectivity on a multi-gaussian field characterized by a single correlation length. When the correlation length of the original field is small, the modified field displays thin high conductivity channels within a matrix of small low-conductivity blocks. Increasing the correlation length of the original field leads to an enlargement of both channels and low-conductivity zones, which causes an increase in connectivity. Fig. 3.8a shows that the slope decreases with increasing correlation length of the original underlying multi-gaussian field. The slope appears to tend asymptotically to a value of 2. The same can be said about the dependence of the slope on connectivity indicators (Eq. 6 and 7). A noisy, but well defined, relationship exists between slope and flow connectivity (Fig. 3.8b) or, even better, transport connectivity (Fig. 3.8c). For values close to 1 (ADE limit), increasing connectivity indicators causes a decrease in slope, until it reaches values close to 2. From there, the slope remains constant despite of further increases of connectivity.

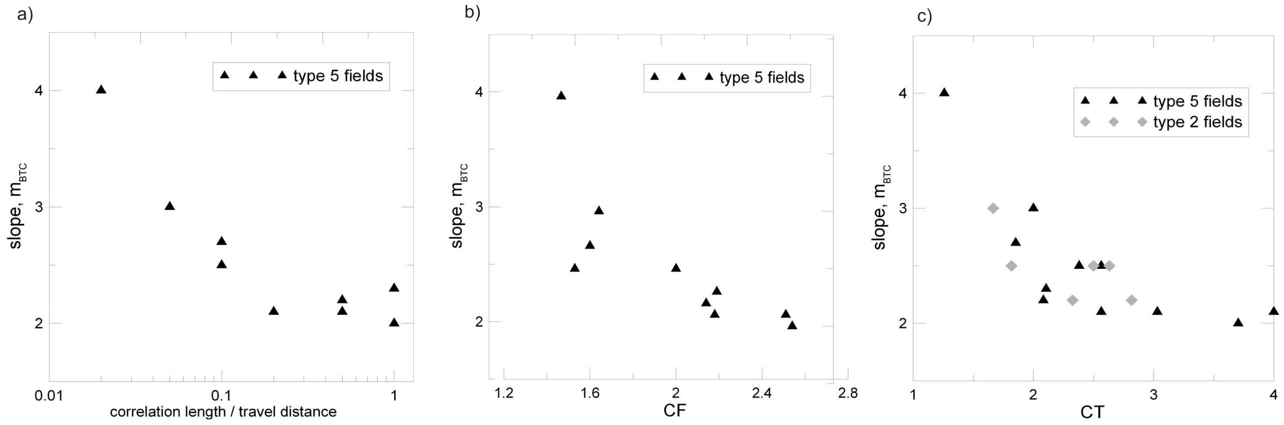

Figure 3.8: Slopes for different types of transmissivity fields versus: a) the correlation lengths of the underlying multi-gaussian field in Type 5 fields(recall that increasing this correlation length results in broader, better connected channels); b) flow connectivity index; and c) transport connectivity index. They all show that the slope m_{BTC} decreases (i.e., tailing becomes increasingly marked) as connectivity increases. The slope appears to tend $m_{BTC} = 2$, but does not decrease further.

3.4.3 Effects of the local-scale equation

In all the cases discussed up to here we assumed that a local ADE exists. Subgrid heterogeneity is modeled by a local-scale dispersivity. We discuss now the effect of local scale transport assumptions on large scale BTCs. The effect of local transverse dispersivity (α_T) is displayed in Fig. 3.9a. Increasing α_T, causes a small delay in first arrival and a small reduction in cut-off time, t_2, but has no impact upon the slope of the BTC. Longitudinal dispersivity (α_L, not shown) has little effect on either the cut-off time or the slope. Only the first arrival time is slightly delayed with decreasing dispersivity. The explanation of this effect is quite apparent form earlier discussions. Transverse dispersion tends to smooth away both from the leading (fast) and the trailing (slow) flow tubes by transferring mass to adjacent flow tubes. This is highlighted by the strong dependence of resident concentrations (not shown) on transverse dispersion. While this is consistent with longstanding understanding (*Taylor*, 1953), it sets a warning on the use of this formulation for reactive transport. Mixing is greatly enhanced by transverse dispersion, yet the memory function is only marginally affected.

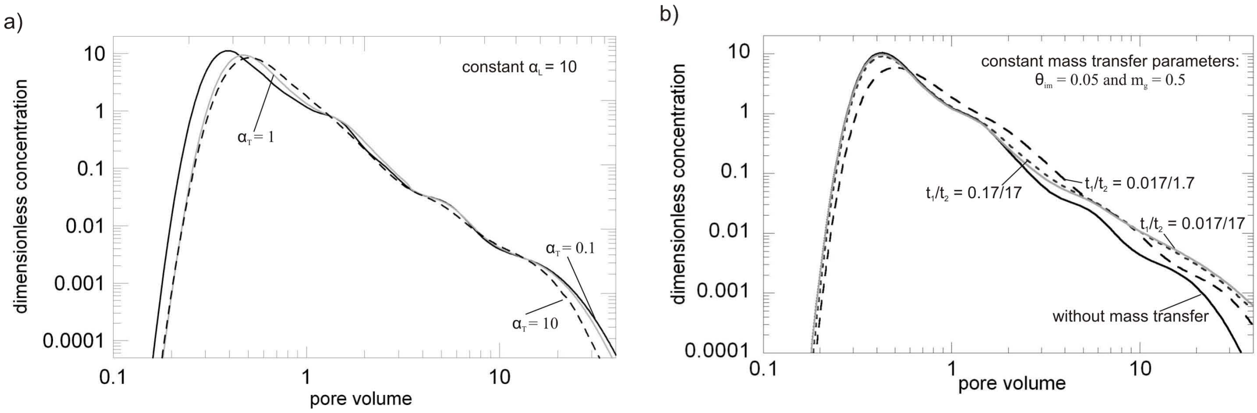

Figure 3.9: BTCs investigating the local scale equation: a) Subgrid heterogeneity is modeled using dispersivity (ADE). When the local transverse dispersivity is varied, the effect on the resulting BTCs is minor. The longitudinal dispersivity was kept constant. b) A non-local small-scale equations is used: a mass transfer term is added with varying memory functions, which causes m_{BTC} to decreases when a large final cutoff time is used.

To investigate the influence of the ADE assumption on the local-scale transport equation, we study now the effect of using a local scale equation with memory. Fig. 3.9b displays the behavior of the BTCs for different memory functions. For characteristic times much smaller than the observation time we find that BTC is virtually identical to the one observed with the ADE, only delayed by the total porosity, which was increased from 0.30 to 0.35. If we set the characteristic times larger than the observation time, the slope decreases. A memory function, with a t_2 slightly larger than peak arrival time, displays a slight decrease in peak concentration and peak arrival time. This means that portion of the local immobile porosity associated to fast characteristic times can be described by the ADE, increasing mobile porosity. If t_2 is increased further, peak arrival time is less increased, but and the slope decreases further. If also t_1 is increased by an order of magnitude and the effects are increased slightly. Remember that the assumed slope of the memory function $m_g = 0.5$ leads to a stronger weighting of large characteristic times (small α_n). Still, we find that the addition of a local scale equation with memory does not make the slope smaller than 2, which would require a much larger immobile porosity and a much larger t_2.

3.4.4 Comparison with BTCs using mass transfer

Finally we use the memory function derived from the above curves to reproduce the BTC with the homogeneous one-dimensional mass transfer model of Eq. 1-4. The only fitting parameters are dispersivity and mobile porosity. They are fitted against early arrival and peak times. Mobile porosity (0.075-0.16) is in all cases a fraction of the original porosity (0.3). The resulting dispersivity ranges between 10.0 and 34.0, where 10.0 is the local (longitudinal) dispersivity. The slope is fitted very well (Fig. 3.10) using an immobile porosity equal to the difference between total and mobile porosity ($\phi_{im} = 0.3 - \phi_m$). We repeated the model with a lower value of t_1 and we reproduced the BTC identically, but with a smaller dispersivity and a smaller mobile porosity. This means that the early time (high α_n terms) of our memory function cannot be estimated simultaneously with porosity and dispersivity from BTC data. This portion of the memory function equilibrates fast with the mobile region while producing some spreading. Hence, from a fitting point of view, neglecting this portion (i.e., increasing t_1) is virtually identical to increasing mobile porosity and dispersivity. This implies that t_1 is arbitrary, but so are mobile porosity and dispersivity. In fact, our formulation leads to a virtually identical fit setting dispersivity to 10 (local value) and mobile porosity equal to zero. It should be noticed that the early portion of the memory function is likely controlled by diffusion processes at the local (pore) scale, which have not been addressed here. In fact, proper representation of these processes requires pore scale modeling (e.g. *Bijeljic and Blunt*, 2006; *Tartakovsky and Neuman*, 2008). The point here is that they cannot be identified from a single, large scale, BTC.

3.5 Discussion and Conclusions

BTCs obtained from detailed simulations of transport through intermediate-scale highly heterogeneous media display the type of tailing often observed in field tracer tests. Intermediate scale heterogeneity means here transport through distances comparable to, or smaller than, the largest

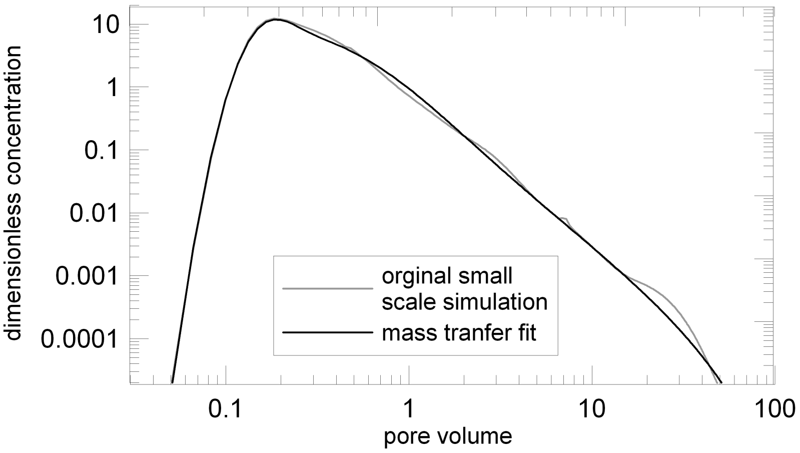

Figure 3.10: Fitted breakthrough curve using the memory function derived from the heterogeneous small scale simulations. The only fitting parameters are dispersivity and mobile porosity. As part of the heterogeneity can be modeled either with the mobile zone dispersion or with the memory function, more than one set of parameters fit the original BTC. When t_1 is chosen small, the mobile zone dispersivity is equal to the local dispersivity of the original heterogeneous field simulation.

heterogeneity scale. That is, transport over media with variability patterns (e.g., high permeability channels) of size comparable to, or larger than, the size of the transport domain. Given the ubiquity of tailing at all scales, this result suggests that stationary *lnT* fields are rare and lends support to views of heterogeneity evolving over a range of scales (*Neuman*, 1990).

The above kind of BTCs cannot be accurately modeled with the ADE, because of their non-Fickian nature, which can be well reproduced with non-local in time formulations (MRMT, CTRW, fADE). All these formulations require specifying a memory function, whose parameters are linked to those that describe heterogeneity. We have parameterized the memory function in terms of its slope in log-log scale and early and late cut-off times, t_1 and t_2.

The slope of the memory function depends most markedly on connectivity indicators. Our simulations displayed no dependence of the slope on other parameters frequently used in describing heterogeneity, such as variance, Hurst coefficient or correlation distance. Yet, it is clear that they do affect BTC tailing (i.e., tailing disappears if the variance tends to zero and connectivity would have increased if we had used much larger correlation distances).

The slope of the BTC is mildly reduced if non-local formulations are adopted for small scale transport. In fact, if the cut-off time, t_2, for the small scale transport is much larger than the travel time of the slow flow tubes, small scale transport will dominate transport over long distances. The issue is non-trivial, non-locality can be caused by diffusive processes (e.g. *Berkowitz et al.*, 2006), which is predictable and would be naturally described by a memory function at the local scale, and by slow advection which we have extensively discussed here. The problem is that non-locality caused by diffusion would be scale independent, while non-locality caused by slow advection depends on both, mean travel time and distance. Specifically, memory function slope remains unchanged, but immobile porosity and late-time cut-off depend on advection time. Tracer tests are often performed under forced gradient conditions (i.e., velocities much larger than those occurring under natural conditions). The memory function derived from such tracer test should be scaled (i.e., t_2 increased in the same proportion than travel time (*Berkowitz et al.*, 2006)) if caused by slow advection, but not if caused by diffusion. Actually since both effects probably overlay, we would have to split the memory function into diffusion and a slow advection for proper scaling.

The minimum slope encountered in this study for all the investigated fields is $m_{BTC} = 2$, while smaller slopes are sometimes observed in field tracer tests. The abundance of slopes close to 2 suggests that we have reached a limit for the type of fields investigated here. Further decrease in slope may be caused by long diffusion times into immobile regions, including heterogeneous diffusivity (*Gouze et al.*, 2008b), by three-dimensionality, especially with variable tortuosity, or by chemical heterogeneity, particularly for solutes that sorb into the least mobile region (e.g., clays).

The scaling behavior of t_2 (late time cut-off) is quite complex. Besides depending on advection time, t_2 appears to increase linearly with the variance of lnT. It is also affected by local scale transverse dispersion. This implies that theoretical developments are needed before memory functions derived from tracer tests can be safely used for predicting long term transport.

A final note of caution must be added. The formulations we tested here are non-local only in time. They work very well, in the sense that they accurately reproduce BTCs. This is a result of our model set-up and the fact that we were only trying to reproduce conservative transport BTCs. Had we tried to simulate reactive transport or spatial distributions of concentrations, non-locality in space may have been needed. An indicator of this is provided by the small dependence of BTCs on local transverse dispersion, which controls mixing (and thus reactions). Therefore, we conclude that, while spreading can be well modeled with appropriately scaled memory function, mixing may not.

Chapter 4

Coupling of Mass Transfer and Reactive Transport for Non-Linear Reactions in Heterogeneous Media[‡]

4.1 Introduction

Multi-component reactive transport modeling at the field scale is necessary for risk assessment and for the design of remediation strategies in groundwater pollution problems. At the local scale, methods are available to address multicomponent reactive transport problems. But it is questionable whether they can be extended to the field scale. Aquifers are known to be heterogeneous at all scales with hydraulic conductivity varying over orders of magnitude even in seemingly perfectly homogeneous aquifers. It has been widely shown that any realistic hydrogeological application must directly or indirectly embed this heterogeneity.

[‡] This chapter is based in the article: Willmann, M., J. Carrera, X. Sánchez-Vila, and O. Silva, 2008, Coupling of Mass Transfer and Reactive Transport for Non-Linear Reactions in Heterogeneous Media, in preparation for submission to *Water Resour. Res.*

For very large travel distances (relative to the largest heterogeneity scale) it has been shown that transport of conservative species satisfies an ADE type equation with upscaled parameters (e.g., *Dagan*, 1989; *Gelhar*, 1993). On the contrary, at intermediate to moderately large travel distances, relevant for most hydrogeological problems, observations display what is known as anomalous (non-Fickian) or non-ergodic (*Kitanidis*, 1988) behavior, so that concentrations cannot be modeled by an ADE, even allowing for upscaled parameters. Furthermore, (*Neuman*, 1990) proposes an universal scaling law stating that aquifers display an evolving range of scales and, therefore, non-ergodic conditions apply to all transport problems, regardless of travel distance.

From a practical perspective, small scale heterogeneity is the critical one in many field applications, because large scale structures can be identified and modeled directly on the numerical grid. This means that upscaling is required to account, at least, for small scale, sub-grid, heterogeneity. To describe effective transport of conservative species at intermediate distances different non-local methods have been developed. The most general one is Continuous Time Random Walk (CTRW) (*Berkowitz et al.*, 2006). Other models are Fractional Advection Dispersion Equations (fADE) (*Benson et al.*, 2000), Multi-Rate Mass Transfer (MRMT) (*Haggerty and Gorelick*, 1995) and memory functions (*Carrera et al.*, 1998). The last two methods are mathematically equivalent. It has been shown (*Dentz et al.*, 2004; *Berkowitz et al.*, 2006) that FADE and MRMT can be expressed as particular cases of CTRW. In short, when only non-localities in time are considered, all methods are equivalent.

All these non-local methods have been very successful in predicting BTCs of field and lab experiments (*Berkowitz and Scher*, 1998; *Kosakowski et al.*, 2001; *McKenna et al.*, 2001; *Levy et al.*, 2003; *Haggerty et al.*, 2004; *Cortis and Berkowitz*, 2004; *Zinn et al.*, 2004; *Le Borgne and Gouze*, 2008) and were also very useful in explaining anomalous transport behavior in heterogeneous aquifers (*Schumer et al.*, 2003; *Dentz and Berkowitz*, 2003; *Berkowitz et al.*, 2006; *Zhang et al.*, 2007; *Berkowitz et al.*, 2008).

The question is whether the success of non-local formulations for representing conservative transport can be extended to reactive transport. Since the nature of reactive transport is extremely sensitive to the nature of reactions (*Rubin*, 1983), we need to distinguish the type of reactions to be addressed. Reactions can be classified as linear or non-linear, as kinetic (slow) or equilibrium (fast), as homogeneous (all reactants in the same phase) or heterogeneous, etc.. Linear reactions (e.g. instantaneous or linear kinetic sorption) should be upscaled without problems with the same model that upscales conservative transport. In fact, MRMT was initially develop as a way to model sorption problems, and has been widely used in this context (*Rubin et al.*, 1997; *Haggerty and Gorelick*, 1998; *Lawrence et al.*, 2002; *Berkowitz et al.*, 2008). Transport of sorptive species in heterogeneous media, was investigated with emphasis on the spatial or the temporal distribution of concentrations since the initial works of (*Selroos and Cvetkovic*, 1992; *Bellin et al.*, 1993).

Regarding equilibrium or kinetic reactions, the situation is more complex. Certainly, linear reactions should properly upscale with the same non-local model as conservative solutes because the overall reaction is controlled by the residence time distribution, which is precisely what the BTC represents. Therefore, any model that reproduces the BTC for a conservative solute should also reproduce the BTC and the overall reaction rate for solute suffering a linear kinetic reaction. This is not necessarily the case for multi-component equilibrium on non-linear kinetic reactions. *De Simoni et al.* (2005, 2007) showed that equilibrium reaction rates are controlled by mixing rates. Reproducing a BTC assures a good reproduction of solute arrivals, but not necessarily mixing. In fact, one can fit a given BTC with models that include mixing or that consist of flow tubes with varying degrees of mass exchange among them (*Medina and Carrera*, 1996; *Luo and Cirpka*, 2008).

The distinctive characteristic of the non-local formulations presented before, with respect to the ADE, is how these models can separate the concepts of spreading and mixing. Spreading, directly related to hydrodynamic dispersion, provides a measure of the area that could potentially be affected by a pollution problem, incorporating the uncertainty in the location of the center of gravity of the polluted area. Mixing, on the other side, indicates the extent of the polluted area, regardless of its location. From these definitions it is evident that reactions are controlled by mixing rather than by spreading, and this should be accounted for in the governing equations for multicomponent reactive transport in heterogeneous media.

More recently the emphasis has moved to the direct computation of reaction rates. Starting from the analytical solution for the local reaction rate developed by (*De Simoni et al.*, 2005, 2007). *Luo et al.* (2008) and *Fernandez-Garcia et al.* (2008) evaluated the global reaction rate for generally heterogeneous and stratified media respectively, concluding that the integrated reaction rate could not be obtained from an upscaled ADE equation. (*Lichtner and Kang*, 2007) used a Lattice-Boltzmann model to simulate pore scale precipitation/dissolution model. They found that in most cases a multi-porosity model was needed to upscale reactive transport locally governed by a single porosity model.

So far it has not been investigated whether reactive and conservative transport may be upscaled in a similar way. The objective of this work is, thus, to investigate whether a Mass Transfer model is an appropriate tool to describe mixing controlled Multi-component reactive transport in heterogeneous aquifers. Our goal is to show that adequate upscaling of conservative transport is sufficient in order to upscale reactive transport. For this purpose we revisit the model proposed in the previous chapter and extend it to reactive transport. We then compare the results obtained by some detailed heterogeneous simulations using the ADE, with those coming from the MRMT model with the known memory function derived from conservative transport.

4.2 The Multi-Rate Mass Transfer Reactive (MRMT-R) Model

In this section we propose a model for multicomponent reactive transport based on an effective dynamics formulation. This is done in three steps, starting with the corresponding model for conservative solute, presented here for completeness, then showing the local scale reactive problem we consider in this paper (mixing induced precipitation), and finally coupling the two models to derive the MRMT-R model.

4.2.1 Conservative transport model based on Multi-Rate Mass Transfer

Amongst the different effective models available in the literature to represent transport in heterogeneous media, we select one based on Multi-Rate Mass Transfer, for reasons that become apparent when extending it to account for reactions. The MRMT model pictures the system as composed by a mobile and a suite of immobile regions that coexist at any given point in the domain. These regions interact, since solute mass is transferred between the mobile and each of the immobile regions. Originally the MRMT model was used to account for rate-limited sorption processes, and widely used in the chemical literature (e.g., *Connaughton et al.*, 1993; *Chen and Wagenet*, 1995). Later it was adapted to conservative transport in heterogeneous media. The underlying idea is that flow paths with varying velocities (residence times) coexist at some elementary volume. Solute is transferred between paths by local diffusion/dispersion. The MRMT model conceptualizes this picture as one zone where water flows and a number of zones where the solute is stagnant (those corresponding to slow advection paths), but that can be reached by diffusion/dispersion. The MRMT model is an obvious simplification of reality. However, it provides sufficient degrees of freedom to accommodate any residence time distribution and, indeed, it can be used to obtain tracer test BTC that are analogous to those measured in the field (e.g., *McKenna et al.*, 2001; *Haggerty et al.*, 2004).

The MRMT model assumes an underlying ADE equation for the mobile zone with an additional sink/source term to account for mass transfer with immobile zones. Therefore, the resulting equation for the concentration in the mobile zone, c_m, can be written as

$$\phi_m \frac{\partial c_m}{\partial t} = \nabla \cdot (\mathbf{D} \nabla c_m) - \mathbf{q} \cdot \nabla c_m - \Gamma \tag{4.1}$$

where D is the dispersion tensor, ϕ_m is the porosity corresponding to the mobile zone, i.e., the ratio between the pores that are accessible by advection in our model, and the total volume, and Γ is the source/sink term controlling the mass transfer between the mobile and the suite of immobile regions, which we write as (*Carrera et al.*, 1998; *Haggerty et al.*, 2000):

$$\Gamma = \phi_{i_{tot}} g * \frac{\partial c_m}{\partial t} \tag{4.2}$$

here $*$ indicating a convolution product. Hence the resulting Eq. 4.2 is non-local in time. $\phi_{i_{tot}}$ is called the total immobile porosity, defined as the void volume fraction that is not accessible by advection. With this definition the actual porosity (measurable in the field) is just $\phi = \phi_m + \phi_{i_{tot}}$. Function g, termed memory function, accounts for the probabilistic distribution of the time that a solute particle remains in the immobile regions. In general, this function will depend on the velocity distribution.

Eqs. 4.1 and 4.2 are basically shared by all non-local in time formulations. As such, they are not appropriate for reactive transport. To do so, we need to localize the transport equation (i.e., to write it in terms of concentrations at a given point and a given time). We start by expanding the memory function as a sum of exponentials

$$g(t) = \sum_{i=1}^{N} \alpha_i b_i e^{-\alpha_i t} \tag{4.3}$$

where α_i is the inverse of the characteristic residence time associated to the $i - th$ term, and b_i is the corresponding fraction of the immobile porosity. Notice that this expansion is equivalent to discretizing the residence time distribution. More interesting, it is equivalent to viewing the immobile region as consisting of N immobile regions, each of which exchanges mass with rate α_i (*Carrera et al.*, 1998; *Haggerty et al.*, 2000):

$$\frac{\partial c_i}{\partial t} = \alpha_i (c_m - c_{im}) \tag{4.4}$$

where c_{im} indicates the concentration of the solute at the immobile zone i (mass of solute per volume of pores of the $i-th$ site). Introducing c_{im} allows rewriting Eq. 4.2 as

$$\Gamma = \sum_{i=1}^{N} \alpha_i \phi_i (c_m - c_{im}) \tag{4.5}$$

where $\phi_i = b_i \phi_{i_{tot}}$ is the immobile porosity associated to exchange rate α_i (or residence time $1/\alpha_i$). Since b_i's must add up to 1, it results:

$$\sum_{i=1}^{N} \phi_i = \phi_{itot} \tag{4.6}$$

In principle a large suite of memory functions could be used. The main feature of these functions is their behavior at large times, since they control the late-time behavior of breakthrough curves (*Haggerty et al.*, 2000). Also, in principle there is a large number of parameters that should be fitted (actually $2N-1$). For this reason in most applications a general shape of the memory function, parameterized by a rather short number of parameters, is proposed (e.g., *Rubin et al.*, 1997; *Lawrence et al.*, 2002; *Haggerty et al.*, 2000). Amongst these, a commonly used model is the truncated power-law (*Dentz et al.*, 2004; *Berkowitz et al.*, 2008), in which function $g(t)$ can be expressed in terms of two characteristic times, t_1 (time at which the power-law behavior starts manifesting), t_2 (time at which concentration starts decaying faster than the power-law), and the slope of the memory function, m_g.

4.2.2 Reactive transport in a single porosity model

The model presented in the previous subsection accounts for a conservative transport undergoing advection, dispersion at the local scale and mass transfer between mobile and less-mobile (mathematically treated as immobile) zones. In this section we extend the model to incorporate a binary precipitation-dissolution system at equilibrium, but it could be extended to any system involving $n \geq 2$ aqueous species with $m \geq 1$ equilibrium reactions along the lines of (*De Simoni et al.*, 2005). The binary system proposed involves two reacting aqueous species, B_1, B_2 (their respective aqueous concentrations being c_1, c_2) in chemical equilibrium with a mineral S at any point in space and time:

$$B_1 + B_2 \longleftrightarrow S \tag{4.7}$$

The concentrations of the aqueous species are non-linearly related by means of the mass action law, which, under the assumption of low ionic strength can be written as

$$c_1 * c_2 = K \tag{4.8}$$

where K is the equilibrium constant. In general K will be a function of ionic strength and temperature. Without loss of generality, and for the sake of simplicity, we disregard this variability. The governing non-linear transport equations becomes

$$\phi_m \frac{\partial c_{m,j}}{\partial t} = \nabla \cdot (\mathbf{D} \nabla c_{m,j}) - \mathbf{q} \cdot \nabla c_{m,j} - r_m \qquad j = 1, 2 \tag{4.9}$$

where r_m is the reaction rate. Note, that in Eq. 4.9 we keep the subindex m in the concentrations and the reaction rate to indicate that they correspond to that of the mobile zone; this distinction will be useful in the sequel. Note also that since r_m is the same in both equations, it is possible to define a linear combination of the concentrations (denoted as component):

$$u_m = c_{m,1} - c_{m,2} \tag{4.10}$$

So that the governing equation for u_m is again a linear transport equation, but with no chemical source/term

$$\phi_m \frac{\partial u_m}{\partial t} = \nabla \cdot (\mathbf{D} \nabla u_m) - \mathbf{q} \cdot \nabla u_m \tag{4.11}$$

The component is not defined uniquely. Another conservative quantity would also be obtained by defining the component as the product of Eq. 4.10 by a scalar. The resulting transport equation (Eq. 4.11) is independent of r_m; that is, precipitation would remove the same amount of moles of the two species, and thus their difference is unaffected by reaction (which is the definition of conservative quantity). Assuming it is possible to obtain a solution for the component u_m, the two concentrations can be obtained explicitly by solving a speciation problem (involving Eqs. 4.8 and 4.10)

$$c_{m,1} = \frac{u_m}{2} + \sqrt{\frac{u_m^2}{4} + K} \qquad\qquad c_{m,2} = -\frac{u_m}{2} + \sqrt{\frac{u_m^2}{4} + K} \tag{4.12}$$

In most applications the main quantity of interest is the reaction rate rather than the actual concentrations of the solute. This would be the case, e.g., in natural attenuation studies, karst formation, mineral precipitation,... The reaction rate can then be obtained from Eq. 4.9. Alternatively, *De Simoni et al.* (2005) derived an explicit expression for the calculation of r directly from the solution of the component, being the product of two terms, one of them depending only on speciation r_{spec} and a second one which depends on the concentration gradients and the dispersion tensor and characterizes mixing r_{mix}

$$r = r_{spec} r_{mix} \tag{4.13}$$

with

$$r_{spec} = \frac{2K}{(u_m^2 + 4K)^3} \qquad\qquad r_{mix} = \nabla^T u_m \mathbf{D} \nabla u_m \tag{4.14}$$

4.2.3 Multi-Rate Mass Transfer Reactive (MRMT-R) model

Combining the two models presented in this section, it is possible to write a model that incorporate non-linear reactions to the MRMT model. An important point to note here is that the incorporation of ”immobile regions” in our effective model is just a mathematical artifact to account for the amount of solute that samples the less mobile parts of the domain. For this reason, sink terms should be included in the ”immobile zones” to account for the precipitation that takes place when the solutes reaching those areas by diffusion (actually here slow advection), are not in chemical equilibrium with the mineral. It is important to state that we can have a different chemical equilibrium condition in each one of the zones (mobile plus N immobile). Thus, despite locally we preserve equilibrium at all points, defining concentration by averaging over scales larger than the pore, equilibrium is not preserved. This issue has significant consequences in the total reaction values, which will be explored later.

Combining Eqs. 4.9 and 4.2, we can write the governing equation for the MRMT-R model

$$\phi_m \frac{\partial c_{m,j}}{\partial t} = \nabla \cdot (\mathbf{D}\nabla c_{m,j}) - \mathbf{q} \cdot \nabla c_{m,j} - \sum_{i=1}^{N} \alpha_i \phi_i (c_{m,j} - c_{im,j,i}) - r_m \qquad j = 1, 2 \tag{4.15}$$

where $c_{im,j,i}$ denotes concentration of species j in the immobile zone i. Introducing Eq. 4.10, the equation satisfied by the conservative component reads

$$\phi_m \frac{\partial u_m}{\partial t} = \nabla \cdot (\mathbf{D}\nabla u_m) - \mathbf{q} \cdot \nabla u_m - \sum_{i=1}^{N} \alpha_i \phi_i (u_m - u_{im,i}) \tag{4.16}$$

where we have introduced $u_{im,i} = c_{im,1,i} - c_{im,2,i}$. Provided we have a way to solve Eq. 4.16 in terms of u_m, the actual concentration values in the mobile zone are given by Eq. 4.12. $u_{im,i}$ satisfies an extension of Eq. 4.4)

$$\frac{\partial u_{im,i}}{\partial t} = \alpha_i (u_m - u_{im,i}) \tag{4.17}$$

And after solving for $u_{im,i}$, the concentrations of the reacting species in each of the zones considered immobile are given as

$$c_{im,1,i} = \frac{u_{im,i}}{2} + \sqrt{\frac{u_{im,i}^2}{4} + K} \qquad\qquad c_{im,2,i} = -\frac{u_{im,i}}{2} + \sqrt{\frac{u_{im,i}^2}{4} + K} \tag{4.18}$$

Finally the reaction rates can be obtained as

$$r = r_m + \sum_{i}^{N} r_{im,i} \tag{4.19}$$

with r_m obtained from Eq. 4.15, and $r_{im,i}$ being

$$r_{im,i} = -\phi_i \frac{\partial c_{im,j,i}}{\partial t} + \phi_i \alpha_i (c_{im,j,i} - c_{m,j}) \tag{4.20}$$

and the value of $r_{im,i}$ being independent of $j = 1$ or 2, that is, of the species used for computing mass balance. It is important to note that in the effective reactive multi-component transport model, upscaling is entirely included in the memory function which is only determined by conservative transport. MRMT-R model presented here is implemented in the finite element code TRANSIN (*Medina and Carrera*, 1996) which was extended for general mass transfer in the previous chapter. Some details of the numerical implementation are given in Appendix A1.

4.3 The MRMT-R Model: Sensitivity Analysis

The MRMT-R model discussed here depends on a number of parameters, including those that define the memory function, mobile and immobile porosity, and the equilibrium constant, among others. In this section we explore the sensitivity of instantaneous and cumulative reaction rate to a number of those parameters.

We perform numerical simulations on a 1D homogeneous field with 3000 elements of length. A gradient is imposed so that water flows in the positive x-direction. The water initially present in the system has a constant chemical signature represented by $u_m = u_{im,i} = 0$, equivalent to consider $c_{m,j} = c_{im,j,i} = 0$. During a short interval at the beginning ($\delta t = 1000$) a pulse of $u = 0.5$ is applied. The physical meaning is that a water with a different chemical composition is entering the domain. This water has a high concentration of c_1 and a low concentration of c_2, but it is still in chemical equilibrium with the mineral. After this time interval, the system is flushed with water with the initial composition ($u = 0$). While the two waters are equilibrated with the mineral, any of their mixtures will not satisfy the mass balance equation, and thus precipitation takes places wherever mixing is occurring. The parameters for the reference case studied (see chapter 2) are a mobile porosity, ϕ_m of 0.147 and a longitudinal dispersivity, α_l, of 33.8 for the mobile zone. The immobile regions are characterized by an immobile porosity, ϕ_{itot}, 0.153 (so that total porosity is 0.3) and the following memory function parameters: slope, m_g, of 1 and characteristic times t_1, t_2, of 8000 and 800000.

4.3.1 Reaction Rate Spatial Distributions in the Mobile and Immobile Zones

Due to the specific boundary conditions, the largest amount of precipitation takes place at the inlet (left) boundary (Fig.4.1a). This is caused by the largest concentration gradient being present at the inlet node. With time reactions extend along the flow path.

In our MRMT reactive model mixing takes place in both the mobile and the N immobile zones, with the overall reaction rate being the sum over all zones. At early times the spatial distribution of reaction rates in the mobile zone resembles what would be obtained in a homogeneous medium when transport is modeled by an ADE, with a characteristic symmetric double peak and a zero value in between. The double peak is still present in the MRMT-R model, but the minimum value is no longer equal to zero, and the fastest moving peak is slightly larger (see Fig.4.1b). The relatively large value of reaction rate obtained in the mobile region reflects the two mixing mechanisms present in Eq. 4.15, i.e., dispersion and exchange with immobile regions. Since r_m is obtained from a mass balance in Eq. 4.15, we cannot distinguish between the two terms. Therefore, we calculate the reaction rate caused by dispersion using Eq. 4.13 and assume that the rate is caused by exchange with immobile regions. The result is also shown in Fig.4.1b,c and points out that mixing due to mass transfer, in this case, is much larger than due to dispersion.

The reaction rate obtained by integrating the reaction rates in all immobile zones is much smaller than that of the mobile zone, and has a single maximum located in between the two peaks of mobile zone reaction rate. For larger times, the reaction rate distribution displays only a single peak (Fig.4.1c) for the particular set of parameters used in these simulations. Here, mobile and

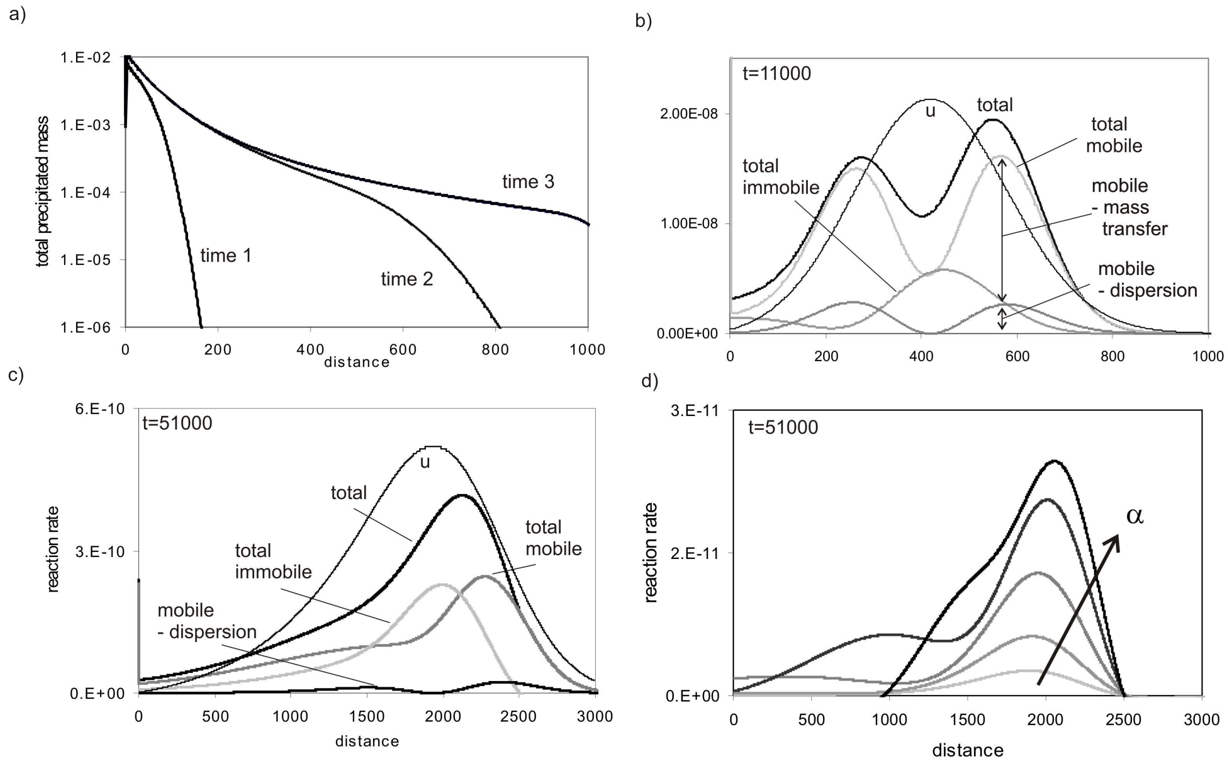

Figure 4.1: Evaluation of the spatial distribution of mineral precipitation: a) total precipitated mass for three different times (1000, 11000, 51000); b) spatial distribution of reaction rate for an early time step (t t1); reaction rate in the mobile zones shows some ADE like behavior with the characteristic double peak and is much stronger than reaction rate in the immobile zone; c) the same plot for a later time step, where no double peaks are displayed anymore (the modeling domain was enlarged here); d) distribution of selected single immobile zones for the same time as c); the total number of immobile zones is 20.

immobile reaction rates have similar shapes, with their maxima shifted towards the front and long backwards tails, the one corresponding to the immobile zone delayed with respect to that of the mobile one. Individual reaction rate for 5 zones out of the total $N = 20$ are shown in Fig.4.1d. For the zones with largest α fast exchange, display a more pronounced peak and a less marked tail. The peak of reaction rate distribution becomes increasingly delayed with decreasing α.

4.3.2 Sensitivity to the equilibrium constant

In Eq. 4.13 the reaction rate is expressed as the product of two independent terms: the mixing factor and the speciation factor. While our work focuses on mixing, the influence of the speciation factor is discussed here briefly. In our simple example the speciation factor is controlled entirely by the equilibrium constant together with the component u. Fig.4.2a illustrates the strong dependence of the speciation factor on the equilibrium constant K. For large u the speciation factor is largest for large K and the opposite holds for low K. Moreover, for small values ($u < \sqrt{K}$) the speciation factor is virtually constant, but drops dramatically for larger $u's$. Non-monotonic dependence with respect to K translates to the quantification of overall precipitation (Fig.4.2b). Together with the non-linearity, it leads to a somewhat impredictable behavior of reaction rates.

We observe a complete distinct behavior of precipitation depending on K. $pK = log_{10}(K) = 2$, is the reference case discussed before. When K is decreased (pK=4) the overall behavior changes slightly. The reaction rate is generally increased and a slight double peak is developed. For $pK = 6$ this is much more pronounced. We see a well developed double peak. The reason here is not as in the previous section incomplete mixing within the immobile zone but that reaction hardly take place at peak concentrations but at much lower ones. This means the mixing is strongest where $pK = 2$ has its peak, but as the mixing factor and the speciation factor are multiplied to get the reaction rate, here we have the maximum of the reaction rate more separated. The influence of K is very large as we want to test here mainly the role of mixing we use mainly $pK = 2$ as examples.

4.3.3 Variation of Parameters that Alter the Shape of the Conservative BTC

Here we analyze the sensitivity of reaction rates to some of the parameters involved in the MRMT-R model: longitudinal dispersivity, α_L, the characteristic time t_2, and the slope of the memory function m_g. Results are shown in Fig.4.3.

We performed additional simulations increasing and decreasing α_L by a factor of 2 ($\alpha_L = 16.9$,

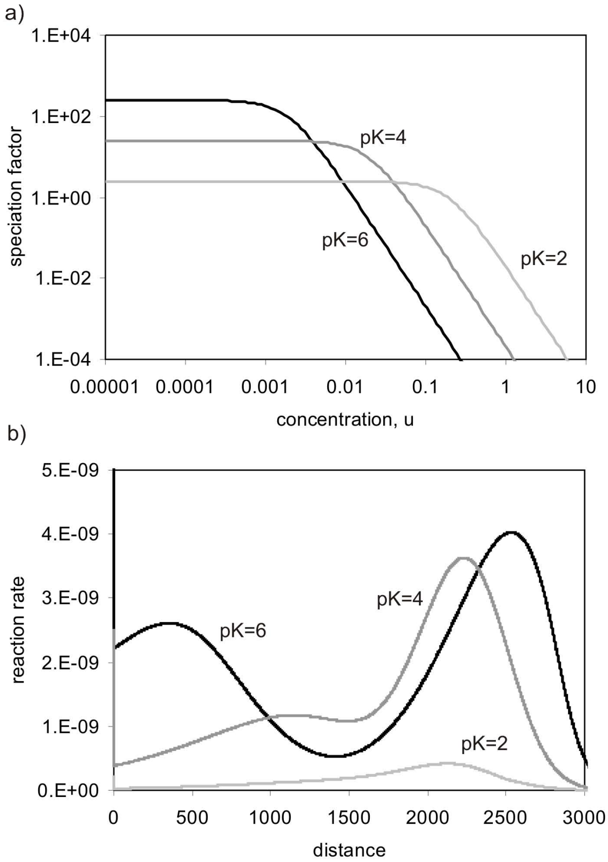

Figure 4.2: a) Speciation factor as a function of concentration for different pK values (notice, that the speciation factor increases with pK for low values of$u$, but decreases for high values); b) spatial distribution of the reaction rate as a function of K. The reaction rates are non-monotonic with K.

33.8 and 67.6). Small α_L values lead to larger values of the peak reaction rates (see Fig.4.3a). The reason is that despite Eq. 4.13 apparently is linear with D, the actual behavior is the opposite since increased α_L values enhance mixing, thus reducing the gradients of the conservative quantities.

t_2 was changed by an order of magnitude ($t_2 = 8 * 10^4, 8 * 10^5, 8 * 10^6$). Large t_2 values lead to single peak asymmetric distributions, with the peak displaced towards the advancing front (Fig.4.3b). The reason is that large t_2 imply less accessible immobile porosity, so that the front is less retarded. For decreasing t_2 the immobile zones become more accessible and the reaction rate exhibits an ADE-like behavior with double peak.

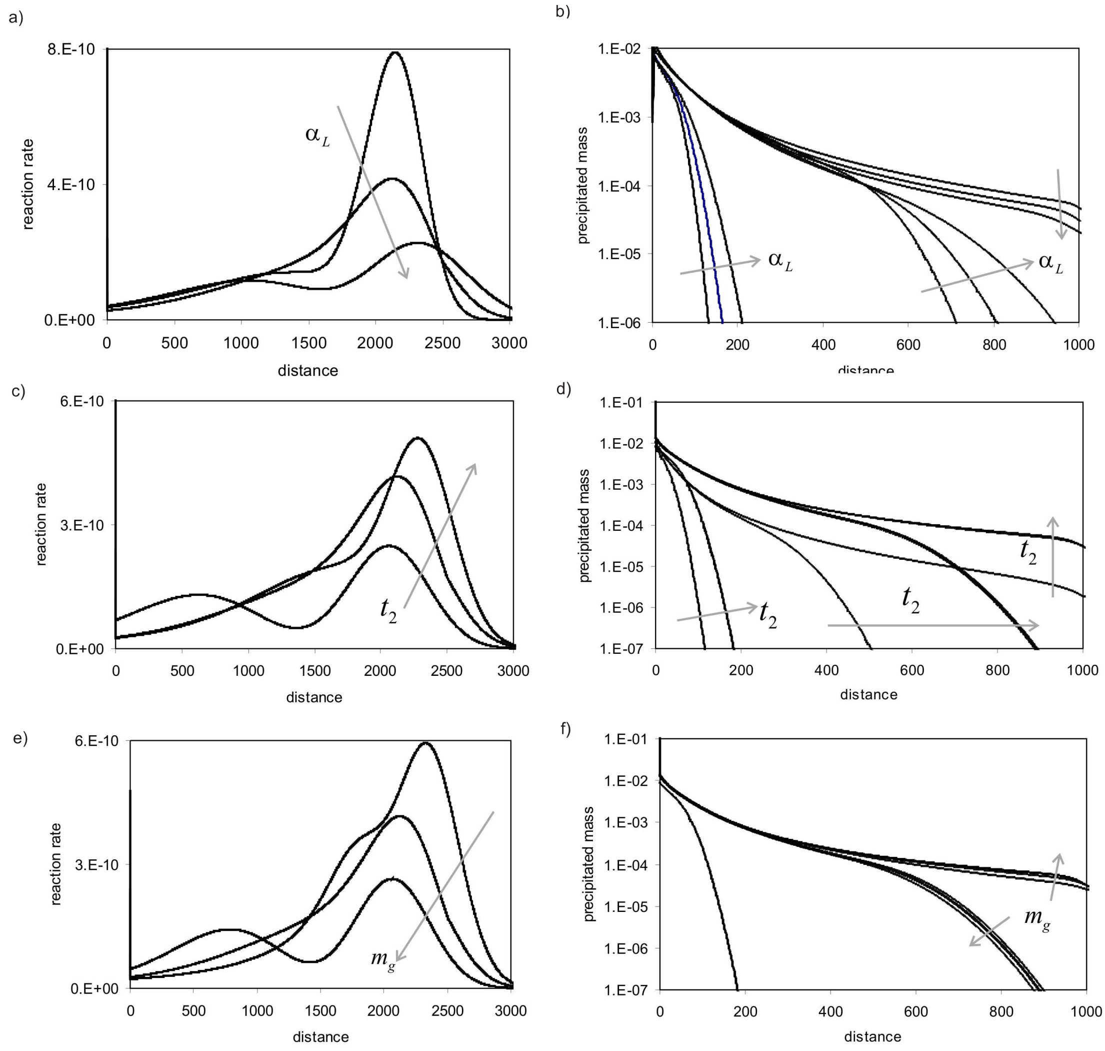

Figure 4.3: Sensitivity of the spatial distribution of total reaction rates (recall Fig.4.1) and total precipitated mass to: a,b) longitudinal dispersivity, c,d) t2, and e,f) slope of the memory function, mg. The curves in a, c and e correspond to a fixed time t=51000

Three values of m_g (0.5, 1.0, and 1.5) are compared (Fig.4.3c). Increasing m_g makes the solution more ADE-like. Contrarily, small m_g values lead to a single peak distribution, with increasing peak value. This can be explained by noticing that m_g can be seen as a weighting function of the exchange rates, so that the largest the m_g value, the smallest the areas with large α_L values, and vice versa.

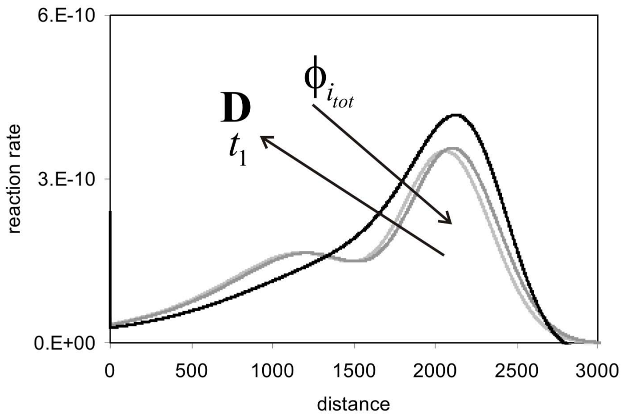

Figure 4.4: Spatial distributions of reaction rate for three combinations of ratios of mobile and immobile porosity, t_1 and dispersivity, that lead to virtually identical conservative tracer BTCs. Notice that the total reaction rate is not affected dramatically though the separation between mobile and immobile precipitation is.

4.3.4 Variation of parameters conserving the shape of the BTC

While in the previous subsection we have shown how the distribution of reaction rates are sensitive to some of the parameters that define the MRMT-R model, this is not the case for all the parameters that are actually involved. The physical reason is that it is equivalent to consider a large dispersion coefficient with a large mobile porosity and a large immobile zone with a small t_1 value. To verify this hypothesis we ran transport simulations with three combinations of parameters that lead to almost identical BTCs. Simulations were performed using immobile porosities equal to 0.153, 0.24 and 0.29, combined with longitudinal dispersivities of 33.6, 10.0, 10.0, and t_1 values of 8000, 170 and 30 respectively. In all cases the mobile porosity is selected so that total porosity is a constant value of 0.3. The corresponding spatial distributions of reaction rates are shown in Fig.4.4.

Depending on the combination of parameters, the reaction rates computed in the mobile and immobile zones (not presented) can be quite different, but the total value (the sum) is practically constant.

4.4 MRMT-R upscaling methodology

In chapter 2 is was shown that an MRMT model could be used to provide an effective picture of conservative transport. They obtained how the memory function is affected by different parameters characterizing the heterogeneity of the system, such as the variance of the log-hydraulic conductivity. The main objective in this section is to find whether and under which conditions, the MRMT-R model is capable of reproducing key features of multicomponent reactive transport in heterogeneous media where an ADE is assumed at the local scale. The working hypothesis is that the memory function that is derived from conservative transport would directly be applicable to reactive transport.

The methodology we use is numerical and can be summarized in the following steps: (1) we create heterogeneous transmissivity fields with some characteristic features; (2) we perform reactive transport simulations in the heterogeneous fields based on a local description of transport governed by an ADE equation with a single sink/source term to account for precipitation/dissolution; (3) we derive a memory function from the breakthrough curves observed for a conservative species; (4) we model reactive transport in a homogenized media by using the MRMT-R model with the parameters derived from the conservative curves, and, (5) we test whether the MRMT-R simulations actually match the observed curves in the heterogeneous media. The different steps are expanded next.

4.4.1 Creation of heterogeneous transmissivity fields

We conceptualize the aquifer as two-dimensional. We are interested in transport at intermediate distances compared to a larger characteristic heterogeneity scale (such as the correlation distance whenever it exists), where power-law tails are frequently observed in the field. According to to the results of chapter 2 tailing occurs due to the presence of connected regions of high conductivity (preferential flow paths). For this reason we use individual realizations of heterogeneous fields obtained as follows (the actual selected fields can be seen in Fig.4.5). The first field studied is an individual unconditional realization of a Multi-Gaussian field with a small correlation length ($\lambda = 20$ in consistent units). This field was generated using the Gaussian sequential simulator GCOSIM3D (*Gómez-Hernández and Journel*, 1993). This first field is used for comparison, since transport in Multi-Gaussian fields has been the topic of extensive research. The second field corresponds to an individual realization of a conditional field honoring a power variogram. The conditioning points are selected to produce a single preferential flow path connecting the high permeability pixels. By construction, this field exhibits an evolving range of scales. The third field is a connected field constructed using the methodology proposed by *Zinn and Harvey* (2003). This results in a field with various connected preferential flow paths surrounded by low conductive regions. The variance of log-transmissivity (Y) is set to 6 in all three fields. The domain size is 1024 by 512 elements of unit size. The flow problem consist of uniform no-flow boundaries on top and bottom and constant head boundaries on the remaining sides, forcing a mean uniform flow from left to right. The overall gradient is 0.0098. Notice that we are interested in looking at the characteristic features of transport in individual realizations, and this is the reason not to pursue a Monte Carlo approach.

4.4.2 Reactive transport simulations

The reactive transport in the heterogeneous fields is assumed to be controlled by a local scale ADE. *Berkowitz et al.* (2006) question the existence of a scale independent local scale equation. Still, we apply the ADE here as we are interested in the loss of information in the upscaling process. The methodology could easily be extended to a different form of the local transport equation. Rather than running a reactive transport model, we took advantage of posing the problem in terms of a single component and we solved a transport of a conservative species (Eq. 4.11) followed by speciation (Eq. 4.12). The initial condition is $u_m = u_{im,i} = 0$.

Similar boundary conditions as those explained in the previous section are considered, just noticing that now conditions should be imposed in all boundary nodes corresponding to the 2D domain. During a short interval at the beginning ($\Delta t = 1000$) a pulse of $u = 0.5$ is applied to the water entering through the left nodes, followed by flushing with water with the initial composition. The remaining parameters for the local scale equation are a porosity of 0.3 and longitudinal and transverse dispersivities of 10 and 1 respectively. Molecular diffusion is neglected as we study here the influence of physical heterogeneity and, thus, slow advection. Reaction rate is calculated at each time step and each node through mass balance consideration, and the precipitated mass is recorded.

4.4.3 Derivation of memory function for conservative transport

In order to apply the Multi-Rate Mass Transfer model we derive the memory function from conservative transport. The three BTCs presented in Fig.4.5 (thus corresponding to a conservative species) can be represented using an MRMT model with a single memory function, which is derived following the methodology outlined in chapter 2. From a given BTC, one derives an upscaled value for longitudinal dispersivity and mobile porosity from the early time arrival of the BTC. The three parameters defining the memory function are taken from late-time behavior. The two characteristic times when the power-law behavior starts and ends t_1 and t_2 and the slope of the BTC m_{BTC}. The slope of the memory function, m_g, is related to the slope of the BTC depending on the boundary condition . They are identical for resident concentration, while for flux-averaged concentration it holds that $m_g = m_{BTC} - 1$. The last relevant parameter in the model, the immobile porosity, is calculated by $\phi_{i_{tot}} = \phi_{tot} - \phi_{mob}$.

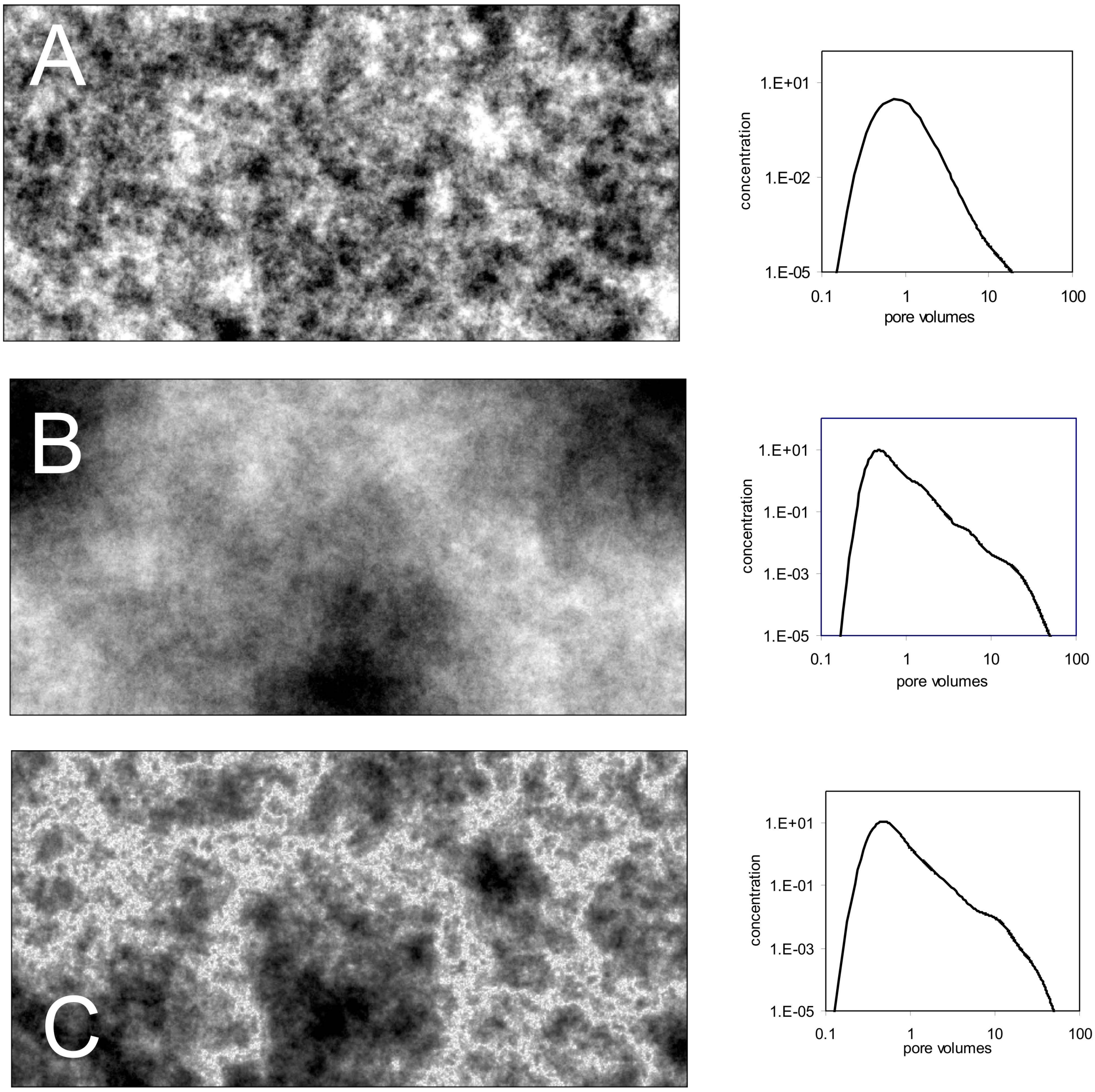

Figure 4.5: Transmissivity fields and corresponding breakthrough curves (BTCs) obtained from conservative transport simulations. BTC's are the cumulated mass collected at the domain's right boundary. The three fields correspond respectively to single realizations of: A) a Multi-Gaussian field with short correlation length, B) a non-stationary field based on a power variogram, and C) a field where connectivity between the high transmissive pixels have been enhanced with respect to those of low conductivity.

4.5 Reproducing the observations in the heterogeneous media by means of an effective model

Reactive transport in the three heterogeneous media shown in Fig.4.5 are now analyzed. The two variables considered are: (1) vertically averaged spatial distribution of the reaction rates, and (2) total precipitated mass over the whole domain. Type A field shows an almost Fickian behavior with a slightly noticeable tail. The curves recorded from the Type B and C fields show an anomalous (non-Fickian) behavior. While these two fields are very different in terms of their internal structure, they render similar breakthrough curves, so that the fitted memory functions are almost identical. Here we compare how reactive transport behaves in these fields and compare the results in terms of reaction rate distribution to those obtained from the effective model.

4.5.1 Reproducing anomalous transport behavior

Looking at fields B and C, we find clear indicators of anomalous transport at intermediate distances ($t_1 < t_c < t_2$). The breakthrough curves for conservative solutes display a power-law behavior. This indicates that it is possible to reproduce the conservative BTCs using a MRMT model.

Field C is characterized by fine channels within a matrix of less conductive material. Fig.4.6a shows a very good match between the heterogeneous and solution and the upscaled mass transfer results in terms of total precipitated mass versus distance for three selected time steps. This is obtained by construction, since total precipitation is controlled by mass balance considerations. The remarkable point is that both the spatial distribution and the time evolution are well reproduced. This observation is independent of the K value (Fig.4.6b,c), despite the very non-linear response to this particular parameter: larger K values (= 0.01) lead to larger precipitation close to the outlet, while smaller K values provide a similar amount of reaction throughout the system for very large times. The spatial distribution of vertically averaged reaction rates at one time step for the type C

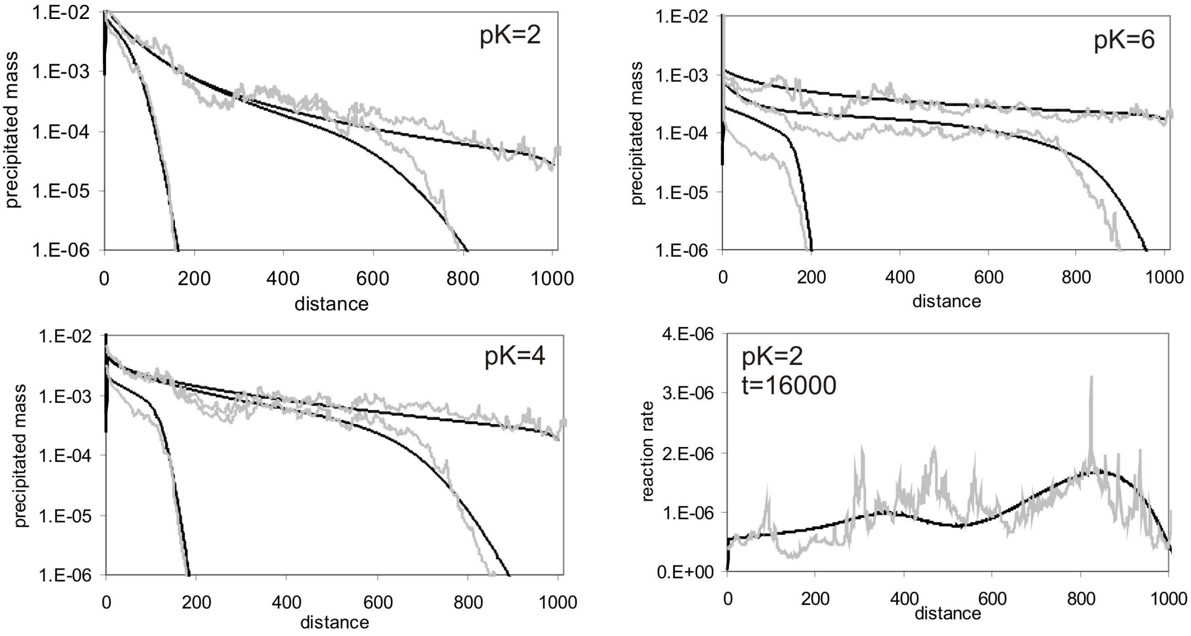

Figure 4.6: Model results for field type C (connected field). a-c) Comparison between the spatial distribution of the vertically averaged precipitated mass in the heterogeneous media with those derived from the effective MRMT-R model for three different time steps (1000, 11000, 51000) and for (a) pK = 2, (b) pK = 4 ,and (c) pK = 6. d) The instantaneous reaction rate for both models at a given time step at pK = 2..

field is shown in Fig.4.6d. The heterogeneous curve has a slight double peak with the largest peak at the front. This behavior is reproduced quite well with the mass transfer model. Already at such early time the effective model is capable of reproducing the main features of the heterogeneous solution. We also compared the reaction rate at later times (not shown), but as most of the mass has left the domain only the tails were fitted.

Type B field (Fig.4.5) is characterized by large scale structures as the transitions from high to low conductive zones is more gradual than in the C field. Still, memory functions in those two fields are almost identical. Fig.4.7 shows the comparison of precipitated mass versus distance for some specific times and different *K* values. The agreement is still quite remarkable. On the contrary, when comparing now the spatial distribution of reaction rate in both models (see Fig.4.7d) the match is rather poor. The heterogeneous medium leads to a double peaked curve,

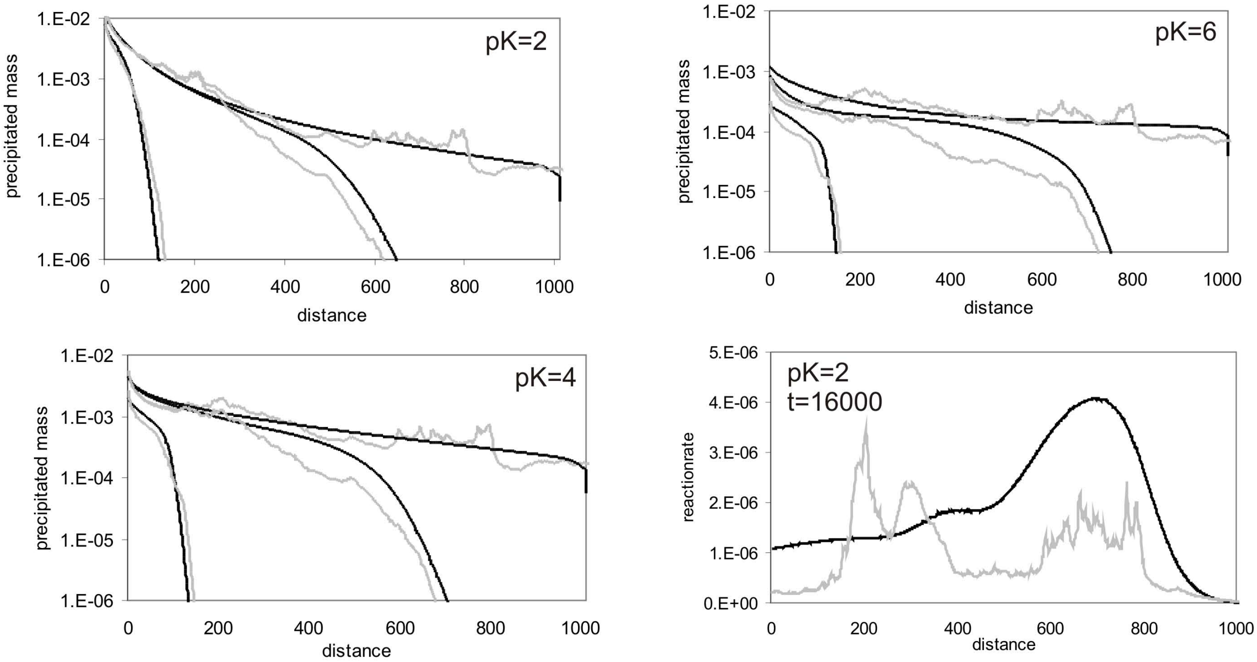

Figure 4.7: Model results for field type B (non-stationary variogram). a-c) Comparison between the spatial distribution of the vertically averaged precipitated mass in the heterogeneous media with those derived from the effective MRMT-R model for three different time steps (1000, 11000, 51000) and for (a) pK = 2, (b) pK = 4 ,and (c) pK = 6. d) The instantaneous reaction rate for both models at a given time step at pK = 2.

while the effective model provides a single one and a long tail. The explanation is that at this distance the chosen memory function is not representative. This is due to the presence of very large low and highly conductive zones (Fig.4.5), so that the local distribution has a very strong impact on the actual spatial distribution, an effect that washes out when integrated along the full domain. At larger travel times (not shown) the agreement improves slightly.

4.5.2 Reproducing Quasi-ergodic transport

Ergodic transport will eventually develop whenever travel distance is much larger than the corresponding correlation length along the mean flow direction. In such a case transport can be described by means of a macro-dispersion equation. This is the reason we incorporated field A in our simulations. The conservative breakthrough curve at the outlet boundary shows a behavior close to Fickian (recall Fig.4.5). The heterogeneous reactive transport results are shown in Fig.4.8a-c. In a) we also show the difference between considering a macro-ADE, with an upscaled dispersivity coefficient of 85.0, or a MRMT model with mobile and immobile porosities and dispersivity equal to 0.2, 0.1 and 45.0 respectively, and the memory function characterized by a slope of 2.0 and characteristic times of 600 and 900000. The curves in the two models are practically identical, the second one still accounts for the minor tail of the conservative BTC. The curves corresponding to the heterogeneous model are much smoother than in the previous two fields. Generally there is a reasonable agreement with respect to the heterogeneous solution except at the outlet. This is mainly due to the decreased dispersion of the MRMT model at that boundary. The agreement is in both cases good. In the field we know that reactive transport models are underestimating the reaction rates in the field. Our results indicate that the ADE is not valid in the field at any scale.

4.6 Sensitivity to boundary condition and transverse dispersivity

4.6.1 Boundary conditions

The slope of a BTC depends strongly on the boundary condition applied; contrarily, the memory function does not change (*Haggerty et al.*, 2000). In all previous simulations an initial pulse is applied at the inlet boundary of the heterogeneous field. This results in a flux-weighted initial condition, leading to a BTC slope of m_{pulse}. Applying a uniform initial distribution leads to a different BTC, with a slope m_{unif}. In chapter 2 it was found that whenever the boundary itself samples all the variability of the system, ($m_{unif} = m_{pulse} - 1$). We look now at the implications to reactive transport. In Fig.4.9 the curves corresponding to the two boundary conditions are compared for Field C. We assure mass conservation in both simulations by adjusting the duration of the pulse input ($t_p = 610$) and the number of rows where constant concentration are initially present (13 rows). We observe that generally the overall precipitation is largest for the flux-averaged boundary case

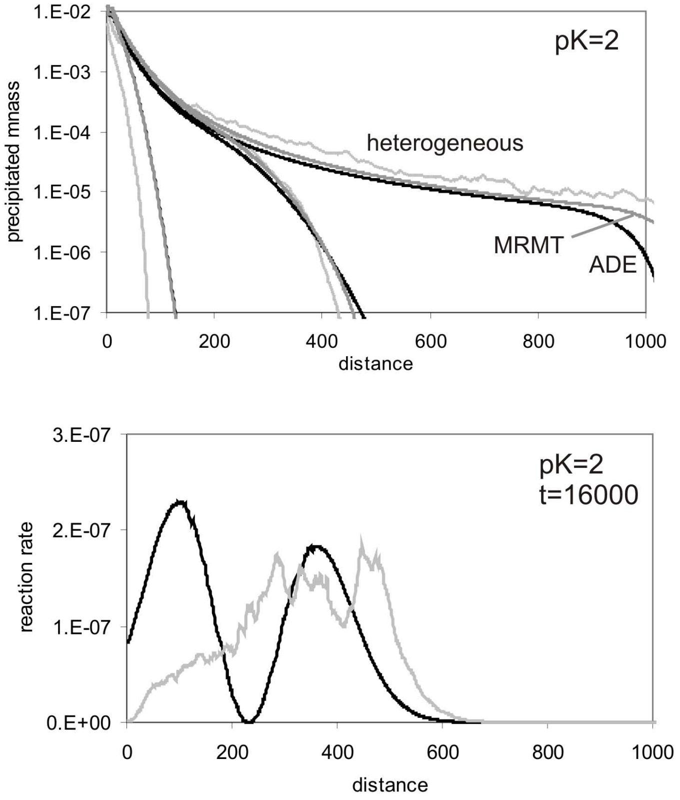

Figure 4.8: Model results for field type A, the multi-Gaussian field. a) Comparison between the spatial distribution of the vertically averaged precipitated mass in the heterogeneous media with those derived from the effective MRMT-R model for three different time steps (1000, 11000, 51000) and for pK = 2. b) The instantaneous reaction rate for both models at a given time step.

than for the uniform one. The peak of total precipitation for the latter case is located right after the zone where fixed initial conditions are applied. Close to the inlet boundary the total precipitation is of the same order of magnitude than the flux-averaged one. Then precipitation becomes smaller and after a distance of about 100 and its shape becomes identical to the flux-averaged one but only with only 20% of the total precipitate. This large difference in mass precipitated is caused by the dominant transport mechanism in this field being flow within the fast flowing channels, so that the largest amount of precipitation takes place along the channels. The homogeneously distributed case seems to have only 20% of the mass within these channels compared to the reference case. The MRMT-R model using the same memory function accounts very well for both solutions with

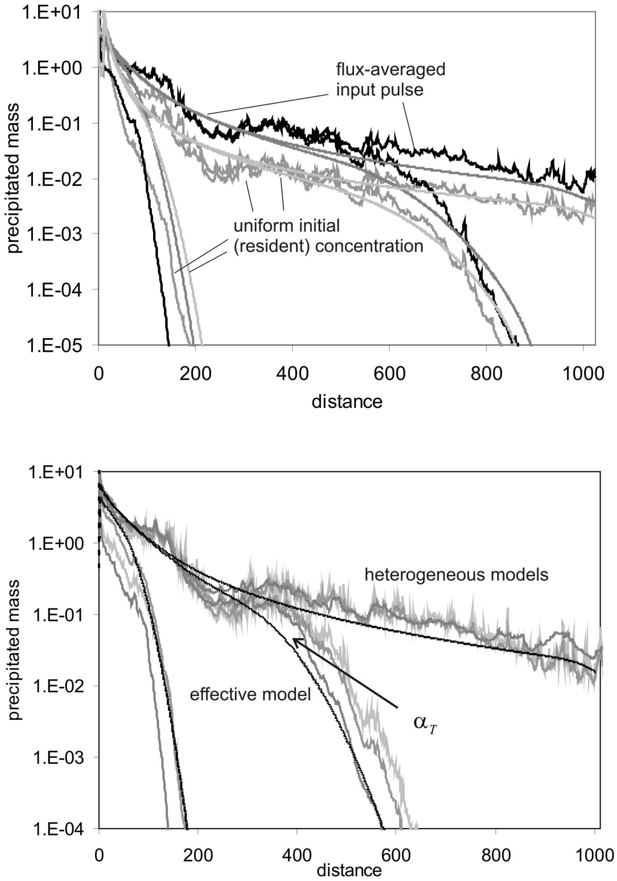

Figure 4.9: Sensitivity analysis for: a) Boundary conditions, including an flux averaged input pulse and initial uniform concentration at the boundary nodes. After a distance of 200 the curves have the same shape but the precipitated mass when a pulse is considered is 5 times larger than for fixed initial concentration. The smoother cures are the effective MRMT-R models which both reproduce very well the heterogeneous solution. b) Transverse dispersivities (0.1, 1.0, 10.0) is varied. The curves look similar but smooth out with increasing dispersivity. The corresponding effective solution represents very well all the heterogeneous curves.

respect to total precipitated mass. Intuitively one expects resident concentration to be used in reactive transport, particularly as reactions takes place also where water is almost stagnant (immobile zone). But from our simulations we conclude that the distinction between flux concentration and resident concentration only depend of the boundary condition of the problem and that MRMT-R is capable of accounting for both.

4.6.2 Transverse dispersion

Transverse dispersion, α_T, seems particularly important for reactive transport as it is the main local scale parameter that controls mixing. And, contrarily to longitudinal dispersion, α_L, α_T is not modeled directly within the effective model. Here we compare for the heterogeneous reference field C the curves of precipitated mass for three different α_T values (Fig.4.9b). It can be seen that the total precipitated mass is only slightly affected by the choice of the α_T value. A large value leads to a smooth curve. It can also be seen that a larger transverse dispersion value delays the precipitation for earlier time steps. This happens with conservative transport as well and it is because large α_T delays the arrival of the mixing front. For comparison the effective mass transfer model is added as well and it can be observed that all three α_Ts are represented well with the model not taking into account α_T. We conclude that α_T while being the controlling factor describing mixing, it is not a dominant factor controlling mixing-controlled reactive transport.

4.7 Conclusions

We present an effective reactive mass transfer model and investigate whether this model based on upscaling of conservative transport is sufficient to upscale mixing controlled multi-component reactive transport. We develop a mass transfer model (MRMT-R) for a binary precipitation dissolution system and use an upscaled memory function derived from conservative transport. Generally, we find that the MRMT-R model an excellent tool for representing mixing controlled reactive transport. In particular:

1. Total precipitation is well reproduced for all the examples studied, in terms of both the total mass precipitated and its spatial distribution. In any case the effective solution is smoother than the heterogeneous one. Reaction rate at early times (relative to t_1) is only matched well if the memory function is already representative for the domain sampled.

2. The distinction between reactions in the mobile and immobile zones is to some extend arbitrary. Fast flowing parts of the domain can either be modeled within the mobile porosity with an upscaled dispersion or within the immobile porosity with large exchange rates. In the latter case the reaction rate of the immobile zone has a similar shape than that of the mobile zone. If additionally the separation between dispersion mobile and mass transfer mobile is made, a better separation can be made: the mass transfer mobile and the immobile reaction rate give the total mass transfer reaction rate. This is much larger than the remaining mobile dispersion one.

3. Applying different boundary conditions changes the reactive transport behavior dramatically. A uniform initial (resident) distribution leads to stronger precipitation close to the boundary condition and less precipitation further away. Surprisingly, the shape further away form the boundary is more or less the same. The MRMT-R model reproduces very well precipitation for both boundary conditions using the same memory function.

4. Transverse dispersivity has only a minor effect on total precipitation even it controls mixing. The larger transverse dispersivity, the smoother the curve. That transverse dispersion can be ignored is important as MRMT-R (and most of the existing upscaled models) does not account for it.

5. The ADE (or macro ADE) represents reactive transport reasonable well at distances where transport can be modeled as Fickian. This is also the case when a very minor tailing exists. The bad performance of the ADE in the field supports the claim that the ADE does not hold at the local scale (e.g. *Berkowitz et al.*, 2006).

Generally we find MRMT-R an excellent tool for upscaling mixing controlled reactive transport in heterogeneous aquifers. In our study only mixing due to physical heterogeneity (tailing due to slow advection) was taken into account. Further studies should explore the influence of chemical heterogeneity like molecular diffusion or variable sorption coefficients, k_d.

Chapter 5

General conclusions

This thesis investigates the influence of heterogeneity of natural aquifers on our analysis of hydrogeological problems for different subsurface processes with varying complexity. The following major conclusions can be drawn:

The interpretation of recovery tests using the simple Theis recovery method can provide valuable information about representative parameters in heterogeneous aquifers, even though the method was developed for homogeneous media. Actually, it may be possible to discriminate between at least two representative transmissivity values, corresponding to the local T values (T_{loc}) surrounding the well, and some regional representative value (T_{reg}). The analysis presented here implies that the rate of early time recovery is informative of T_{loc}, whereas that of late time data yields information about T_{reg}. This result is valid as long as early time effects can be filtered out. The results presented here have several practical implications about the design and interpretation.

Regarding test design the following recommendations are advisable:

1. Pumping duration. Pumping duration should be chosen depending on the scale, L_c, to be characterized. At the very least, t_p should equal SL_c^2/T, where S and T are local estimates of storativity and transmissivity, respectively. Preferably, pumping durations should be much longer,

for example, 10 SL_c^2/T, especially if T_{reg} is expected to be smaller than T.

2. Recovery period. The design should allow for a long recovery period, not shorter than twice the pumping duration, and, if possible, much longer than twice the duration. Notice that this increase in time can be achieved at very low cost because time scale is logarithmic and only a few measurements have to be added. Because drawdowns become small for late time recovery, the reliability of these drawdowns needs to be assessed by comparing them to measurement errors.

3. Pumping rate. Late time residual drawdown is sensitive to total volume of water pumped, V_W, as $s \sim V_W/4$ (that is, it does not depend on the time evolution of pumping rate). Average pumping rate, V_W/t_P, should be designed for a sizable value of s. Recovery tests are not highly sensitive to high frequency changes in flow rate, but early time recovery is sensitive. Still, using V_W/t_P may become the only realistic option when pumping rate cannot be controlled.

4. Natural head trends. Heads should be monitored prior to the test so as to ensure either that they have stabilized prior to pumping or that a natural trend can be fitted. It should be noticed that much information is contained in late time residual drawdowns that are small. Residual drawdowns are equal to the difference between heads during recovery, which can be measured accurately, and natural heads. Efforts should be made to estimate the latter natural heads as accurately as possible. These efforts include not only prior stabilization, but also monitoring boreholes unaffected by the test. Mistaken natural head evolution would lead to wrong T_{reg} estimation.

Regarding the interpretation of recovery tests the following recommendations are advisable:

1. At any given time the head recovery plot can yield two slopes: m_1, tangent, and m_2, secant though the origin. Using them, T_{m1} and T_{m2} can be calculated.

2. When both pumping and recovery times are large it is possible to obtain good estimates of both T_{loc} and T_{reg}. Better estimations are obtained when the local value at the well is smaller than the regional T value, provided that sizable pumping rates can be sustained.

3. T_{loc} is better represented by T_{m1}. Early time effects (for example, skin effect) should be ruled out by calculating the corresponding sampling radius. A small radius indicates that these effects are still relevant and mask T_{loc} that cannot be estimated.

4. If pumping duration and recovery are long enough, late time T_{m1} and T_{m2} will tend to T_{reg}. The advantage of using T_{m2} is that it converges to the large scale value much faster than T_{m1}. If recovery is too short to resolve T_{reg} ($T_{m1} \neq T_{m2}$), T_{m2} can be used to approximate T_{reg}. The resulting value should be suspected. T_{m2} lies between T_{loc} and T_{reg}. Therefore, T_{reg} will be larger than T_{m2} if T_{loc} is small, and vice versa.

Upscaling of conservative transport using mass transfer models linking memory parameters to physical parameters of heterogeneity leads to the following conclusions:

1. The above kind of BTCs cannot be accurately modeled with the ADE, because of their non-Fickian nature, which can be well reproduced with non-local in time formulations (MRMT, CTRW, fADE). All these formulations require specifying a memory function, whose parameters are linked to those that describe heterogeneity. We have parametrized the memory function in terms of its slope in log-log scale and early and late cut-off times, t_1 and t_2.

2. The slope of the memory function depends most markedly on connectivity indicators. Our simulations displayed no dependence of the slope on other parameters frequently used in describing heterogeneity, such as variance, Hurst coefficient or correlation distance. Yet, it is clear that they do affect BTC tailing (i.e., tailing disappears if the variance tends to zero and connectivity would have increased if we had used much larger correlation distances).

3. The slope of the BTC is mildly reduced if non-local formulations are adopted for small scale transport. In fact, if the cut-off time, t_2, for the small scale transport is much larger than the travel time of the slow flow tube, small scale transport will dominate transport over long distances. The issue is non-trivial, non-locality can be caused by diffusive processes (e.g. *Berkowitz et al.*, 2006), which is predictable and would be naturally described

by a memory function at the local scale, and by slow advection which we have extensively discussed here. The problem is that non-locality caused by diffusion should be scale independent, while non-locality caused by slow advection depends on both, mean travel time and distance. Specifically, memory function slope remains unchanged, but immobile porosity and late-time cut-off depend on advection time. Tracer tests are often performed under forced gradient conditions (i.e., velocities much larger than those occurring under natural conditions). The memory function derived from such tracer test should be scaled (i.e., t_2 increased in the same proportion than travel time (*Berkowitz et al.*, 2006)) if caused by slow advection, but not if caused by diffusion. Actually since both effects probably overlay, we would have to split the memory function into diffusion and a slow advection for proper scaling.

4. The minimum slope encountered in this study for all the investigated fields is $m_{BTC} = 2$, while smaller slopes are sometimes observed in field tracer tests. The abundance of slopes close to 2 suggests that we have reached a limit for the type of fields investigated here. Further decrease in slope may be caused by long diffusion times into immobile regions, including heterogeneous diffusivity (*Gouze et al.*, 2008b), by threedimensionality, especially with variable tortuosity, or by chemical heterogeneity, particularly for solutes that sorb into the least mobile region (e.g., clays).

5. The scaling behavior of t_2 (late time cut-off) is quite complex. Besides depending on advection time, t_2 appears to increase linearly with the variance of lnT. It is also affected by local scale transverse dispersion. This implies that theoretical developments are needed before memory functions derived from tracer tests can be safely used for predicting long term transport.

Upscaling multi-component reactive transport using mass transfer based on physically based parameters derived from conservative leads to the following conclusions:

1. MRMT-R is found an excellent tool for upscaling mixing controlled reactive transport in heterogeneous aquifers. Total precipitation is very well reproduced for all the examples studied, in terms of both the total mass precipitated and its spatial distribution. In any case the effective solution is smoother than the heterogeneous one. Reaction rate at early times (relative to t_1) is only matched well if the memory function is already representative for the domain sampled.

2. The distinction between reactions in the mobile and immobile zones is to some extend arbitrary. Fast flowing parts of the domain can either be modeled within the mobile porosity with an upscaled dispersion or within the immobile porosity with large exchange rates. In the latter case the reaction rate of the immobile zone has a similar shape than that of the mobile zone. If additionally the separation between dispersion mobile and mass transfer mobile is made, a better separation can be made: the mass transfer mobile and the immobile reaction rate give the total mass transfer reaction rate. This is much larger than the remaining mobile dispersion one.

3. Applying different boundary conditions changes the reactive transport behavior dramatically. A uniform initial (resident) distribution leads to stronger precipitation close to the boundary condition and less precipitation further away. Surprisingly, the shape further away form the boundary is more or less the same. The MRMT-R model reproduces very well precipitation for both boundary conditions using the same memory function.

4. Transverse dispersivity has only a minor effect on total precipitation even it controls mixing. The larger transverse dispersivity, the smoother the curve. That transverse dispersion can be ignored is important as MRMT-R (and most of the existing upscaled models) does not account for it.

5. The ADE (or macro ADE) represents reactive transport reasonable well at distances where transport can be modeled as Fickian. This is also the case when a very minor tailing exists. The bad performance of the ADE in the field supports the claim that the ADE does not hold

at the local scale (e.g. *Berkowitz et al.*, 2006).

Appendix A

A.1 Implementation of a discrete mass-transfer scheme

We describe the implementation of our mass transfer scheme into a standard transport code without solving explicitly for each immobile zone. The exchange term Γ is a sum of exchange terms between the mobile zone and each of the immobile zones f_n:

$$\Gamma = \sum_{n=1}^{N} f_n \tag{A.1}$$

The exchange is described by:

$$f_n = -\phi_{in}\alpha_n(c_{in} - c) \tag{A.2}$$

where c_{in} is the concentration in immobile zone n. Mass balance in the n-th immobile zone yields:

$$\frac{dc_{in}}{dt} = \alpha_n(c_{in} - c) \tag{A.3}$$

The equation may be solved together with Eq. 1 while treating c_{in} as unknown. However, numerical solution is greatly simplified by eliminating it, much in the spirit of *Carrera et al.* (1998). Assuming that the time is discretized and that c varies linearly during the time step (i.e., $\partial c/\partial t$ remains constant), we get:

$$c_{in}(t) = c^k + (c_{in}^k - c^k)e^{\alpha_n t} + \frac{\partial c}{\partial t}[t - \frac{1}{\alpha_n}(1 - e^{-\alpha_n \Delta t})] \tag{A.4}$$

Substituting $\partial c/\partial t$ by its time discretized approximation, $\Delta c/\Delta t$, and using the resulting value for c_{in} to eliminate it from Eq. A2, while evaluating f_n at time $\theta\Delta t$:

$$f_n^{k+\theta} = \phi_{in}\frac{\Delta c}{\Delta t}(1 - e^{-\alpha_n \theta \Delta t}) + \alpha_n \phi_{in}(c_{in}^k - c^k)e^{-\alpha_n \theta \Delta t} \tag{A.5}$$

Notice that now f_n (source/sink per unit aquifer volume) is expressed in terms of only one unknown, $\Delta c/\Delta t$. Therefore, adding f_n to any numerical solver requires two operations:

1. Add the coefficient of $\Delta c/\Delta t$, $\phi_{in}(1 - e^{-\alpha_n \theta \Delta t})$, to the diagonal of the storage matrix for each immobile zone and each node (typically multiplied by the aquifer volume associated to the node, in finite element or finite difference codes)
2. Add the remaining term, $\alpha_n \phi_{in}(c_{in}^k - c^k)e^{-\alpha_n \theta \Delta t}$, to the right hand side (sinks and sources) vector (also for each immobile zone and node, and multiplied with the associated volume, if needed)

We do not solve here explicitly for immobile concentrations. If needed, as for reactive transport simulations, this can be easily done as an extra step using Eq. A4 after the system has been solved and $\Delta c/\Delta t$ is known.

A.2 Implementation of the discrete MRMT-R

Here the implementation of the MTMT-R model into a standard numerical code is outlined. The implementation of the general, conservative MRMT scheme was outlined in Appendix A.1. Additionally, after solving transport for the component u, the mass balance for the reaction rate in the mobile zone (Eq. 4.15) and all immobile zones (Eq. 4.20) have to be calculated at each time step. Both are mass balance equations where s only unknown is the reaction rate. Generally, this implementation of this reactive mass transfer scheme is straight forward. Still, two difficulties exist. The treatment of boundary conditions involving explicitly u and solving the problem implicitly.

The boundary conditions have to be corrected for those operations that involve explicit values of u (like for fixed concentration or flux dependent mass inflow). The mass balance in Eq. 4.15 only closes if this correction is performed. The respective mathematical operation setting the boundary conditions has to be reverted and performed again with c_2 replacing u. For solving transport at an implicit scheme it is critical to set the time correctly for the weighting of u and c_2. One can either calculate the reaction rate at at time $k + \theta$ or the reaction rates at times k and $k + 1$ are weighted by θ. We found much lower mass balance error for the latter case.

Bibliography

Agarwal, R. (1980), A new method to account for producing time effects when drawdown type curves are used to analyze pressure built-up and other test data, *SPE 9289, SPE-AIME 55th Annual Technical Conference and Exhibition*, *Dallas, Texas*.

Agarwal, R., A.-H. R., and R. H.J.J. (1970), An investigation of wellbore storage and skin effect in unsteady liquid flow. 1. analytical treatment, *AIME Trans*, pp. 279–290.

Alcolea, A., J. Carrera, and A. Medina (2008), Regularized pilot points method for reproducing the effect of small scale variability: Application to simulations of contaminant transport, *J. Hydrol.*, *355(1-4)*, 76–90, doi:10.1016/j.jhydrol.2008.03.004.

Banton, O., and L. Bangoy (1996), A new method to determine storage coefficient from pumping test data, *Ground Water*, *35*, 772–777.

Becker, M. W., and A. Shapiro (2000), Tracer transport in fractured crystalline rock: Evidence of nondiffusive breakthrough tailing, *Water Resour. Res.*, *36(7)*, 1677—-1686.

Becker, M. W., and A. Shapiro (2003), Interpreting tracer breakthrough tailing from different forced-gradient tracer experiment configurations in fractured bedrock, *Water Resour. Res.*, *39(1)*, 1024, doi:10.1029/2001WR001190.

Bellin, A., A. Ronaldo, W. J. P. Bosma, S. E. A. T. M. van der Zee, and Y. Rubin (1993), Linear equilibrium adsorbing solute transport in physically and chemically heterogeneous porous formations 1. analytical solutions, *Water Resour. Res.*, *29 (12)*, 4019–4030.

Benson, D. A., S. W. Wheatcraft, and M. M. Meerschaerdt (2000), The fractional-order governing equation of lévy motion, *Water Resour. Res.*, *36 (6)*, doi:10.1029/2000WR900032.

Berkowitz, B., and H. Scher (1997), Anomalous transport in random fracture networks, *Phys. Rev. Lett.*, *79*(20), 4038–4041, doi:10.1103/PhysRevLett.79.4038.

Berkowitz, B., and H. Scher (1998), Theory of anomalous chemical transport in fracture networks, *Phys. Rev. E*, *57(5)*, 5858–5869.

Berkowitz, B., and H. Scher (2008), Exploring the nature of non-fickian transport in laboratory experiments, *Adv. Water Resour.*, *in press*, doi:doi:10.1016/j.advwatres.2008.05.004.

Berkowitz, B., A. Cortis, M. Dentz, and H. Scher (2006), Modeling non-fickian transport in geological formations as a continous time random walk, *Rev. Geophys.*, *44*, doi:10.1029/2005RG000178.

Berkowitz, B., S. Emmanuel, and H. Scher (2008), Non-fickian transport and multple-rate mass transfer in heterogeneous media, *Water Resour. Res.*, *44*, W03,402, doi:10.1029/2007WR005906.

Bijeljic, B., and M. J. Blunt (2006), Pore-scale modeling and continuous time random walk analysis of dispersion in porous media, *Water Resour. Res.*, *42*, W01,202, doi:doi:10.1029/2005WR004578.

Bourdet, D. (2002), *Well Test Analysis: The Use of Advanced Interpretation Models*, *Handbook of Petroleum Exploration and Production*, vol. 3, 1st edn. ed., Elsevier, Amsterdam.

Butler, J. J. (1990), The role of pumping tests in site characterization: some theoretical considerations, *Ground Water*, *28*, 394–40.

Butler, J. J., and W. Liu (1993), Pumping tests in nonuniform aquifers: The radially asymmetric case, *Water Resour. Res.*, *29*, 259–269.

Carrera, J. (1993), An overview of uncertainties in modelling groundwater solute transport, *J. Contam. Hydrol.*, *13(1-4)*, 23–48, doi:10.1016/0169-7722(93)90049-X.

Carrera, J., X. Sánchez-Vila, I. Benet, A. Medina, G. Galarza, and J. Guimera (1998), On matrix diffusion: formulations, solution methods and qualitative effects, *Hydrogeol. J.*, *6(1)*, 178–190, doi:10.1007/s100400050143.

Chen, W., and R. J. Wagenet (1995), Solute transport in porous media with sorption-site heterogeneity, *Environ. Sci. Technol.*, *29*, 11.

Chenof, a. C. R., D. (2002), Methods to determine storativity of infinite confined aquifers from a recovery test, *Ground Water*, *10*, 385–389.

Chu, L., and A. Grader (1999), Transient pressure and rate analysis for active and interference wells in composite systems, *In Situ*, *23*, 297–332.

Cirpka, O. A., and A. J. Valocchi (2007), Two-dimensional concentration distribution for mixing-controlled bioreactive transport in steady state, *Adv. Water Resour.*, *30(6-7)*, 1668–1679, doi: 10.1016/j.advwatres.2006.05.022.

Connaughton, D. F., J. R. Stedinger, L. W. Lion, and M. L. Shuler (1993), Description of time-varying desorption kinetics: release of naphthalene from contaminated soils, *Environ. Sci. Technol.*, *27*, 2397 – 2403, doi:10.1021/es00048a013.

Copty, N., and A. Findikakis (2004), Stochastic analysis of pumping test drawdown data in heterogeneous geologic formations, *J. Hydraul. Res.*, *42*, 59–67.

Cortis, A., and B. Berkowitz (2004), Anomalous transport in ”classical” soil and sand columns, *Soil Sci. Soc. Am. J.*, *68*, 1539–1548.

Cortis, A., and C. Knudby (2006), A continuous time random walk approach to transient flow in heterogeneous porous media, *Water Resour. Res.*, *42*, W10,201, doi:10.1029/2006WR005227.

Dagan, G. (1989), *Flow and transport in porous formations*, 465 pp., Springer-Verlag, Berlin Heidelberg New York.

De Simoni, M., J. Carrera, X. Sánchez-Vila, and A. Guadagnini (2005), A procedure for the solution of multicomponent reactive transport problems, *Water Resour. Res.*, *41*, W11,410, doi: 10.1029/2005WR004056.

De Simoni, M., X. Sánchez-Vila, J. Carrera, and M. Saaltink (2007), A mixing ratios-based formulation for multicomponent reactive transport, *Water Resour. Res.*, *43*, W07,419, doi: 10.1029/2006WR005256.

Dentz, M., and B. Berkowitz (2003), Transport behavior of solute transport in continous time random walks and multi-rate mass transfer, *Water Resour. Res.*, *39 (5)*, 1111, doi:10.1029/ 2001WR001163.

Dentz, M., H. Kinzelbach, S. Attinger, and W. Kinzelbach (2000), Temporal behavior of a solute cloud in a heterogeneous porous medium 1. point-like injection, *Water Resour. Res.*, *36(12)*, 3591—-3604.

Dentz, M., A. Cortis, H. Scher, and B. Berkowitz (2004), Time behavior of solute transport in heterogeneous media: Transition from anomalous to normal transport, *Adv. Water Resour.*, *27*, 155–173.

Di Donato, G., E. Obi, and M. J. Blunt (2003), Anomalous transport in heterogeneous media demonstrated by streamline-based simulation, *Geophys. Res. Lett.*, *30(12)*, 1608, doi:10.1029/ 2003GL017196.

Farrell, J., and M. Reinhard (1994), Desorption of halogenated organics from model solids, sediments, and soil under unsaturated conditions: 2. kinetics, *Environ. Sci. Technol.*, *28(1)*, 63–72.

Fernandez-Garcia, D., X. Sánchez-Vila, and A. Guadagnini (2008), Reaction rates and effective parameters in stratified aquifers, *Adv. Water Resour.*, *31(10)*, 1364–1376, doi:10.1016/j. advwatres.2008.07.001.

Freeze, R., and J. Cherry (1979), *Groundwater*, Prentice Hall, Eaglewood Cliffs, NJ.

Freyberg, D. L. (1986), A natural gradient experiment on solute transport in a sand aquifer 2. spatial moments and the advection and dispersion of nonreactive tracers, *Water Resour. Res.*, *22(13)*, 2031—-2046.

Gelhar, L. (1993), *Stochstic Subsurface Hydrology*, Princton Hall, Old Tappan, New York.

Gómez-Hernández, J., and A. Journel (1993), Joint sequential simulation of multigaussian fields, in *Geostat Troia 1992*, vol. 1, edited by Soares, pp. 85–94, Kluwer Publ.

Goode, D. (1997), Composite recovery type curves in normalized time from theis' exact solution, *Ground Water*, *35(4)*, 672–678.

Gouze, P., T. L. Borgne, R. Leprovost, G. Lods, T. Poidras, and P. Pezard (2008a), Non-fickian dispersion in porous media: 1. multiscale measurements using single-well injection withdrawal tracer tests, *Water Resour. Res.*, *44*, W06,426, doi:10.1029/2007WR006278.

Gouze, P., M. Yasmin, T. L. Borgne, M. Dentz, and J. Carrera (2008b), Non-fickian dispersion in porous media explained by heterogeneous microscale matrix diffusion, *Water Resour. Res.*, *in press*.

Guimerà, J., and J. Carrera (2000), A comparison of hydraulic and transport parameters measured in low-permeability fractured media, *J. Contam. Hydrol.*, *41(3-4)*, 261–281, doi:10.1016/S0169-7722(99)00080-7.

Hadermann, J., and W. Heer (1996), The grimsel (switzerland) migration experiment: integrating field experiments, laboratory investigations and modelling, *J. Contam. Hydrol.*, *21(1-4)*, 87–100, doi:doi:10.1016/0169-7722(95)00035-6.

Haggerty, R., and S. M. Gorelick (1995), Multiple-rate mass transfer for modeling diffusion and surface reactions in media with pore scale heterogeneity, *Water Resour. Res.*, *31 (10)*, 2383–2400.

Haggerty, R., and S. M. Gorelick (1998), Modeling mass transfer processes in soil columns with pore-scale heterogeneity, *Soil Sci. Soc. Am. J.*, *62(1)*, 62–74.

Haggerty, R., S. A. McKenna, and L. C. Meigs (2000), On the late-time behavior of tracer test breakthrough curves, *Water Resour. Res.*, *36 (12)*, 3467–3479.

Haggerty, R., C. F. Harvey, C. F. von Schwerin, and L. C. Meigs (2004), What controls the apparent timescale of solute mass transfer in aquifers and soils? a comparison of experimental results, *Water Resour. Res.*, *40*, W01,510, doi:10.1029/2002WR001716.

Kitanidis, P. K. (1988), Prediction by the method of moments of transport in a heterogeneous formation, *J. Hydrol.*, *102*, 453—-473.

Knudby, C., and J. Carrera (2005), On the relationship between indicators of geostatistical, flow and transport connectivity, *Adv. Water Resour.*, *28*, 405–421, doi:10.1016/j.advwatres.2004.09.001.

Kosakowski, G., B. Berkowitz, and H. Scher (2001), Analysis of field observations of tracer transport in a fractured till, *J. Contam. Hydrol.*, *47(1)*, 29–51.

Kreft, A., and A. Zuber (1978), On the physical meaning of the dispersion equation and its solutions for different initial and boundary conditions, *Chem. Eng.*, *33*, 1471—1480.

Lallemand-Barres, P., and P. Peaudecerf (1978), Recherche des relations entre a valeur de la dispersivite macroscopique d'un milieu aquifere, ses autres caracteristiques et les conditions de mesure, *Etude Bibliographique, Bull., Bureau de Recherches Géologiques et Minières*, *III (4)*, 277—284.

Lawrence, A. E., X. Sanchez-Vila, and Y. Rubin (2002), Conditional moments of the breakthrough curves of kinetically sorbing solute in heterogeneous porous media using multirate mass transfer models for sorption and desorption, *Water Resour. Res.*, *38(11)*, 1248, doi: 10.1029/2001WR001006.

Le Borgne, T., and P. Gouze (2008), Non-fickian dispersion in porous media: 2. model validation from measurements at different scales, water resour. res., 44, w06427, doi:10.1029/2007wr006279, *Water Resour. Res.*, *44*, W06,427, doi:10.1029/2007WR006279.

Le Borgne, T., M. Dentz, and J. Carrera (2008a), Spatial markov processes for modeling lagrangian particle dynamics in heterogeneous porous media, *Physical Review E*, *78*, 026,308.

Le Borgne, T., M. Dentz, and J. Carrera (2008b), Lagrangian statistical model for transport in highly heterogeneous velocity fields, *Physical Review Letters*, *101*, 090,601.

Levy, M., M. B. BerkowitzLevy, and B. Berkowitz (2003), Measurement and analysis of non-fickian dispersion in heterogeneous porous media, *J. Contam. Hydrol.*, *64(3-4)*, 203–226.

Lichtner, P. C., and Q. Kang (2007), Upscaling pore-scale reactive transport equations using a multiscale continuum formulation, *Water Resour. Res.*, *43*, W12S15, doi:10.1029/2006WR005664.

Luo, J., and O. A. Cirpka (2008), Travel-time based descriptions of transport and mixing in heterogeneous domains, *Water Resour. Res.*, *in press*, doi:10.1029/2007WR006035.

Luo, J., M. Dentz, J. Carrera, and P. Kitanidis (2008), Effective reaction parameters for mixing controlled reactions in heterogeneous media, *Water Resour. Res.*, *44*, W02,416, doi:10.1029/2006WR005658.

Martinez-Landa, L., and J. Carrera (2005), An analysis of hydraulic conductivity scale effects in granite (full-scale engineered barrier experiment (febex), grimsel, switzerland), *Water Resour. Res.*, *41(3)*, W03,006.

McKenna, S., L. Meigs, and R. Haggerty (2001), racer tests in a fractured dolomite 3. double porosity, multiple-rate mass-transfer processes in two-well convergent flow tests, *Water Resour. Res.*, *35 (7)*, 1143–1154.

Medina, A., and J. Carrera (1996), Coupled estimation of flow and solute transport parameters, *Water Resour. Res.*, *32(10)*, 3063—3076.

Meier, P., J. Carrera, and X. Sanchez-Vila (1998), An evaluation of jacob's method for the interpretation of pumping tests in heterogeneous formations, *Water Resour. Res.*, *34(5)*, 1011–1025.

Meier, P., J. Carrera, and X. Sanchez-Vila (1999), A numerical study on the relationship between transmissivity and specific capacity in heterogeneous aquifers, *Ground Water*, *37(4)*, 611–617.

Meier, P., A. Medina, and J. Carrera (2001), Geostatistical inversion of cross-hole pumping tests for identifying preferential flow channels within a shear zone, *Ground Water*, *39(1)*, 10–17.

Meigs, L. C., and R. L. Beauheim (2001), Tracer tests in a fractured dolomite 1. experimental design and observed tracer recoveries, *Water Resour. Res.*, *37(5)*, 1113—1128.

Moench, A., and P. Hsieh (1985), Evaluation of slug tests in wells containing a finite thickness skin - comment, *Water Resour. Res.*, *21(9)*, 1459–1461.

Neretnieks, I., and A. Rasmuson (1984), An approach to modelling radionuclide migration in a medium with strongly varying velocity and block sizes along the flow path, *Water Resour. Res.*, *20(12)*, 1823—-1836.

Neretnieks, I., T. Eriksen, and P. Tahtinen (1982), Tracer movement in a single fissure in granitic rock: Some experimental results and their interpretation, water resour. res., 18(4), 849–858, *Water Resour. Res.*, *18(4)*, 849—-858.

Neuman, S., and V. Di Federico (2003), Multifaceted nature of hydrogeologic scaling and its interpretation, *Rev. Geophys.*, *41 (3)*, doi:10.1029/RG000130.

Neuman, S., and D. Tartakovsky (2008), Perspective on theories of anomaloustransport in heterogeneous media, *Adv. Water Resour.*, doi:10.1016/j.advwatres.2008.08.005.

Neuman, S. P. (1990), Universal scaling of hydraulic conductivities and dispersivities in geologic media, *Water Resour. Res.*, *22(8)*, 1749–1758.

Neuman, S. P., A. Guadagnini, and M. Riva (2004), Type-curve estimation of statistical heterogeneity, *Water Resour. Res.*, *40*, W04,201, doi:10.1029/2003WR002405.

Ondiviela, M., E. Vasquez-Sune, J. Carrera, and D. Plana (2001), Estudio hidrogeologico para el tunel de la c/ mallorca de la penetracion de la linea de alta velocidad en barcelona [hydrogeological study for the tunnel at mallorca street about the influence of the high velocity train], *Tech. rep.*, Hydrogeology Group, UPC, Barcelona.

Papadopulus, I., and H. Cooper (1967), Drawdown in a well of large diameter, *Water Resour. Res.*, *3(1)*, 241–244.

Rasmuson, A., and I. Neretnieks (1986), Radionuclide migration in strongly fissured zones: The sensitivity to some assumptions and parameters, *Water Resour. Res.*, *22(4)*, 559—-569.

Renard, P., and G. de Marsily (1997), Calculating equivalent permeability: a review, *Adv. Water Resour.*, *20(5-6)*, 253–278, doi:10.1016/S0309-1708(96)00050-4.

Rubin, Y. (1983), Transport of reactive solute in porous media: Relation between mathematical nature of problem formulation and chemical nature of reactions, *Water Resour. Res.*, *19(5)*, 1231—-1252.

Rubin, Y., M. A. Cushey, and A. Wilson (1997), The moments of the breakthrough curves of instantaneously and kinetically sorbing solutes in heterogeneous geologic media: Prediction and parameter inference from field measurements, *Water Resour. Res.*, *33(11)*, 2465–2481.

Sánchez-Vila, X., and J. Carrera (1997), Directional effects on convergent flow tracer tests, *Math. Geol.*, *29(4)*, 551–569.

Sánchez-Vila, X., and J. Carrera (2004), On the striking similarity between the moments of breakthrough curves for a heterogeneous medium and a homogeneous medium with a matrix diffusion term, *J. Hydrol.*, *294(1-3)*, 164–175, doi:doi:10.1016/j.jhydrol.2003.12.046.

Sánchez-Vila, X., I. Colominas, and J. Carrera (1993), *FAITH: User's Guide*, Technical University of Catalonia, Barcelona.

Sánchez-Vila, X., J. Girardi, and J. Carrera (1995), A synthesis of approaches to upscaling of hydraulic conductivities, *Water Resour. Res.*, *31(4)*, 867–882.

Sánchez-Vila, X., P. Meier, and J. Carrera (1999), Pumping tests in heterogeneous aquifers: An analytical study of what can be obtained from their interpretation using jacob's method, *Water Resour. Res.*, *35(4)*, 943–952.

Schad, H., and G. Teutsch (1994), Effects of the investigation scale on pumping test results in heterogeneous porous aquifers, *J. Hydrol.*, *159(1-4)*, 61–77, doi:10.1016/0022-1694(94)90249-6.

Schumer, R., D. A. Benson, M. M. Meerschaert, and B. Baeumer (2003), Fractal mobile/immobile solute transport, *Water Resour. Res.*, *39(10)*, 1296, doi:10.1029/2003WR002141.

Selroos, J. O., and V. Cvetkovic (1992), Modeling solute advection coupled with sorption kinetics in heterogeneous formations, *Water Resour. Res.*, *28 (5)*, 1271–1278.

Shapiro, A., and P. Hsieh (1998), How good are estimates of transmissivity from slug tests in fractured rock?, *Ground Water*, *36(1)*, 37–48.

Shapiro, A. M. (2001), Effective matrix diffusion in kilometer-scale transport in fractured crystalline rock, *Water Resour. Res.*, *37(3)*, 507—522.

Shapiro, A. M., R. A. Renken, R. W. Harvey, M. R. Zygnerski, and D. W. Metge (2008), Pathogen and chemical transport in the karst limestone of the biscayne aquifer: 2. chemical retention from diffusion and slow advection, *Water Resour. Res.*, *in press*, doi:10.1029/2007WR006059.

Streltsova, T. (1988), *Well Testing in heterogeneous formations*, Wiley, New York.

Tartakovsky, A., and S. P. Neuman (2008), Effects of peclet number on pore-scale mixing and channeling of a tracer and on directional advective porosity, *Geophysical Research Letters*, *in press*.

Taylor, G. I. (1953), Dispersion of soluble matter in solvent flowing slowly through a tube, *Proc. Roy. Soc. A.*, *219*, 186—-203.

Theis, C. (1935), The relation between the lowering of the piezometric surface and the rate and duration of discharge of a well using ground water storage, *Trans. Am. Geophys. Union*, *16*, 519–524.

Valocchi, A. J. (1985), Validity of the local equilibrium assumption for modeling sorbing solute transport through homogeneous soils, *Water Resour. Res.*, *21(6)*, 808—-820.

Vesselinov, V., S. Neuman, and W. Illman (2001), Three-dimensional numerical inversion of pneumatic cross-hole tests in unsaturated fractured tuff 2. equivalent parameters, high-resolution stochastic imaging and scale effects, *Water Resour. Res.*, *37(12)*, 3019–3041.

Wang, P. P., C. Zheng, and S. M. Gorelick (2005), A general approach to advective–dispersive transport with multirate mass transfer, *Adv. Water Resour.*, *28(1)*, 33–42, doi:doi:10.1016/j.advwatres.2004.10.003.

Wen, X.-H., and J. J. Gómez-Hernández (1996), Upscaling hydraulic conductivities in heterogeneous media: An overview, *J. Hydrol.*, *183,(1-2)*, ix–xxxii.

Werth, C. J., J. A. Cunningham, P. V. Roberts, and M. Reinhard (1997), Effects of grain-scale mass transfer on the transport of volatile organics through sediments 2. column results, *Water Resour. Res.*, *33 (12)*, 2727—-2740.

Yeh, T.-C. J., and S. Liu (2000), Hydraulic tomography: Development of a new aquifer test method, *Water Resour. Res.*, *36(8)*, 2095–2105.

Zhang, Y., B. Baeumer, and D. A. Benson (2006), Relationship between flux and resident concentrations for anomalous dispersion, *Geophys. Res. Lett.*, *33*, L18,407, doi:10.1029/2006GL027251.

Zhang, Y., D. A. Benson, and B. Baeumer (2007), Predicting the tails of breakthrough curves in regional-scale alluvial systems, *Ground Water*, *45 (4)*, 473–484, doi:10.1111/j.1745-6584.2007.00320.x.

Zheng, L., J.-Q. Guo, and Y. Lei (2005), An improved straight-line fitting method for analyzing pumping test recovery data, *Ground Water*, *43(6)*, 939–942, doi:10.1111/j.1745-6584.2005.00094.x.

Zinn, B., and C. F. Harvey (2003), When good statistical models of aquifer heterogeneity go bad: A comparision of flow, dispersion, and mass transfer in connected and multivariate gaussian hydraulic conductivity fields, *Water Resour. Res.*, *39 (3)*, doi:10.10292001WR001146.

Zinn, B., L. C. Meigs, C. F. Harvey, R.Haggerty, W. J. Peplinski, and C. F. von Schwerin (2004), Experimental visualization of solute transport and mass transfer processes in two-dimensional conductivity fields with connected regions of high conductivity, *Environ. Sci. Technol.*, *38 (14)*, 3916 –3926, doi:10.1021/es034958g.